Kalman Filter Implementation to Determine Orbit and Attitude of a Satellite in a Molniya Orbit

Elizabeth M. Keil

Thesis submitted to the faculty of the Virginia Polytechnic Institute and State University in partial fulfillment of the requirements for the degree of

Master of Science

In

Aerospace and Ocean Engineering

Robert W. McGwier

Craig A. Woolsey

Cornel Sultan

2 May 2014

Blacksburg, VA

Keywords: Attitude, Orbit, Determination, Kalman Filter

Kalman Filter Implementation to Determine Orbit and Attitude of a Satellite in a Molniya Orbit

Elizabeth M. Keil

Abstract

This thesis details the development and implementation of an attitude and orbit determining Kalman filter algorithm for a satellite in a Molniya orbit. To apply the Kalman Filter for orbit determination, the equations of motion of the two body problem were propagated using Cowell's formulation. Four types of perturbing forces were added to the propagated model in order to increase the accuracy of the orbit prediction. These four perturbing forces are Earth oblateness, atmospheric drag, lunar gravitational forces and solar radiation pressure. Two cases were studied, the first being the implementation of site track measurements when the satellite was over the ground station. It is shown that large errors, upwards of ninety meters, grow as time from last measurement input increases. The next case studied was continuous measurement inputs from a GPS receiver on board the satellite throughout the orbit. This algorithm greatly decreased the errors seen in the orbit determining algorithm due to the accuracy of the sensor as well as the continuous measurement inputs throughout the orbit. It is shown that the accuracy of the orbit determining Kalman filter also depends on the length of time between each measurement update. The errors decrease as the time between measurement updates decreases. Next the Kalman filter is applied to determine the satellite attitude. The rotational equations of motion are propagated using Cowell's Formulation and numerical integration. To increase the fidelity of the model four disturbing torques are included in the rotational equations of motion model: gravity gradient torque, solar pressure torque, magnetic torque, and aerodynamic torque. Four cases were tested corresponding to four different on board attitude determining sensors: magnetometer, Earth sensor, sun sensor, and star tracker. A controlled altitude path was chosen to test the accuracy of each of these cases and it was shown that the algorithm using star tracker measurements was three hundred times more accurate than that of the magnetometer algorithm.

Table of Contents

1 INTRODUCTION ……..…… 1

1.1 Background and Motivation ……..… 1

1.2 The Satellite ……. 2

1.3 The Orbit ……..……..... 4

2 FUNDAMENTALS OF KALMAN FILTERS …..…….…….……..7

2.1 Kalman Filter ……..……...……...……. 8

2.2 Kalman Filter for Linearized System ……...….. 11

2.3 Extended Kalman Filter ……...…….. 13

3 ORBIT DETERMINATION …… 15

3.1 Defining a Satellite Orbit .…….. 15

3.2 Laws Governing a Satellite Orbit ....……. 20

3.3 Predicting a Satellites Orbit using the Two Body Problem …… 22

3.4 Perturbations of the Satellites Orbit ……...…….. 23

3.5 Development of the State Matrix with Perturbing Forces ……...…… 32

3.6 Kalman Filter Implementation for Site Track Orbit Determination ……... 38

3.7 Orbit Determining Kalman Filter Implementation with GPS……..…….…….... 44

4 ATTITUDE DETERMINATION ..…….…….…..… 49

4.1 Representing Attitude ..……..……..……..… 49

4.2 Rotational Equations of Motion …….…… 52

4.3 Disturbing Torques…….…….…… 54

4.4 Attitude Control …….…….…… 59

4.5 On-Board Attitude Sensors ……..……..…. 61

4.6 Kalman Filter Implementation for Attitude Determination …….. 63

4.7 Results of Attitude Determination Algorithm ……..….. 67

5 CONCLUSION …….……..…..… 78

5.1 Future Work……...……..……..… 79

BIBLIOGRAPHY …….……..… 81

APPENDIX: Development of State Matrix for Earth's Oblateness ...…….…… 83

List of Figures

Figure 1.1: Dimensions and orientation of satellite used in this thesis ……..…… 2

Figure 1.2: View of Molniya Orbit used in this thesis ……...…… 4

Figure 1.3: Altitude of Satellite in Molniya Orbit …… 5

Figure 1.4: Molniya Orbit Ground Track …….. 6

Figure 2.1: The two main steps in a Kalman Filter …… 7

Figure 2.2: Extend Kalman Filter Representation ……... 14

Figure 3.1: Earth Centered Reference Frame …….. 16

Figure 3.2: ECI, ECEF and SEZ Reference Frames …… 17

Figure 3.3: Depiction of Orbital Elements ……... 19

Figure 3.4: Illustration of Kepler's 2nd law ……. 20

Figure 3.5: Zonal Harmonic used in this Thesis …….. 25

Figure 3.6: Orientation of Third Body ……. 28

Figure 3.7: Diagram of Third Body ……. 29

Figure 3.8: Unperturbed and perturbed orbit using all four perturbation accelerations …….. 31

Figure 3.8: Visualization of Orbit and Occurrence of Measurements from Ground Station ….. 38

Figure 3.8: Visualization of ground station collecting and sending range data to satellite ……. 39

Figure 3.10: Predicted and actual orbit determined using site track …… 41

Figure 3.11: Close up of Predicted and Actual Orbit Determined using Site Track ……... 42

Figure 3.12: Error of Orbit Determined using Site Track over one Orbit ……... 43

Figure 3.13: Error of Orbit Determined using Site Track over multiple orbits …….. 43

Figure 3.14: Error of Orbit Determined using GPS sensor ……..… 45

Figure 3.15: Orbit Determined using GPS sensor ……... 45

Figure 3.16: Zoomed In Orbit Determined using GPS sensor …… 46

Figure 3.17: Zoomed in orbit determined using GPS sensor …….. 46

Figure 3.18: Errors in orbit determined using GPS sensor with measurement updates every second ……. 47

Figure 3.18: Errors in orbit determined using GPS sensor with measurement updates every two minutes …… 47

Figure 3.20: Mean errors in orbit verse time between measurement updates ……. 48

Figure 4.1: Orbital and Body Frame Representations ……. 50

Figure 4.2: Euler Angles ……..... 51

Figure 4.3: Disturbance Torque Effects vs. Altitude ……... 54

Figure 4.4: Sunlight on Satellite …….. 55

Figure 4.5: Incident angles of Sunlight with respect to Body Frame …….. 56

Figure 4.7: Gravity Gradient Torque ……... 57

Figure 4.11: Desired motion of satellite ……. 59

Figure 4.12: Satellite Maneuver …….. 61

Figure 4.13: Satellite Attitude Determine Using Magnetometer …… 67

Figure 4.14: Satellite Attitude Determine Using Magnetometer ……. 68

Figure 4.15: Errors in Satellite Attitude Determine Using Magnetometer …….. 68

Figure 4.16: Probability Distribution of Errors in Satellite Attitude Determine Using Magnetometer ……. 69

Figure 4.17: Satellite Attitude Determine Using Earth Sensor …… 70

Figure 4.18: Satellite Attitude Determine Using Earth Sensor …… 70

Figure 4.19: Errors in Satellite Attitude Determine Using Earth Sensor ……. 71

Figure 4.20: Probability Distribution of Errors in Satellite Attitude Determine Using Earth Sensor …….. 71

Figure 4.20: Satellite Attitude Determine Using Sun Sensor …….. 72

Figure 4.21: Satellite Attitude Determine Using Sun Sensor …….. 73

Figure 4.23: Errors in Satellite Attitude Determine Using Sun Sensor ……... 73

Figure 4.24: Distribution of errors in satellite attitude determined using sun sensor ……. 74

Figure 4.25: Satellite Attitude Determine Using Star Tracker …… 75

Figure 4.26: Satellite Attitude Determine Using Star Tracker …… 75

Figure 4.27: Errors in Satellite Attitude Determine Using Star Tracker ……. 76

Figure 4.28: Distribution of errors in satellite attitude determined using star tracker …… 76

Figure 4.28: Summary of distribution of errors in satellite attitude determined ……. 77

List of Tables

Table 1.1: Characteristics of Satellite …… 3

Table 4.1: Errors and update times for Attitude Sensors …… 63

Chapter 1

Introduction

This thesis demonstrates how Kalman Filters can be used to determine a satellites orbit and attitude. Up to date and accurate knowledge of a satellite's position and orientation is necessary for a satellite to perform the mission it was designed for and communicate with the satellite ground station. On-board attitude and orbit determination typically requires a multitude of sensors and is computationally expensive. This chapter will explain the motivation behind this thesis as well as the fictitious satellite and orbit used in this Kalman Filter model.

1.1 Background and Motivation

The goal of this thesis is to accurately compute the orbit and attitude of a satellite with as little computational effort as possible. Although on-board processing capabilities have greatly increased in the past couple of decades, it is still a priority to minimize the amount of computational effort required by the on-board processors while maintaining a desired level of accuracy. Kalman Filters allow for accurate prediction of a given state (attitude, position, velocity etc) without requiring expansive past data to be stored and computed, which allows for efficient on-board computation. The on-board computation, along with the sensors that measure the satellite orbit and attitude, make up the attitude determination system of the satellite. Satellite attitude determining systems vary in size but typically consist of four to five on-board sensors as well as the necessary processing equipment. The goal of this thesis is to develop an attitude determining system which utilizes a smaller number of sensors and is computationally inexpensive so that it can be implemented on a small payload. If a small payload is able to autonomously determine the host satellite orbit and attitude it would reduce the number of interfaces needed between the host and payload, reducing the complexity that comes with integrating payloads to host satellites. The first step in developing a minimized attitude determination system is to define the physical characteristics of the satellite. This is done in the following section.

1.2 The Satellite

To accurately estimate the orbit and attitude of a satellite, the physical aspects of the satellite must first be define. The fictitious satellite used in this thesis has a cylindrical shape with two solar arrays on either side of the cylinder. Figure 1.1 shows the dimensions of the satellite and defines the orientation of the satellite in the body frame.

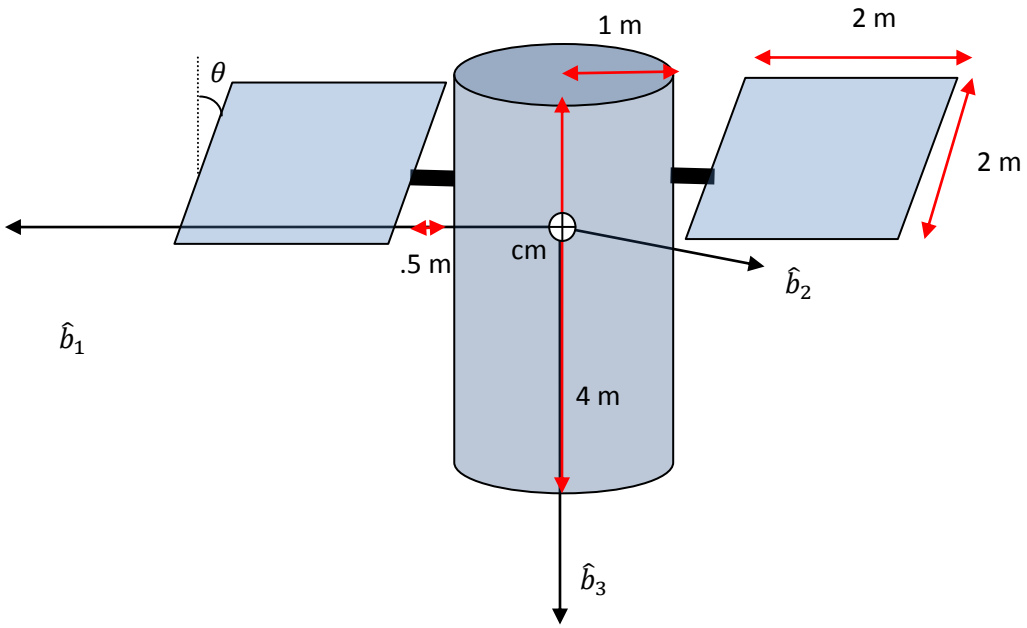

Figure 1.1: Dimensions and orientation of satellite used in this thesis

The satellites dimensions are needed to calculate the moment of inertia matrix, which will be essential in determining how environmental torque affects the satellite attitude. The principal moment of inertia matrix can be calculated using the parallel axis theorem:

$$I^o = I^c + m[r^{co^T} r^{co} \mathrm{I} - r^{co} r^{co^T}]$$

where r^{co} is the vector originating at the satellite's center of mass and pointing to the origin of a chosen reference frame, $\hat{o}$. I^c is the moment of inertia matrix for the given object and I^o is that objects moment of inertia matrix with respect to the reference frame, $\hat{o}$. In this case, the origin of the reference frame is choosen to be the center of the cylinder. The position of each solar array and connecting rod is defined with respect to the origin of the cylinder. Once the moment of inertia matrices for each rod and array are calculated with respect to the cylinders origin, they can be added together:

$$I^o{}_{total} = I^o{}_{cylinder} + I^o{}_{solararray1} + I^o{}_{solararray2} + I^o{}_{rod1} + I^o{}_{rod2}$$

The principal axes theorem can be used again to translate the total moment of inertia matrix from the center of the cylinder to the satellite's center of mass.

$$I^{cm} = I^{o}{}_{total} - m[r^{co^T} r^{co} \mathrm{I} - r^{co} r^{co^T}]$$

Once the total moment of inertia matrix has been formed, eigenvalue decomposition can be used to find the principal moments and axes of inertia. For this satellite, the principal moment of inertia matrix is

$$I_{Principal} = \begin{bmatrix} I_{b_1} & 0 & 0 \\ 0 & I_{b_2} & 0 \\ 0 & 0 & I_{b_3} \end{bmatrix} = \begin{bmatrix} 2000.7 & 0 & 0 \\ 0 & 2019.3 & 0 \\ 0 & 0 & 647.3 \end{bmatrix}$$

This matrix will be used to determine how the satellite rotates with respect to the center of mass under environmental and controlled torques. A satellite is stable about the major and minor axes and unstable about the semi-major axis. From the principal moment of inertia matrix, $I_{b_3} < I_{b_1} < I_{b_2}$, therefore this satellite is unstable about the $\hat{b}_1$ axis.

Notice that the orientation of the satellite's solar arrays varies over the period of the orbit since they will always be oriented with the normal of the array pointing towards the sun. This necessity means the principal moment of inertia matrix for the satellite varies depending on the satellite position in the orbit. Therefore, the effects of the disturbing torques on the satellite, which depend on the moment of inertia matrix, depend on the position of the satellite in its orbit. In order to determine the attitude of the satellite the position of the satellite is needed. This will be further discussed in Chapter 4.

Not only are the dimensions of the satellite needed to estimate the orbit and attitude of the satellite, other characteristics are required, such as center of solar pressure, center of drag etc. Table 1.1 defines these characteristics for the satellite used in this thesis.

Mass	m	800 kg	
Average cross-sectional area	A	8 m^2	
Coefficient of drag	C_D	2.2	
Coefficient of Reflectivity	C_R	0.6	
	b_1	b_2	b_3
Center of mass	0	0	0
Center of aerodynamic pressure, C_{pa}	0	0	-0.5 m
Center of solar pressure, C_{sp}	0	0	-0.8 m

Table 1.1: Characteristics of Satellite

1.3 The Orbit

For this thesis, the chosen orbit is the Molniya orbit, seen in Figure 1.2. The Molniya orbit is a highly elliptical orbit with an inclination of 63.4 degrees and period of one half of a sidereal day. In this orbit the satellite's distance to Earth varies drastically over one period. As seen in Figure 1.3, at perigee the altitude of the satellite is roughly 5000 km and at apogee the altitude of the satellite is over 40,000 km. As will be explained in Chapter 2, a satellite at apogee in the Molniya orbit is traveling much slower than when it is at perigee. This allows for nearly persistent collection by a satellite's sensors while at apogee, making this orbit essential for communication satellites.

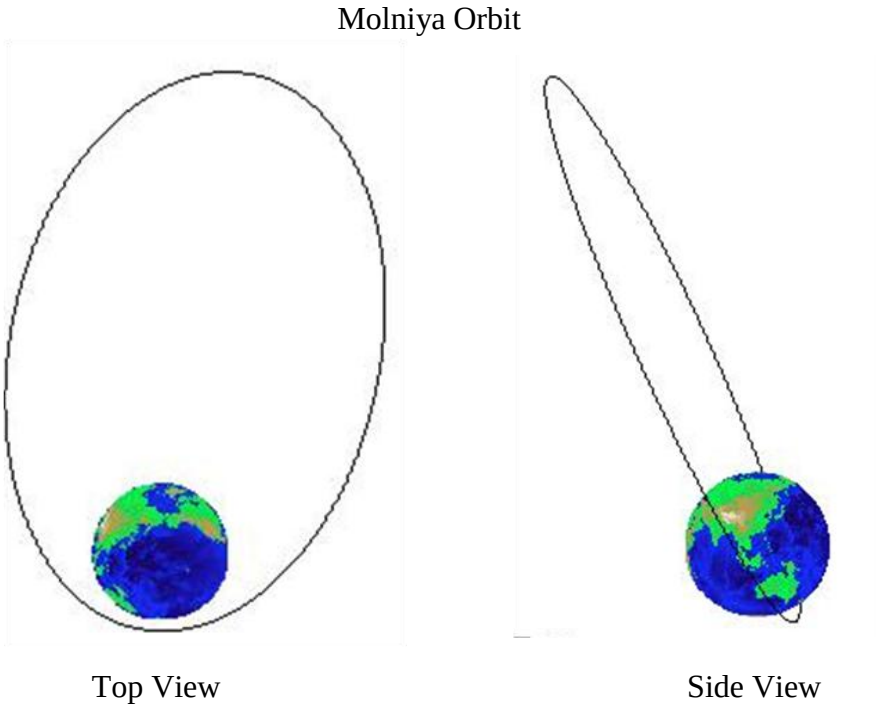

Figure 1.2: View of Molniya Orbit used in this thesis

In this thesis, the Molniya orbit was chosen because of the large variation in altitude. Both perturbing orbital forces and disturbing environmental torques acting on the satellite vary with altitude. As shown in Figure 1.3, the forces and torques strongest at the satellite's apogee are different than those forces and torques affecting the satellites motion when it is at perigee. At lower altitudes a satellite experiences a considerable more amount of drag due to the Earth's atmosphere. Also at low Earth orbit, a satellite is more affected by the Earth's oblateness, which is the increase in mass around the equatorial region. At higher altitudes, upwards of 10,000 kilometers, perturbing forces such as solar radiation pressure and gravitational attraction from the Moon affect the satellite's orbit. Since the forces influencing the orbit and attitude of the

satellite vary over just one period, the attitude determination system must take in to consideration more perturbing forces and torques than a satellite in an orbit where the attitude does not vary greatly.

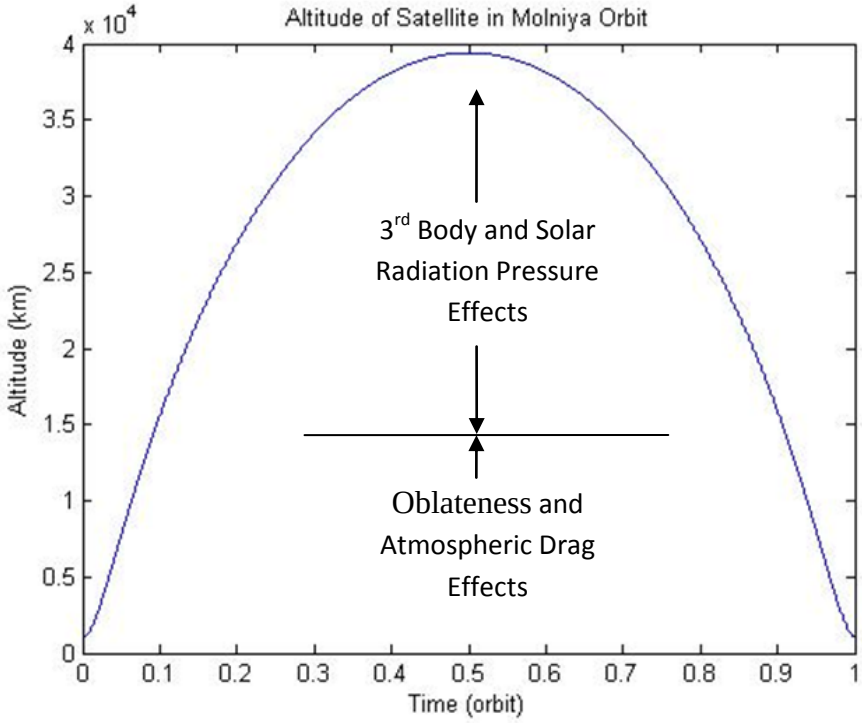

Figure 1.3: Altitude of Satellite in Molniya Orbit

The ground track of the Molniya orbit is seen in Figure 1.4. When the satellite is at apogee, above 30 degrees latitude, the satellite is traveling much slower than when it is at perigee, below -30 degrees latitude. In this thesis, the fictitious satellite ground station is in Sydney, Australia. Since the Earth rotates 180 degrees during each satellite orbit, the satellite only passes by this ground station every other orbit. Therefore a full day must go by before the satellite can pass over the ground station and collect orbit determining information. As discussed in Chapter 3, this makes orbit determining algorithms using site track measurements less accurate than algorithms with on-board sensors due to the limited time in which the satellite is getting measurement updates. Also, since the ground station in this thesis is located at the perigee of the satellite orbit, the number of measurements gathered and provided to the on-board Kalman filter is even more limited since the ground station is only in view for roughly an hour.

In this thesis a Kalman filter is used to determine the orbit and attitude of the satellite in a Molniya orbit. The algorithm requires an accurate model to predict the satellite orbit and attitude and then updates the predictions with input measurements from on board sensors or ground station communication. In Chapter 2, the general theory behind Kalman filters is explained. In

Chapter 3, the Kalman filter is applied to determine the satellite orbit by first propagating the two body equations of motion and then adding in perturbing forces due to the Earth's oblateness,

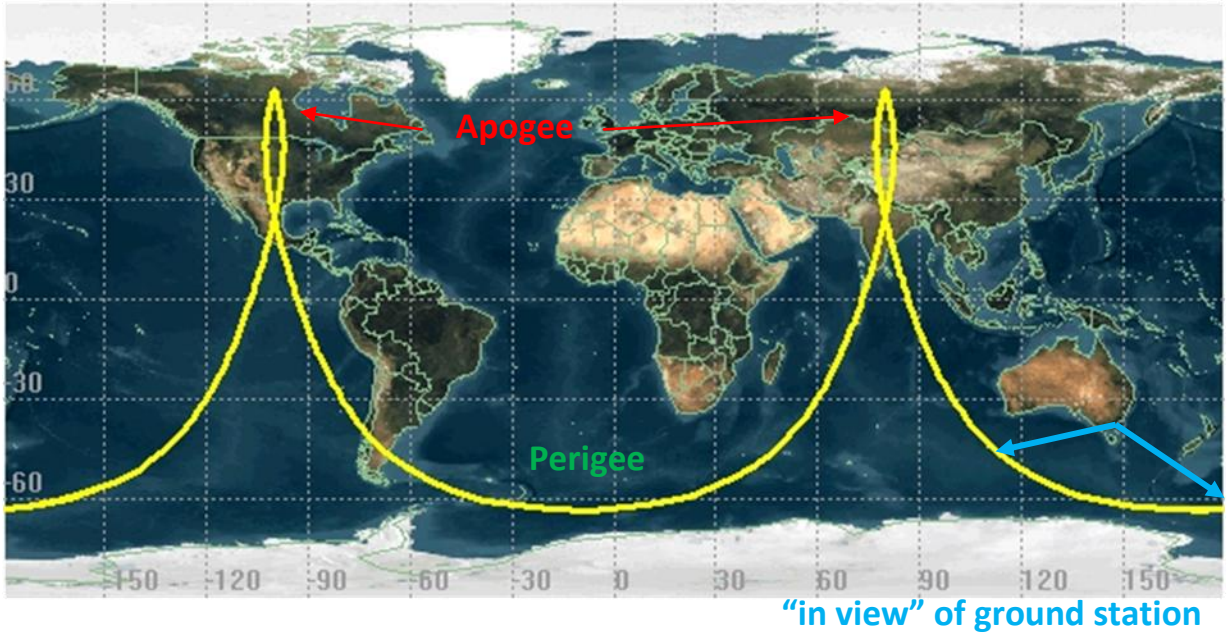

Figure 1.4: Molniya Orbit Ground Track

atmospheric drag, gravitational effect of the Moon and solar radiation pressure. Then two cases are studied, the first being the input measurements coming from the ground station using the pointing of the ground antenna tracking the satellite to provide the satellite with its range, azimuth and elevation. For this case the measurement input only occurs for a brief time once a day. The second case uses an on-board GPS receiver to update the filter with position measurements throughout the orbit.

Then in Chapter 4, the Kalman filter method is applied to determine the satellite attitude, taking in to consideration the disturbing torques a satellite experiences over the period of its orbit. Similar to the orbit determination, the satellites attitude is determined by propagating the rotational equations of motion and adding in the following disturbance torques: gravity gradient, aerodynamic drag, solar radiation pressure and magnetic torque. The attitude determining algorithm is then updated using measurements from one of four possible on-board sensors each with different error magnitudes. The sensors are: magnetometer, Earth sensor, a Sun sensor and star tracker.

Chapter 2

Fundamentals of Kalman Filters

The Kalman Filter, developed by Rudolf E. Kalman is a linear quadratic estimator that uses a series of measurements, which contain a level of noise and inaccuracies, over time to estimate a systems current state. The Kalman Filter has numerous applications and in this thesis the Kalman Filter will be used to estimate a satellite orbit and attitude using various types of measurement inputs. There are two main stages in the Kalman Filter algorithm, a "predict" stage and then a "correct" stage. In the prediction stage, the algorithm uses models, such as the equations of motion for an orbiting satellite, to predict the system's state over time along with the state's uncertainties. The "correct" phase occurs when a measurement is received. The algorithm updates the estimated state with the measurement data with a certain level of weighted average. The algorithm then begins the predict phase all over again. This recursive algorithm

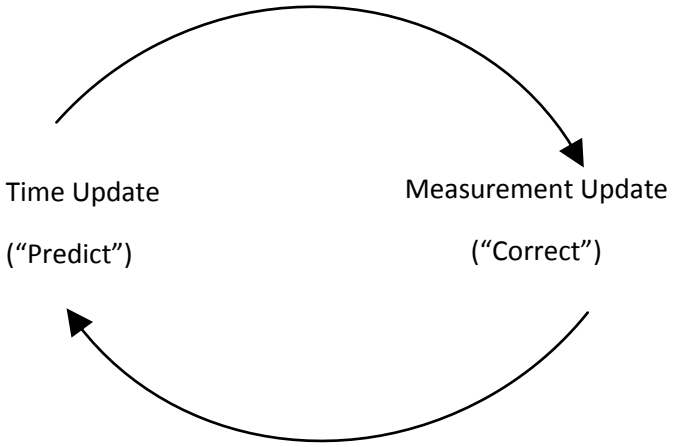

Figure 2.1: The two main steps in a Kalman Filter

allows for real time state calculation without requiring past data and measurements to be stored. Since only the current state and data from the next measurement are required, necessary data storage is minimal.

The Kalman filter uses measurements and the system's dynamic model to estimate the systems state over time. The dynamic model is a linear, time-varying, finite-dimensional state-space system defined as

$$\dot{x}(t) = F(t)x(t) + w$$

$$y(t) = H(t)x(t) + v$$

where $x(t)$ is the state vector, $F(t)$ is the state matrix and w is the process noise. $H(t)$ is the observation matrix, $y(t)$ is the output vector and v is the observation noise.

For this thesis, the Kalman filter is used to determine the orbit and attitude of the satellite. In the case of orbit determination, the state vector is made up of the satellite position and velocity relative to an inertial Earth centered reference frame and is: $x(t) = \lceil \mathrm{r_i}\ \mathrm{r_j}\ \mathrm{r_k}\ \mathrm{v_i}\ \mathrm{v_j}\ \mathrm{v_k} \rfloor^T$. For attitude determination, the state vector is made up of angles and rates of the satellite body frame with respect to its orbital frame: $x(t) = \lceil \theta_1\ \theta_2\ \theta_3\ \dot{\theta}_1\ \dot{\theta}_2\ \dot{\theta}_3 \rfloor^T$. These two cases will be explained further in Chapter 3 and 4. The next few sections explain three types of Kalman filters and their different elements.

2.1 Kalman Filter

The basic Kalman filter can be applied to systems with linear equations of motion. The Kalman Filter uses the state transition matrix,Φ, to propagate the state and its errors exactly since the equations of motion are linear. The inputs of the filter are the initial state, $\widehat{\boldsymbol{X}}_k$, initial state error, $\widehat{\boldsymbol{P}}_k$, the covariance of the process noise, $\boldsymbol{Q}$, the covariance of the observation noise, $\boldsymbol{R}$, and the measurements, z. The covariance of the process noise allows for measurement noise and enables the tuning of the filter. The process and observation noise is assumed to be zero mean Gaussian white noise.

The state transition matrix, Φ, is determined using a Taylor series to determine the state vector at a certain time t.

$$\bar{\bar{\boldsymbol{X}}}_{k+1} = \widehat{\boldsymbol{X}}_k + \dot{\widehat{\boldsymbol{X}}}_k \Delta t + \ddot{\widehat{\boldsymbol{X}}}_k \frac{\Delta t}{2!} + \cdots$$

Substituting in the dynamic model equation gives

$$\bar{\bar{\boldsymbol{X}}}_{k+1} = \hat{\boldsymbol{X}}_k + \boldsymbol{F}\hat{\boldsymbol{X}}_k \Delta t + \boldsymbol{F}^2 \hat{\boldsymbol{X}}_k \frac{\Delta t^2}{2!} + \cdots$$

Therefore,

$$\bar{\bar{\boldsymbol{X}}}_{k+1} = \boldsymbol{\Phi}\hat{\boldsymbol{X}}_k$$

where the state transition matrix is

$$\boldsymbol{\Phi} = \boldsymbol{I} + \boldsymbol{F}\Delta t + \boldsymbol{F}^2 \frac{\Delta t^2}{2!} + \cdots$$

The covariance matrix, **P**, of the predicted state vector is calculated from the previous covariance matrix, the state transition matrix and the covariance of the process noise

$$\bar{\bar{\boldsymbol{P}}}_{k+1} = \boldsymbol{\Phi}\hat{\boldsymbol{P}}_k\boldsymbol{\Phi}^{\mathrm{T}} + \mathbf{Q}$$

The algorithm computes the observation matrix, $H(t)$, once, at the beginning of the algorithm. For the orbit determining Kalman filter, the observation matrix is

$$\mathbf{H} = \frac{\partial \mathbf{z}}{\partial \mathbf{X}} = \begin{bmatrix} \frac{\partial \mathrm{r_i}}{\partial \mathrm{r_i}} & \frac{\partial \mathrm{r_i}}{\partial \mathrm{r_j}} & \frac{\partial \mathrm{r_i}}{\partial \mathrm{r_k}} & \frac{\partial \mathrm{r_i}}{\partial \mathrm{v_i}} & \frac{\partial \mathrm{r_i}}{\partial \mathrm{v_j}} & \frac{\partial \mathrm{r_i}}{\partial \mathrm{v_k}} \\ \frac{\partial \mathrm{r_j}}{\partial \mathrm{r_i}} & \frac{\partial \mathrm{r_j}}{\partial \mathrm{r_j}} & \frac{\partial \mathrm{r_j}}{\partial \mathrm{r_k}} & \frac{\partial \mathrm{r_j}}{\partial \mathrm{v_i}} & \frac{\partial \mathrm{r_j}}{\partial \mathrm{v_j}} & \frac{\partial \mathrm{r_j}}{\partial \mathrm{v_k}} \\ \frac{\partial \mathrm{r_k}}{\partial \mathrm{r_i}} & \frac{\partial \mathrm{r_k}}{\partial \mathrm{r_j}} & \frac{\partial \mathrm{r_k}}{\partial \mathrm{r_k}} & \frac{\partial \mathrm{r_k}}{\partial \mathrm{v_i}} & \frac{\partial \mathrm{r_k}}{\partial \mathrm{v_j}} & \frac{\partial \mathrm{r_k}}{\partial \mathrm{v_k}} \\ \frac{\partial \mathrm{v_i}}{\partial \mathrm{r_i}} & \frac{\partial \mathrm{v_i}}{\partial \mathrm{r_j}} & \frac{\partial \mathrm{v_i}}{\partial \mathrm{r_k}} & \frac{\partial \mathrm{v_i}}{\partial \mathrm{v_i}} & \frac{\partial \mathrm{v_i}}{\partial \mathrm{v_j}} & \frac{\partial \mathrm{v_i}}{\partial \mathrm{v_k}} \\ \frac{\partial \mathrm{v_j}}{\partial \mathrm{r_i}} & \frac{\partial \mathrm{v_j}}{\partial \mathrm{r_j}} & \frac{\partial \mathrm{v_j}}{\partial \mathrm{r_k}} & \frac{\partial \mathrm{v_j}}{\partial \mathrm{v_i}} & \frac{\partial \mathrm{v_j}}{\partial \mathrm{v_j}} & \frac{\partial \mathrm{v_j}}{\partial \mathrm{v_k}} \\ \frac{\partial \mathrm{v_k}}{\partial \mathrm{r_i}} & \frac{\partial \mathrm{v_k}}{\partial \mathrm{r_j}} & \frac{\partial \mathrm{v_k}}{\partial \mathrm{r_k}} & \frac{\partial \mathrm{v_k}}{\partial \mathrm{v_i}} & \frac{\partial \mathrm{v_k}}{\partial \mathrm{v_j}} & \frac{\partial \mathrm{v_k}}{\partial \mathrm{v_k}} \end{bmatrix}$$

The Kalman Filter can be "tuned" by adjusting the covariance of the process noise, $\boldsymbol{Q}$, and the covariance of the observation noise, $\boldsymbol{R}$. In this thesis, $\boldsymbol{Q}$ and $\boldsymbol{R}$ are taken to be diagonal and constant although this does not have to be the case. To tune the Kalman filter, an initial guess for each of the noise matrices is selected and the algorithm is run. Then the matrices can be changed in order to improve the results. For the case of orbit determination, the initial guess for the noise matrices are

$$\mathbf{Q} = \mathbf{R} = \begin{bmatrix} \sigma_{r_i}{}^2 & 0 & 0 & 0 & 0 & 0 \\ 0 & \sigma_{r_j}{}^2 & 0 & 0 & 0 & 0 \\ 0 & 0 & \sigma_{r_k}{}^2 & 0 & 0 & 0 \\ 0 & 0 & 0 & \sigma_{v_i}{}^2 & 0 & 0 \\ 0 & 0 & 0 & 0 & \sigma_{v_j}{}^2 & 0 \\ 0 & 0 & 0 & 0 & 0 & \sigma_{v_k}{}^2 \end{bmatrix}$$

where σ is the expected errors of each state.

Once the initial inputs are defined iterative process begins by propagating the state and error covariance over time. Once a measurement occurs, the predicted state and errors are corrected. The basic Kalman filter is summarized below.

Kalman Filter

Input $\{\widehat{\boldsymbol{X}}_k, \widehat{\boldsymbol{P}}_k, z, \boldsymbol{Q}, \boldsymbol{R}\}$

Output $\{\boldsymbol{X}_{k+1}, \boldsymbol{P}_{k+1}\}$

$\boldsymbol{\Phi}(\mathrm{t_{k+1}}, \mathrm{t_k}) = \dfrac{\partial \widehat{\boldsymbol{X}}_{k+1}}{\partial \widehat{\boldsymbol{X}}_k}$ State Transition matrix

$\mathbf{H}_{k+1} = \dfrac{\partial z}{\partial \overline{\overline{\boldsymbol{X}}}_{k+1}}$ Observation Matrix

Prediction

$\overline{\overline{\boldsymbol{X}}}_{k+1} = \boldsymbol{\Phi}\widehat{\boldsymbol{X}}_k$ Predicted State

$\overline{\overline{\boldsymbol{P}}}_{k+1} = \boldsymbol{\Phi}\widehat{\boldsymbol{P}}_k\boldsymbol{\Phi}^{\mathrm{T}} + \mathbf{Q}$ Predicted Error Covariance

Update

$\boldsymbol{K}_{k+1} = \overline{\overline{\boldsymbol{P}}}_{k+1}\boldsymbol{H}_{k+1}^T \left[\boldsymbol{H}_{k+1}\overline{\overline{\boldsymbol{P}}}_{k+1}\boldsymbol{H}_{k+1}^T + \boldsymbol{R}\right]^{-1}$ Kalman Gain

$\widehat{\boldsymbol{X}}_{k+1} = \overline{\overline{\boldsymbol{X}}}_{k+1} + \boldsymbol{K}_{k+1}\left[\mathbf{z} - \boldsymbol{H}_{k+1}\overline{\overline{\boldsymbol{X}}}_{k+1}\right]$ State Estimate

$\widehat{\boldsymbol{P}}_{k+1} = [I - \boldsymbol{K}_{k+1}\boldsymbol{H}_{k+1}]\,\overline{\overline{\boldsymbol{P}}}_{k+1}$ Error Covariance Estimate

A Kalman filter is optimal when the model used to determine the state matches the real system exactly and the variance of the noise is known exactly. In this thesis, neither the model nor the covariance is known exactly since the state model for an orbiting satellite can only be estimated. Also, in this thesis, the equations of motion are not linear and need to be linearized before applying the Kalman filter. This is done in the following section.

2.2 Kalman Filter for Linearized System

In a Kalman Filter the equations of motion that define the problem are used to develop the state matrix, $F(t)$,. In this thesis, the equations of motion need to be linearized in order to apply the Kalman filter. To do this, the partial derivatives of the equations of motion and perturbations are taken with respect to each element of the state vector. For orbit determination using only the two body equations of motion, the state matrix is

$$\mathbf{F}_{2-\text{body}} = \frac{\partial \dot{\mathbf{X}}}{\partial \mathbf{X}} = \begin{bmatrix} \frac{\partial v_i}{\partial r_i} & \frac{\partial v_i}{\partial r_j} & \frac{\partial v_i}{\partial r_k} & \frac{\partial v_i}{\partial v_i} & \frac{\partial v_i}{\partial v_j} & \frac{\partial v_i}{\partial v_k} \\ \frac{\partial v_j}{\partial r_i} & \frac{\partial v_j}{\partial r_j} & \frac{\partial v_j}{\partial r_k} & \frac{\partial v_j}{\partial v_i} & \frac{\partial v_j}{\partial v_j} & \frac{\partial v_j}{\partial v_k} \\ \frac{\partial v_k}{\partial r_i} & \frac{\partial v_k}{\partial r_j} & \frac{\partial v_k}{\partial r_k} & \frac{\partial v_k}{\partial v_i} & \frac{\partial v_k}{\partial v_j} & \frac{\partial v_k}{\partial v_k} \\ \frac{\partial a_i}{\partial r_i} & \frac{\partial a_i}{\partial r_j} & \frac{\partial a_i}{\partial r_k} & \frac{\partial a_i}{\partial v_i} & \frac{\partial a_i}{\partial v_j} & \frac{\partial a_i}{\partial v_k} \\ \frac{\partial a_j}{\partial r_i} & \frac{\partial a_j}{\partial r_j} & \frac{\partial a_j}{\partial r_k} & \frac{\partial a_j}{\partial v_i} & \frac{\partial a_j}{\partial v_j} & \frac{\partial a_j}{\partial v_k} \\ \frac{\partial a_k}{\partial r_i} & \frac{\partial a_k}{\partial r_j} & \frac{\partial a_k}{\partial r_k} & \frac{\partial a_k}{\partial v_i} & \frac{\partial a_k}{\partial v_j} & \frac{\partial a_k}{\partial v_k} \end{bmatrix}$$

$$= \begin{bmatrix} 0 & 0 & 0 & & & \\ 0 & 0 & 0 & & & \\ 0 & 0 & 0 & & & \\ -\frac{\mu}{r^3} + \frac{3\mu r_i^2}{r^5} & \frac{3\mu r_i r_j}{r^5} & \frac{3\mu r_i r_k}{r^5} & & & \\ \frac{3\mu r_i r_j}{r^5} & -\frac{\mu}{r^3} + \frac{3\mu r_j^2}{r^5} & \frac{3\mu r_j r_k}{r^5} & & & \\ \frac{3\mu r_i r_k}{r^5} & \frac{3\mu r_j r_k}{r^5} & -\frac{\mu}{r^3} + \frac{3\mu r_k^2}{r^5} & & & \end{bmatrix} \begin{matrix} 1 & 0 & 0 \\ 0 & 1 & 0 \\ 0 & 0 & 1 \\ & & \\ 0 & 0 & 0 \\ 0 & 0 & 0 \\ 0 & 0 & 0 \end{matrix}$$

As will be shown in later chapters, much of the Kalman filter development is in determining this state matrix since each perturbing force and torque affects the final state matrix. The state transition matrix is calculated once, at the beginning of the algorithm and includes all the perturbing forces needed to best estimate the state. This algorithm is summarized below.

Kalman Filter – Linearized System

Input $\{\widehat{\boldsymbol{X}}_k, \widehat{\boldsymbol{P}}_k, z, \boldsymbol{Q}, \boldsymbol{R}\}$

Output $\{\boldsymbol{X}_{k+1}, \boldsymbol{P}_{k+1}\}$

$\boldsymbol{F} = \frac{\partial \dot{\boldsymbol{X}}_{t_o}}{\partial \boldsymbol{X}_{t_o}}$ *found one time*

$\boldsymbol{\Phi} = \boldsymbol{I} + \boldsymbol{F}\Delta t + \boldsymbol{F}^2 \frac{\Delta t}{2!}$

$\mathbf{H}_{k+1} = \frac{\partial z}{\partial \hat{\boldsymbol{X}}_{k+1}}$

Prediction

$\bar{\boldsymbol{X}}_{k+1}$ *predicted with Cowell's Method* — Predicted State

$\delta \bar{x}_{k+1} = \boldsymbol{\Phi} \delta \hat{x}_k$ — Predicted State Update

$\bar{\boldsymbol{P}}_{k+1} = \boldsymbol{\Phi} \widehat{\boldsymbol{P}}_k \boldsymbol{\Phi}^{\mathrm{T}} + \mathbf{Q}$ — Predicted Error Covariance

Update

$\tilde{b} = z - \boldsymbol{H}_{k+1} \bar{\boldsymbol{X}}_{k+1}$

$\boldsymbol{K}_{k+1} = \bar{\boldsymbol{P}}_{k+1} \boldsymbol{H}_{k+1}^T \left[\boldsymbol{H}_{k+1} \bar{\boldsymbol{P}}_{k+1} \boldsymbol{H}_{k+1}^T + \boldsymbol{R}\right]^{-1}$ — Kalman Gain

$\delta \hat{x}_{k+1} = \delta \bar{x}_{k+1} + \boldsymbol{K}_{k+1}\left[\tilde{b}_{k+1} - \boldsymbol{H}_{k+1} \delta \bar{x}_{k+1}\right]$ — State Update Estimate

$\widehat{\boldsymbol{X}}_{k+1} = \bar{\bar{\boldsymbol{X}}}_{k+1} + \delta \hat{x}_{k+1}$ — State Estimate

$\widehat{\boldsymbol{P}}_{k+1} = [I - \boldsymbol{K}_{k+1} \boldsymbol{H}_{k+1}]\, \bar{\bar{\boldsymbol{P}}}_{k+1}$ — Error Covariance Estimate

2.3 Extended Kalman Filter

The Kalman filter used in this thesis is the Extended Kalman Filter (EKF). The difference between the basic Kalman filter and the Extended Kalman filter is that the state transition matrix is calculated at every time step rather than at just the beginning of the algorithm. This is required since the perturbing forces that make up the state matrix change with respect to the satellite position in the orbit and therefore with time. So at every time step, the satellite position must be used to recalculate the state matrix and state transition matrix. This is computationally expensive but decreases the errors in the orbit determining algorithm. The summary of the EKF is seen below.

Extended Kalman Filter

Input $\{\widehat{\boldsymbol{X}}_k, \widehat{\boldsymbol{P}}_k, z, \boldsymbol{Q}, \boldsymbol{R}\}$

Output $\{\boldsymbol{X}_{k+1}, \boldsymbol{P}_{k+1}\}$

$$\mathbf{H}_{k+1} = \frac{\partial z}{\partial \widehat{\boldsymbol{X}}_{k+1}}$$

Prediction

$\overline{\boldsymbol{X}}_{k+1}$ *predicted with Cowell's Method* — Predicted State

$$\boldsymbol{F} = \frac{\partial \dot{\boldsymbol{X}}_{k+1}}{\partial \boldsymbol{X}_{k+1}}$$

$$\dot{\boldsymbol{\Phi}} = \boldsymbol{F}(t)\boldsymbol{\Phi}$$

$\delta \bar{x}_{k+1} = 0$ — Predicted State Update

$\overline{\boldsymbol{P}}_{k+1} = \boldsymbol{\Phi}\widehat{\boldsymbol{P}}_k\boldsymbol{\Phi}^{\mathrm{T}} + \mathbf{Q}$ — Predicted Error Covariance

Update

$$\tilde{b} = z - \boldsymbol{H}_{k+1}\overline{\boldsymbol{X}}_{k+1}$$

$\boldsymbol{K}_{k+1} = \overline{\boldsymbol{P}}_{k+1}\boldsymbol{H}_{k+1}^{T}\,[\boldsymbol{H}_{k+1}\overline{\boldsymbol{P}}_{k+1}\boldsymbol{H}_{k+1}^{T} + \boldsymbol{R}]^{-1}$ — Kalman Gain

$\delta \hat{x}_{k+1} = \boldsymbol{K}_{k+1}\tilde{b}_{k+1}$ — State Update Estimate

$\widehat{\boldsymbol{X}}_{k+1} = \overline{\overline{\boldsymbol{X}}}_{k+1} + \delta \hat{x}_{k+1}$ — State Estimate

$\widehat{\boldsymbol{P}}_{k+1} = [I - \boldsymbol{K}_{k+1}\boldsymbol{H}_{k+1}]\,\overline{\overline{\boldsymbol{P}}}_{k+1}$ — Error Covariance Estimate

Figure 2.2 shows how, at each time step, the state and errors are propagated from $\hat{X}_0, \hat{P}_0$ to $\bar{X}_1, \bar{P}_1$ and then the state and errors are updated when a measurement is observed, resulting in $\hat{X}_1, \hat{P}_1$.

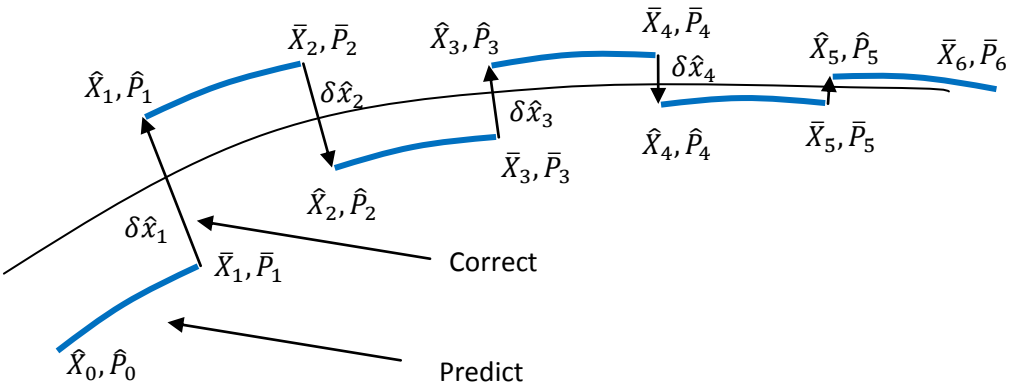

Figure 2.2: Extend Kalman Filter Representation

Chapter 3 will explain how the Kalman filter is applied in order to determine the position of the satellite in its orbit. The derivation of the state matrix is the lengthiest step in the process; requiring the development for individual state matrices for each perturbing force and then summing them in order to get the final state matrix. Then two cases are analyzed, the first provides the filter with a group of measurements once a day in the form of the satellite's range, azimuth and elevation from a ground station. The second case predicts the orbit using position and velocity measurements from an onboard GPS sensor throughout the duration of the orbit.

Similarly, Chapter 4 will estimate the satellite attitude by applying the Kalman filter algorithm. Once again, the development of the state matrix will require the most work seeing as how each disturbing torque influences the matrix. Then four cases are studied pertaining to the four types of on-board attitude sensors.

Chapter 3

Orbit Determination

In order for a satellite to perform the mission it was designed for, it must accurately determine its location in space. Knowledge of the satellite location, called orbit determination, is used by ground stations to command the satellite, maintain the orbit from degradation or to maneuver the satellite to a desired location. The position of a satellite is used for station keeping maneuvers, mission planning and even collision avoidance. Although space is a vast place, the accurate knowledge of the location of each satellite is essential to prevent intergalactic space collisions. Having an accurate on-board orbit determining system allows a satellite and its ground station to accurately plan missions and the necessary maneuvers that mission drives.

In this chapter, the fundamentals of orbit determination will be explain as well as the derivation of the orbit determining Kalman filter used in this thesis. To increase the level of accuracy of the Kalman filter, multiple orbit perturbing forces are added to the algorithm, making the Kalman filter derivation a lengthy but necessary process. First off, the fundamentals of orbit determination will be explained. Then, the Kalman filter will be developed in order to accurately determine the satellite orbit using two cases, site track measurements and GPS sensor measurements.

3.1 Defining a Satellite Orbit

To define an orbit, an inertial reference frame must be developed such that, at any location, the satellite's position and velocity can be described. An inertial reference frame is a set of three mutually perpendicular vectors whose origin remains fixed with respect to space. Therefore the inertial reference frame is one that is not accelerating. However, there is no truly inertial location in space since all points in space are accelerating. Therefore, for any given problem, a reference

frame that is as close to inertial as possible must be selected. In the case of a satellite orbiting the Earth, an Earth centered reference frame is inertial enough since the motion of the Earth throughout space need not be considered. The reference frames that will be used in this thesis are explained below.

3.1.1 Reference Frames

First, the Earth Centered Inertial reference frame, or ECI frame, is a reference frame with its origin at the center of the Earth. As shown in Figure 3.1, the I-axis points in the direction of Earth's vernal equinox, the K-axis points towards the North Pole and the J-axis completes the triad and lies within the equatorial plane. The satellite's position can then be defined as the vector, $\vec{r}$, in this ECI frame.

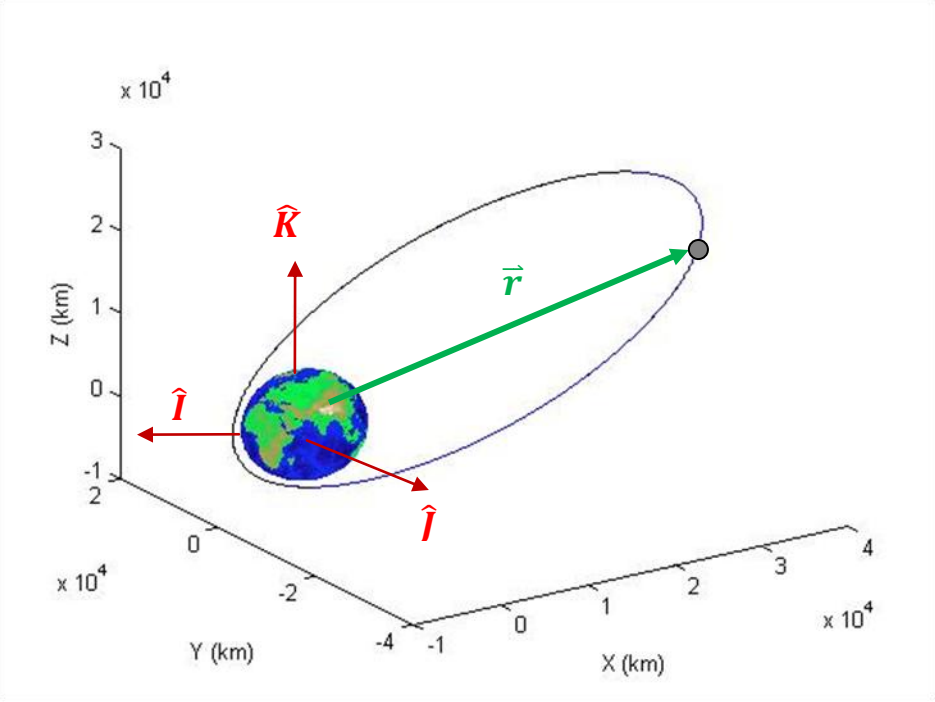

Figure 3.1: Earth Centered Reference Frame

The ECI frame remains relatively fixed over time, therefore the Earth rotates about the K axis of the ECI frame. Another reference frame needs to be defined that remains fixed with the Earth and therefore rotates along with the Earth. This reference frame is appropriately called the Earth Centered Earth Fixed reference frame, or ECEF. This frame is similar to the ECI frame however the $\hat{I}_{local}$ points towards the location of the prime meridian, or 0 degrees longitude.

Later on in this chapter, another reference frame will be needed to determine the satellite's position. This reference frame determines the satellite's position as it relates to a point on the surface of the Earth, such as a ground station. The reference frame is called the Topocentric

Horizon Coordinate System. It is commonly called SEZ since the vectors that make up the coordinate system point due south and due east from the ground station as well as directly out, or zenith, from the ground station. Figure 3.2 shows how the SEZ frame relates to the ECEF and ECI frame.

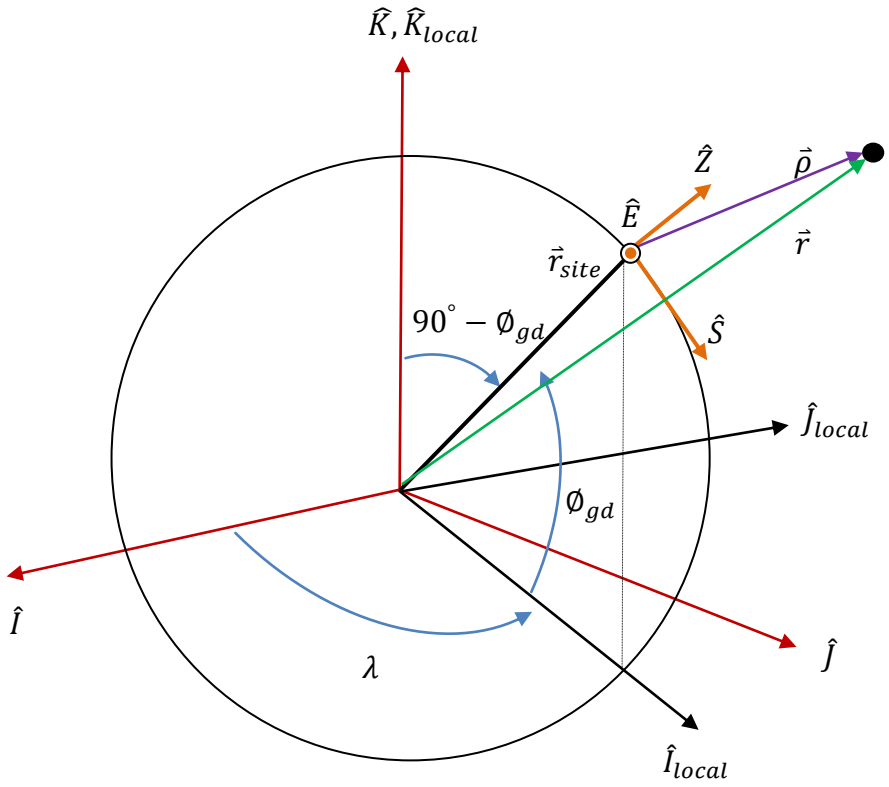

Figure 3.2: ECI, ECEF and SEZ Reference Frames

A satellite's position can be described in the SEZ frame by three parameters: range, azimuth, and elevation. The range of a satellite, ρ_{SEZ}, is the distance from the satellite to the ground station. The azimuth of the satellite, β, is the angle measured from the north, clockwise to the location beneath the satellite. The elevation of the satellite, el, is the angle to the satellite measured from the horizon. These three parameters can be determined from a ground antenna pointing toward the satellite and will be used as the site track measurements in one of the Kalman filter cases. In order to determine the satellite location in the ECI frame, using parameters defined in the SEZ frame, coordinate transformations must occur. A coordinate transformation takes in to account the rotations required to transform the ECI frame in to the SEZ frame. Then, any vector in the SEZ frame can be transformed back in to the ECI frame and used to define the satellite in the ECI frame. This process is called the transformation of reference frames and is explained in the next section.

3.1.2 Transformation between Reference Frames

In order to define a satellites position in the ECI frame using measurements in the SEZ frame, the measurements must be transformed into the ECI frame. In order to transform vector components from one reference frame to another, the vector is multiplied by a rotation matrix. For example, if a vector $\vec{e} = [e_a \; e_b \; e_c]^T$ needed to be transformed from an *a,b,c* frame to a *u,v,w* frame it would need to be multiplied by a rotation matrix R^{ua}.

$$\vec{e}_{uvw} = \begin{bmatrix} u_1 & u_2 & u_3 \\ v_1 & v_2 & v_3 \\ w_1 & w_2 & w_3 \end{bmatrix} \begin{bmatrix} e_a \\ e_b \\ e_c \end{bmatrix} = R^{ua}\vec{e}_{abc}$$

The rotation matrices used to transform the vectors come in one of three forms depending on which of the three axes the rotation is about.

$$R_1(\theta) = \begin{bmatrix} 1 & 0 & 0 \\ 0 & \cos\theta & -\sin\theta \\ 0 & \sin\theta & \cos\theta \end{bmatrix} \quad R_2(\theta) = \begin{bmatrix} \cos\theta & 0 & \sin\theta \\ 0 & 1 & 0 \\ -\sin\theta & 0 & \cos\theta \end{bmatrix} \quad R_3(\theta) = \begin{bmatrix} \cos\theta & -\sin\theta & 0 \\ \sin\theta & \cos\theta & 0 \\ 0 & 0 & 1 \end{bmatrix}$$

Then the final rotation matrix can be developed my multiplying each of the individual rotation matrices needed to complete the rotation. For example, the final rotation matrix for a rotation about the third, first, then second axes is

$$R_{312} = \quad R_2 R_1 R_3$$

To transform a vector in the SEZ frame to the ECI frame, it must first be rotated counter clockwise about the E-axis in order to align the Z-axis with the K-axis. This is done by using a 2-rotation by the negative of $90 - \emptyset_{gd}$.

$$R_2\left(\emptyset_{gd} - 90\right) = \begin{bmatrix} \cos(\emptyset_{gd} - 90) & 0 & \sin(\emptyset_{gd} - 90) \\ 0 & 1 & 0 \\ -\sin(\emptyset_{gd} - 90) & 0 & \cos(\emptyset_{gd} - 90) \end{bmatrix} = \begin{bmatrix} \sin\left(\emptyset_{gd}\right) & 0 & \cos\left(\emptyset_{gd}\right) \\ 0 & 1 & 0 \\ -\cos\left(\emptyset_{gd}\right) & 0 & \sin\left(\emptyset_{gd}\right) \end{bmatrix}$$

Another rotation is required to rotate the S-axis, which is now the $\hat{I}_{local}$ axis, to the I-axis. This is done by rotating counterclockwise about the K-axis by the angle, λ, which requires the R_3 rotation matrix.

$$R_3(-\lambda) = \begin{bmatrix} \cos(-\lambda) & -\sin(-\lambda) & 0 \\ \sin(-\lambda) & \cos(-\lambda) & 0 \\ 0 & 0 & 1 \end{bmatrix}$$

So the final rotation comes out to

$$\vec{\rho}_{ECI} = R_3(-\lambda)R_2(\emptyset_{gd} - 90)\vec{\rho}_{SEZ} = \begin{bmatrix} \sin(\emptyset_{gd})\cos(\lambda) & -\sin(\lambda) & \cos(\emptyset_{gd})\cos(\lambda) \\ \sin(\emptyset_{gd})\sin(\lambda) & \cos(\lambda) & \cos(\emptyset_{gd})\sin(\lambda) \\ -\cos(\emptyset_{gd}) & 0 & \sin(\emptyset_{gd}) \end{bmatrix} \vec{\rho}_{SEZ}$$

The last step in transforming position vector in the SEZ frame to the ECEF frame is just the translation of the origin from a point on the surface of the Earth to the center of the Earth. This is done using basic addition

$$\vec{r}_{ECI} = \vec{\rho}_{ECI} + \vec{r}_{site\ ECI}$$

This transformation will be used when measurements of range, azimuth and elevation of a satellite from the ground station are inputted in to the Kalman filter that is estimating the position of the satellite in terms of the ECI frame.

3.1.3 Orbital Elements

Another important way to describe a satellite orbit is using orbital elements. In this thesis, the effects of the perturbing forces that influence a satellite orbit will be described in orbital elements; therefore a brief overview of these elements is given here.

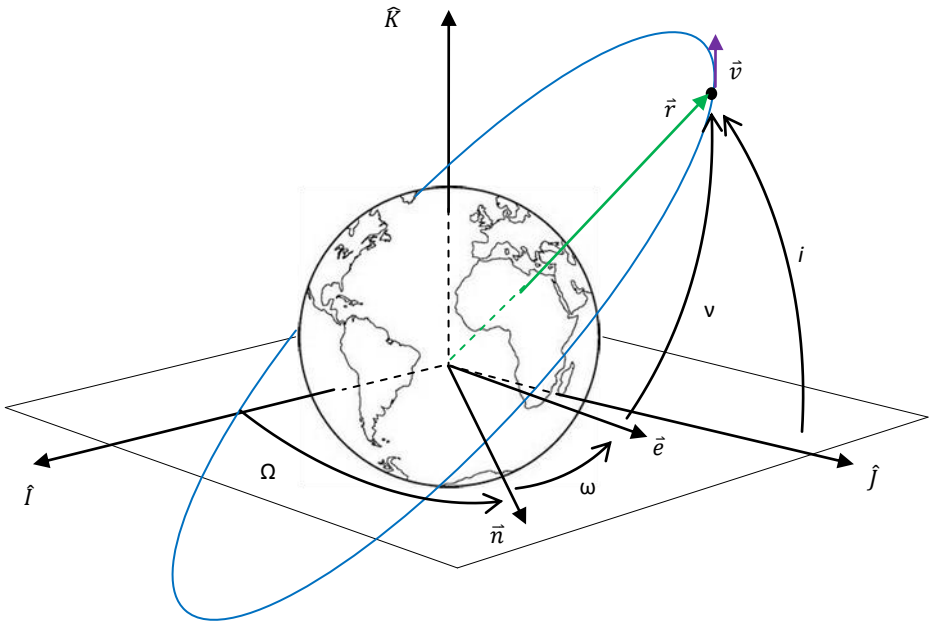

Figure 3.3: Depiction of Orbital Elements

The orbital elements describe the location of the satellite at any given time. Figure 3.3 depicts the orbit of the satellite as an ellipse that is inclined with respect to the Earth's equator. The first of the orbital elements is the semimajor axis of this ellipse, *a*. The eccentricity of this ellipse is the second of the orbital elements, *e*. The third orbital element is the inclination of the ellipse with respect to the Earth's equatorial plane and is denoted, *i*. The right ascension of the ascending nodes, Ω, is the angle from the I-axis to the ascending node, $\vec{n}$, which is the vector pointing from the center of the Earth to the point where the orbit crosses the equatorial plane going from south to north. The argument of perigee, ω, is the angle between the ascending node, $\vec{n}$, and the location of the orbit's perigee, or closest approach, denoted, $\vec{e}$. Last, the true anomaly, *v*, is the angle between the satellite's current position in the orbit with respect to $\vec{e}$. These orbital elements are all that are needed to find the position and velocity of the satellite in the ECI frame. Next, the laws that govern the motion of a satellite orbiting Earth are explained.

3.2 Laws Governing a Satellite Orbit

Kepler's and Newton's Laws, which were first developed to describe the motion of planets about the sun, are essential to determine a satellite orbit. These laws can be applied to any two body problem, where one body orbits another due to gravitational forces, such as a satellite about the Earth.

3.2.1 Kepler's Laws

Kepler's laws are as follows:

1. The orbit of each planet is an ellipse with the Sun at one focus.
2. The line joining the planet to the Sun sweeps out equal areas in equal times.
3. The square of the period of a planet is proportional to the cube of its mean distance to the Sun

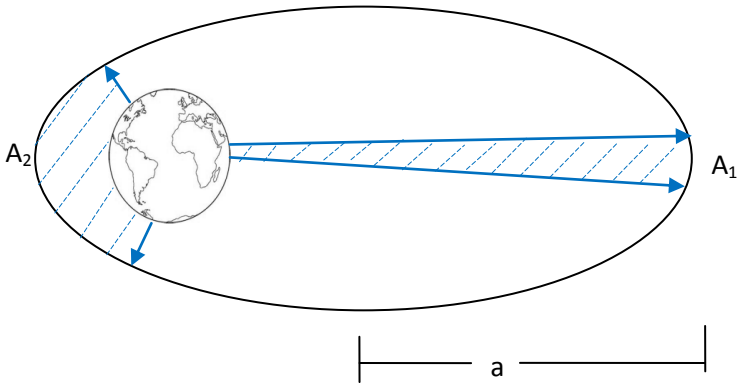

Figure 3.4: Illustration of Kepler's 2nd law

Figure 3.4 illustrates Kepler's second law, showing that a satellite will trace out equal areas of an ellipse in equal times. In order to trace out equal areas in equal times, the satellite travels much faster when close to the Earth, at perigee, then when it is at apogee, furthest from the Earth. Later, it will be shown that this increased speed causes increased errors in the orbit determining Kalman filter.

3.2.2 Newton's Laws

Newton's second law and his law of gravitation are also essential to predicting a satellite orbit. Newton's second law states that the sum of all forces acting on a body, *F*, is equal to the mass of that body, m, times the body's acceleration, *a*. Therefore,

$$\sum \vec{F} = m\vec{a}$$

Newton's law of gravitation applies his second law to the gravitational forces between two bodies. Therefore the gravitational force of the Earth, acting on a satellite is

$$\vec{F} = -\frac{Gm_{Earth}m_{sat}}{r^3}\vec{r}$$

where G is the gravitational constant. With this equation, the acceleration of a satellite can be determined from just the satellite's position relative to the body in which it orbits.

3.2.3 Assumptions of the Two Body Problem

There are four key assumptions of the two body problem and they are

1. The mass of the satellite is negligible when compared to the mass of the attracting body, in this case, the Earth
2. The coordinate system used to define the motion is inertial
3. The bodies of the satellite and Earth are spherically symmetric
4. No other forces act on the system except for the gravitational forces of the attracting body

For this thesis, assumption 1 holds; the satellite's mass is negligible when compared to the mass of the Earth. Also, assumption 2 holds loosely; the ECI frame is determined to be inertial enough for this two-body problem. The motion of the Earth through space is neglected. However, in this thesis, both Assumption 3 and 4 do not hold, resulting in perturbation forces and disturbing torques on the satellite. Assumption 3 does not hold, since neither the Earth nor the satellite is a perfect sphere. The Earth has more mass about the equatorial region than at the poles; therefore the gravitational force on the satellite varies between the equatorial plane and poles. Also, the satellite is not a sphere, but rather a cylindrical shape with extending solar panels. This non-spherical shape means the force from Earth's gravity varies from point to point along the satellite

body. Assumption 4 does not hold since there are additional external forces such as drag from the Earth's atmosphere acting on the satellite. These variations to the two-body problem will be discussed further throughout this thesis.

3.3 Predicting the Satellite Orbit using the Two Body Problem

In this thesis, the satellite orbit is propagated using the laws explained above and a numerical integration method called Cowell's Formulation, explained below.

3.3.1 Cowell's Formulation

From Newton, the acceleration of a satellite in the two body problem can be described by the following equation

$$\vec{\mathbf{a}} = -\frac{\mu\vec{\mathbf{r}}}{\mathrm{r}^3}$$

where $\mu = \mathrm{Gm}_{\mathrm{Earth}}$. However the two-body problem neglects the real-world perturbation effects such as atmospheric drag and the Earth's oblateness. These perturbations, which will be discussed in detail in the following sections, create an additional acceleration that acts on the satellite. This acceleration can be added to the two-body acceleration and numerically integrated to find a more accurate satellite orbit.

$$\vec{\mathbf{a}} = -\frac{\mu\vec{\mathbf{r}}}{\mathrm{r}^3} + \vec{\mathbf{a}}_{\mathrm{perturbed}}$$

Cowell's Formulation numerically integrates the second order differential equations of motion. To use this method a state vector is developed such as the one below for orbit determination.

$$x = \begin{bmatrix} x_1 \\ x_2 \\ x_3 \\ x_4 \\ x_5 \\ x_6 \end{bmatrix} = \begin{bmatrix} r_i \\ r_j \\ r_k \\ v_i \\ v_j \\ v_k \end{bmatrix}$$

Then the derivative of the state vector is

$$\dot{x} = \begin{bmatrix} v_i \\ v_j \\ v_k \\ a_i \\ a_j \\ a_k \end{bmatrix} = \begin{bmatrix} v_i \\ v_j \\ v_k \\ -\frac{\mu r_i}{r^3} + a_{i_{perturbed}} \\ -\frac{\mu r_j}{r^3} + a_{j_{perturbed}} \\ -\frac{\mu r_k}{r^3} + a_{k_{perturbed}} \end{bmatrix} = \begin{bmatrix} x_4 \\ x_6 \\ x_6 \\ -\frac{\mu x_1}{r^3} + a_{i_{perturbed}} \\ -\frac{\mu x_2}{r^3} + a_{j_{perturbed}} \\ -\frac{\mu x_3}{r^3} + a_{k_{perturbed}} \end{bmatrix}$$

Cowell's method uses numerical integration to integrate the derivative of the state vector to determine the state vector over time. In this thesis, Matlab's numerical integration function *ode45* is used to numerically integrate $\dot{X}$ over time using a fixed time step.

3.4 Perturbations of the Satellite Orbit

This section is devoted to finding the acceleration of the satellite due perturbing forces, $\vec{\mathbf{a}}_{\text{perturbed}}$. Four perturbing forces will be added to the two-body problem, explained in previous sections, in order to increase the accuracy of the satellite orbit determination algorithm. These four perturbing forces are: Earth's oblateness, Earth's atmospheric drag, the Moon's gravitational force, and the pressure due to solar radiation. The first two perturbing forces, Earth's oblateness and atmospheric drag, affect the orbit of a satellite while it is relatively close to the Earth (~1000 km altitude). Their affects diminish with increased altitude. While the oblateness and atmospheric drag diminish with altitude, the effects of Moon's gravity and the pressure from solar radiation increase with altitude. Since this particular satellite is in a highly elliptical orbit it experiences both the perturbing forces that are strongest at low altitudes as well as the perturbing forces that are stronger at higher altitudes. Therefore the accelerations due to all four of these perturbing forces are added to the general two-body acceleration.

$$\vec{\mathbf{a}}_{\text{perturbed}} = \vec{\mathbf{a}}_{\text{spherical}} + \vec{\mathbf{a}}_{\text{drag}} + \vec{\mathbf{a}}_{\text{3rdbody}} + \vec{\mathbf{a}}_{\text{SR}}$$

3.4.1 Earth's Oblateness

As was explained in Section 3.2.3 one of the assumptions of the two body problem is that the satellite and the Earth are symmetrically spherical. The fact that the satellite is not spherically symmetric will cause aerodynamic disturbing torques that will be discussed in Chapter 4. The fact that the Earth is not spherically symmetric is addressed here. The oblateness of the Earth refers to the increase in mass around the Earth's equatorial region. This increased mass around the equator creates its own gravitational force on the satellite.

The perturbing acceleration due to the Earth's oblateness is derived from the aspherical potential function

$$U = \frac{\mu}{r}\left[1 + \sum_{l=2}^{\infty}\sum_{m=0}^{l}\left(\frac{R_\oplus}{r}\right)^l P_{l,m}[\sin(\phi_{gc_{sat}})]\{C_{l,m}\cos(m\lambda_{sat}) + S_{l,m}\sin(m\lambda_{sat})\}\right]$$

where $R_\oplus$ is the radius of the Earth, $\phi_{gc_{sat}}$ and λ_{sat} are the latitude and longitude of the sub-satellite point on the Earth, and $P_{l,m}$ is the associated Legendre functions.

The acceleration due to the Earth's oblateness is then found by taking the gradient of the aspherical potential function in spherical coordinates with respect to $\vec{r}_{ECI}$, using the chain rule.

$$\vec{a} = \frac{\partial U}{\partial r}\frac{\partial r}{\partial \vec{r}} + \frac{\partial U}{\partial \lambda}\frac{\partial \lambda}{\partial \vec{r}} + \frac{\partial U}{\partial \phi_{gc}}\frac{\partial \phi_{gc}}{\partial \vec{r}}$$

This then gives the final acceleration in the ECI frame as

$$a_i = \left\{\frac{1}{r}\frac{\partial U}{\partial r} - \frac{r_k}{r^2\sqrt{r_i^2 + r_j^2}}\frac{\partial U}{\partial \phi_{gc_{sat}}}\right\}r_i - \left\{\frac{1}{r_i^2 + r_j^2}\frac{\partial U}{\partial \lambda_{sat}}\right\}r_j$$

$$a_j = \left\{\frac{1}{r}\frac{\partial U}{\partial r} - \frac{r_k}{r^2\sqrt{r_i^2 + r_j^2}}\frac{\partial U}{\partial \phi_{gc_{sat}}}\right\}r_j + \left\{\frac{1}{r_i^2 + r_j^2}\frac{\partial U}{\partial \lambda_{sat}}\right\}r_i$$

$$a_k = \frac{1}{r}\frac{\partial U}{\partial r}r_k + \frac{\sqrt{r_i^2 + r_j^2}}{r^2}\frac{\partial U}{\partial \phi_{gc_{sat}}}$$

where

$$\frac{\partial U}{\partial r} = -\frac{\mu}{r}\sum_{l=2}^{\infty}\sum_{m=0}^{l}\left(\frac{R_\oplus}{r}\right)^l (l+1)P_{l,m}[\sin(\phi_{gc_{sat}})]\{C_{l,m}\cos(m\lambda_{sat}) + S_{l,m}\sin(m\lambda_{sat})\}$$

$$\frac{\partial U}{\partial \phi_{gc}} = \frac{\mu}{r}\sum_{l=2}^{\infty}\sum_{m=0}^{l}\left(\frac{R_\oplus}{r}\right)^l \left\{P_{l,m+1}\left[\sin(\phi_{gc_{sat}})\right] - m\tan(\phi_{gc_{sat}})P_{l,m}\left[\sin(\phi_{gc})\right]\right\} \times \{C_{l,m}\cos(m\lambda_{sat}) + S_{l,m}\sin(m\lambda_{sat})\}$$

$$\frac{\partial U}{\partial \lambda} = \frac{\mu}{r}\sum_{l=2}^{\infty}\sum_{m=0}^{l}\left(\frac{R_\oplus}{r}\right)^l mP_{l,m}\left[\sin(\phi_{gc_{sat}})\right]\{S_{l,m}\cos(m\lambda_{sat}) - C_{l,m}\sin(m\lambda_{sat})\}$$

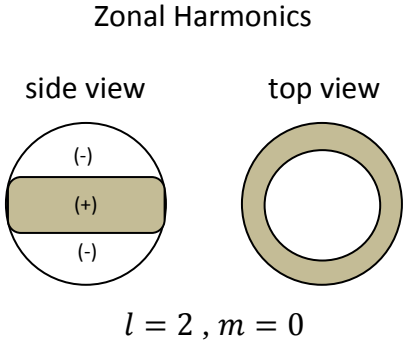

Figure 3.5: Zonal Harmonic used in this Thesis

For the second order zonal harmonics, as shown in Figure 3.5, l=2 and m=0. The zonal gravitational coefficient becomes $C_{l,m} = C_{2,0} = -0.0010826269$ and the sectorial harmonic becomes $S_{l,m} = S_{2,0} = 0$. For this case, the associated Legendre functions are

$$P_{2,0}\left[\sin\left(\phi_{gc_{sat}}\right)\right] = \frac{1}{2}\{3\sin^2\left(\phi_{gc_{sat}}\right) - 1\}$$

$$P_{2,1}\left[\sin(\phi_{gc_{sat}})\right] = 3\sin\left(\phi_{gc_{sat}}\right)\cos\left(\phi_{gc_{sat}}\right)$$

The partial derivatives become

$$\frac{\partial U}{\partial r} = -\frac{3}{2}\frac{\mu {R_\oplus}^2 C_{2,0}}{r^3}\{3\sin^2\left(\phi_{gc_{sat}}\right) - 1\}$$

$$\frac{\partial U}{\partial \phi_{gc}} = 3\frac{\mu {R_\oplus}^2 C_{2,0}}{r^3}\sin\left(\phi_{gc_{sat}}\right)\cos\left(\phi_{gc_{sat}}\right)$$

$$\frac{\partial U}{\partial \lambda} = 0$$

Therefore the final acceleration due to perturbations from Earth's oblateness for second order zonal harmonics is

$$a_i = \left\{[-\frac{3}{2}\frac{\mu {R_\oplus}^2 C_{2,0}}{r^4}\{3\sin^2\left(\phi_{gc_{sat}}\right) - 1\}] - \frac{r_k}{r^2\sqrt{r_i^2 + r_j^2}}[3\frac{\mu {R_\oplus}^2 C_{2,0}}{r^3}\sin\left(\phi_{gc_{sat}}\right)\cos\left(\phi_{gc_{sat}}\right)]\right\} r_i$$

$$a_j = \left\{[-\frac{3}{2}\frac{\mu {R_\oplus}^2 C_{2,0}}{r^4}\{3\sin^2\left(\phi_{gc_{sat}}\right) - 1\}] - \frac{r_k}{r^2\sqrt{r_i^2 + r_j^2}}[3\frac{\mu {R_\oplus}^2 C_{2,0}}{r^3}\sin\left(\phi_{gc_{sat}}\right)\cos\left(\phi_{gc_{sat}}\right)]\right\} r_j$$

$$a_k = [-\frac{3}{2}\frac{\mu {R_\oplus}^2 C_{2,0}}{r^4}\{3\sin^2\left(\phi_{gc_{sat}}\right) - 1\}]r_k + \frac{\sqrt{r_i^2 + r_j^2}}{r^2}\,3\frac{\mu {R_\oplus}^2 C_{2,0}}{r^3}\sin\left(\phi_{gc_{sat}}\right)\cos\left(\phi_{gc_{sat}}\right)$$

This process can be repeated for sectorial and tesseral harmonics until the level of accuracy of the acceleration due to Earth's oblateness is reached. In this thesis, only the perturbation from second order zonal harmonics is considered since it is almost 1000 times larger than perturbations from the third order harmonics.

The Earth's oblateness affects a satellite orbit since the gravitational pull of the bulge creates secular variations in the argument of perigee and right accession of the ascending node. Since the bulge around the equator pulls the satellite toward the equatorial plane, the satellite will reach the line of nodes, $\vec{n}$, more quickly than it would for a spherically symmetric Earth. This creates a "spinning top" like precession in the satellites orbit. Periodic variations in all orbital elements are also caused by the harmonics of the Earth's shape.

3.4.2 Atmospheric Drag

The next most influential perturbing force for low earth orbiting satellites is the effect of atmospheric drag. The molecules that make up the Earth's atmosphere create friction on the satellite, making drag a non conservative perturbation, reducing the total energy of the system. The acceleration of the satellite due to atmospheric drag is

$$\vec{\mathbf{a}}_{\text{drag}} = -\frac{1}{2}\frac{\mathrm{c_D A}}{\mathrm{m}}\gamma \mathrm{v}_{\mathrm{rel}}^2 \frac{\vec{\mathbf{v}}_{\mathbf{rel}}}{|\vec{\mathbf{v}}_{\mathbf{rel}}|}$$

where $\mathrm{c_D}$ is the dimensionless coefficient of drag that quantifies the susceptibility of the satellite to drag. The coefficient of drag depends on the shape of the satellite and in this thesis the satellite coefficient of drag is $\mathrm{c_D} = 2.2$. A is the cross-sectional area of the satellite defined to be the area which is normal to the satellite velocity vector. In this thesis, the cross-sectional area of the satellite is taken to be 8 m^2 and its mass, m, is 800 kg. The atmospheric density, γ, is the density of Earth's atmosphere at the current altitude of the satellite and is the most difficult aspect of the acceleration to determine. Not only does the atmospheric density vary with altitude, the density is affected by temperature, winds, tides and even the location of the ground station. There are two types of atmospheric models used to determine the density. They are static or time varying models. A static model considers

- *Latitudinal variations*: variations in the density of the atmosphere due to altitude. Since the Earth is oblate, when a satellite passes over the equatorial region relative altitude is less and therefore the atmospheric density is larger.

- *Longitudinal variations*: variations in the density due to local altitude, such as mountain ranges, cause significant variations in the atmospheric models due to local wind, temperature etc.

A time-varying atmospheric model has additional complexities to consider including diurnal variations in which the atmosphere lags in the direction of the Sun, where it is warmest. Other affects such as the sun spot cycle and even the 27-day solar rotation cycle create changes in the Earth's atmosphere. It is extremely difficult to model all of these effects.

In this thesis, the atmospheric density is determined using the following equations

$$\gamma = \gamma_0 e^{-h/h_0} = \gamma_0 e^{-(|r|-R_\oplus)/h_0}$$

where $\gamma_0 = 3.019 \times 10^{-15} \frac{kg}{m^3}$ and $h_0 = 1000$ km.

The velocity vector used in the calculation of the acceleration due to drag is taken relative to the Earth's rotating atmosphere. The rotation of the atmosphere is approximated as the rotation of the Earth. This is an assumption since the rotation of the atmosphere depends on the altitude; when closer to Earth's surface the atmosphere's rate is close to that of Earth's, however as altitude increases the rate of the atmosphere decreases. The velocity vector is found using the transport theorem. The relative velocity vector is

$$\vec{\mathbf{v}}_{\mathbf{rel}} = \frac{d\vec{\mathbf{r}}}{dt} - \vec{\omega}_\oplus \times \vec{\mathbf{r}} = \begin{bmatrix} \frac{dr_i}{dt} + \omega_\oplus r_j \\ \frac{dr_j}{dt} + \omega_\oplus r_i \\ \frac{dr_k}{dt} \end{bmatrix} = \begin{bmatrix} v_i + \omega_\oplus r_j \\ v_j + \omega_\oplus r_i \\ v_k \end{bmatrix}$$

Therefore the acceleration due to atmospheric drag becomes:

$$\vec{\mathbf{a}}_{\text{drag}} = -\frac{1}{2}\frac{c_D A}{m}\gamma_0 e^{-\left(\sqrt{r_i^2+r_j^2+r_k^2}-R_\oplus\right)/h_0} \sqrt{v_i^2+v_j^2+v_k^2} \begin{bmatrix} v_i + \omega_\oplus r_j \\ v_j + \omega_\oplus r_i \\ v_k \end{bmatrix}$$

As explained earlier, atmospheric drag is a non conservative perturbing force which causes the satellite to lose energy. This in turn causes a decrease in the orbits semimajor axis and eccentricity. Therefore, over time, the orbit becomes more circular and the altitude of the satellite

decreases. Therefore, station keeping maneuvers are required to maintain any satellite orbit including the highly elliptical orbit of the satellite in this thesis.

3.4.3 Perturbation due to Moon

The Earth's oblateness and atmospheric drag play a crucial role in perturbing orbits at low altitudes (~ 1000 km), however as the altitude of a satellite increases the Moon's gravitational pull becomes a more influential perturbation force. Since a satellite in a Molniya orbit reaches altitudes upwards of 35,000 km, third-body perturbation effects due to the Moon are essential to accurate orbit estimation. As seen in Figure 3.6, the Moon creates a gravitational force on the satellite in the direction of the Moon, which pulls the satellites orbit toward the lunar plane, changing the inclination of the orbit.

The acceleration of the satellite due to the Moon's gravitational pull is

$$\vec{\mathbf{a}}_{3-\text{body}} = \mathrm{Gm}_2 \left(\frac{1}{\mathrm{d}^3} \vec{\mathbf{d}} - \frac{1}{\mathrm{r'}^3} \vec{\mathbf{r'}} \right)$$

where $\vec{\mathbf{d}}$ and $\vec{\mathbf{r'}}$ are shown in Figure 3.7 and defined as

$$\vec{\mathbf{d}} = \vec{r}_{moon} - \vec{r}_{sat} = \begin{bmatrix} r_{i_{moon}} - r_{i_{sat}} \\ r_{j_{moon}} - r_{j_{sat}} \\ r_{k_{moon}} - r_{k_{sat}} \end{bmatrix}$$

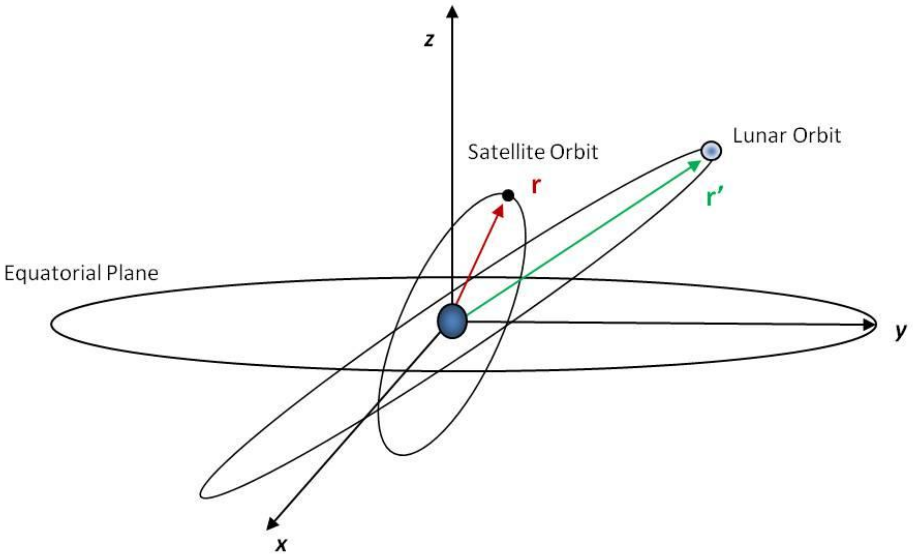

Figure 3.6: Orientation of Third Body

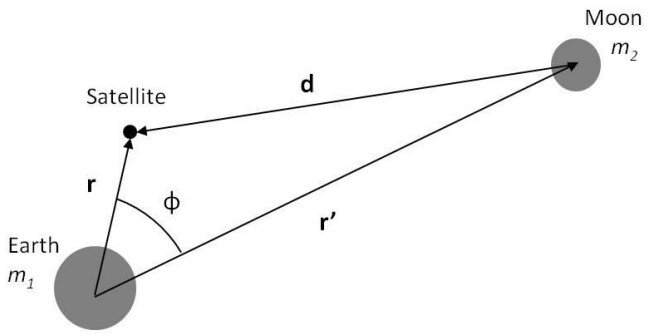

Figure 3.7: Diagram of Third Body

The acceleration due to the Moon can be written in the ECI frame as

$$\vec{\mathbf{a}}_{\text{Moon}} = \text{GM}_{\text{Moon}}\left(\frac{1}{|\vec{\mathbf{r}}_{\text{moon}} - \vec{\mathbf{r}}_{\text{sat}}|^3}(\vec{\mathbf{r}}_{\text{moon}} - \vec{\mathbf{r}}_{\text{sat}}) - \frac{1}{|\vec{\mathbf{r}}_{\text{moon}}|^3}\vec{\mathbf{r}}_{\text{moon}}\right)$$

$$= \text{GM}_{\text{Moon}}\left[\frac{1}{\left[(r_{i_m} - r_{i_{sat}})^2 + (r_{j_m} - r_{j_{sat}})^2 + (r_{k_m} - r_{k_{sat}})^2\right]^{3/2}}\begin{bmatrix} r_{i_m} - r_{i_{sat}} \\ r_{j_m} - r_{j_{sat}} \\ r_{k_m} - r_{k_{sat}} \end{bmatrix} - \frac{1}{|\vec{\mathbf{r}}_{\text{m}}|^3}\begin{bmatrix} r_{i_m} \\ r_{j_m} \\ r_{k_m} \end{bmatrix}\right]$$

The Sun's gravitational force on the satellite is not added as a perturbing force in this thesis since its affect on the satellite orbit is about half that of the Moon's, which is already a small effect. The overall affect of the Moon's gravitational force on the satellite is similar to the oblateness of the Earth, causing perturbation in the line of nodes and argument of perigee; however the variations are about the lunar plane rather than the equatorial plane.

3.4.4 Perturbation due to Solar Radiation Pressure

The final perturbing force considered in this thesis is the pressure created on the satellite due to the Sun's radiation. Similarly to the Earth's atmospheric drag, solar radiation particles create friction on the satellite, and therefore solar radiation pressure is a non-conservative perturbing force. This force decreases the overall energy of the satellite, reducing the semi major axis of the orbit. There are also annual variations in the argument of perigee and eccentricity due to the relative location of the Earth with respect to the Sun over one year.

The acceleration of the satellite due to solar radiation pressure is

$$\vec{\boldsymbol{a}}_{SR} = -\frac{p_{SR} c_R A_{\odot}}{m} \frac{\vec{r}_{sat\odot}}{\left|\vec{r}_{sat\odot}\right|}$$

Where p_{SR} is the solar pressure per unit area and is found using Einstein's law, $E = mc^2$in the form $mc = \frac{E}{c}$ and the solar-radiation constant, $SF = 1353 \frac{W}{m^2}$..

$$p_{SR} = \frac{E}{c} = \frac{SF}{c} = \frac{1353 \frac{W}{m^2}}{3 \times 10^8 \frac{m}{s}} = 4.51 \times 10^{-6} \frac{W.s}{m^3} = 4.51 \times 10^{-6} \frac{N}{m^2}$$

Reflectivity of the satellite, c_R, is typically between 0 and 2, and is 0.6 for the satellite in this thesis. The exposed surface area of the satellite to the sun, $A_{\odot}$, is taken to be 14 m^2 since both the solar arrays will be facing the sun at all time and the surface area of the central body will vary from 3 to 8 m^2. $\vec{r}_{sat\odot}$ is the vector from the satellite to the sun, therefore

$$\vec{r}_{sat\odot} = \vec{r}_{\odot} - \vec{r}_{sat} = \begin{bmatrix} r_{i_{\odot}} - r_{i_{sat}} \\ r_{j_{\odot}} - r_{j_{sat}} \\ r_{k_{\odot}} - r_{k_{sat}} \end{bmatrix}$$

Substituting in this vector gives the acceleration of the satellite due to solar radiation pressure in the ECI frame as

$$\vec{\boldsymbol{a}}_{SR} = -\frac{p_{SR} c_R A_{\odot}}{m} \frac{1}{\sqrt{(r_{i_{\odot}} - r_{i_{sat}})^2 + (r_{j_{\odot}} - r_{j_{sat}})^2 + (r_{k_{\odot}} - r_{k_{sat}})^2}} \begin{bmatrix} r_{i_{\odot}} - r_{i_{sat}} \\ r_{j_{\odot}} - r_{j_{sat}} \\ r_{k_{\odot}} - r_{k_{sat}} \end{bmatrix}$$

Notice, knowledge of the location of the Sun is required to determine the acceleration of the satellite at any given point. In this thesis, the Sun's position is taken as stationary over the time period in which the orbit is determined. Each time the algorithm is run, the Sun's location must be inputted and the perturbing acceleration recalculated.

3.4.5 Summary of Perturbation Forces

To summarize, the acceleration due to each of the perturbing forces explained above can be added to the two-body acceleration and numerically integrated to find the satellite's position and velocity. The numerical integration is done using MatLab's *ode45* which integrates the time derivative of the state vector. A plot of the perturbed and unperturbed orbit is seen in Figure 3.8.

$$\dot{X} = \begin{bmatrix} v_i \\ v_j \\ v_k \\ -\frac{\mu r_i}{r^3} + a_{i_{nonspherical}} + a_{i_{drag}} + a_{i_{3-body}} + a_{i_{SR}} \\ -\frac{\mu r_j}{r^3} + a_{j_{nonspherical}} + a_{j_{drag}} + a_{j_{3-body}} + a_{j_{SR}} \\ -\frac{\mu r_k}{r^3} + + a_{k_{nonspherical}} + a_{k_{drag}} + a_{k_{3-body}} + a_{k_{SR}} \end{bmatrix}$$

The inputs needed to calculate the perturbation acceleration are the position of the satellite, the latitude and longitude of the sub-satellite point and the position of the Sun and the Moon relative to the center of the Earth. The position of the Sun and Moon relative to the Earth is taken as constant for the period of the satellite and therefore can be inputted once at the beginning of the algorithm. The sub-satellite point changes over time and therefore will need to be recalculated with each time step. At each time step,

$$\theta_{g_{k+1}} = \theta_{g_k} + \omega_{\oplus}\Delta t \qquad \phi_{gc_{sat}} = sin^{-1}\left(\frac{r_k}{r}\right) \qquad \lambda_{sat} = tan^{-1}\left(\frac{r_j}{r_i}\right) - \theta_{g_{k+1}}$$

where θ_g is the Greenwich sidereal time. Therefore the final initial inputs needed to compute the perturbation acceleration are: the satellite's initial position, velocity and characteristics, the Earth to Sun vector, the Earth to Moon vector and the initial Greenwich sidereal time.

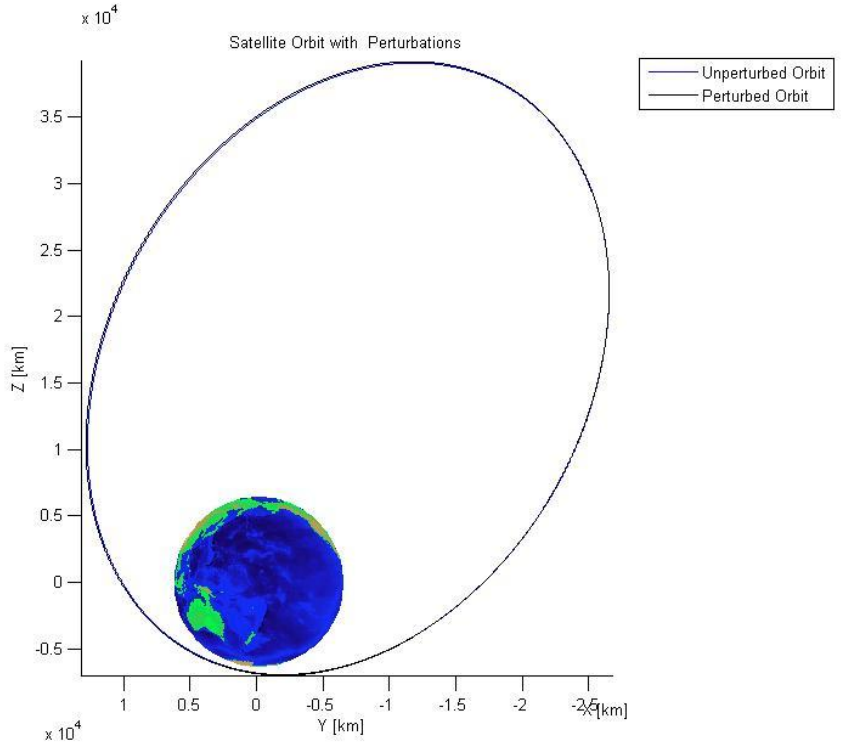

Figure 3.8: Unperturbed and perturbed orbit using all four perturbation accelerations

3.5 Development of State Matrix with Perturbing Forces

The state matrix, F, is made up of the equations of motion that define the problem, therefore it must be calculated for each of the perturbing forces in order to apply the Kalman filter to orbit determination. Much of the Kalman filter development is in determining this state matrix since each perturbing force and torque affects the final state matrix. The state transition matrix also needs to be linearized in order to apply the Kalman filter. To do this, the partial derivatives of the equations of motion and perturbations are taken with respect to each element of the state vector. For an orbit in which no disturbing forces are considered, the F matrix is only dependent on the 2-body equations:

$$\mathbf{X_{2-body}} = \begin{bmatrix}\vec{\mathbf{r}}\\ \vec{\mathbf{v}}\end{bmatrix} = \begin{bmatrix} r_i\\ r_j\\ r_k\\ v_i\\ v_j\\ v_k\end{bmatrix} \text{ and } \dot{\mathbf{X}}_{\mathbf{2-body}} = \begin{bmatrix}\vec{\mathbf{v}}\\ \vec{\mathbf{a}}\end{bmatrix} = \begin{bmatrix}\vec{\mathbf{v}}\\ -\frac{\mu\vec{r}}{r^3}\end{bmatrix} = \begin{bmatrix} v_i\\ v_j\\ v_k\\ -\frac{\mu r_i}{r^3}\\ -\frac{\mu r_j}{r^3}\\ -\frac{\mu r_k}{r^3}\end{bmatrix}$$

therefore

$$\mathbf{F}_{2-\text{body}} = \frac{\partial\dot{\mathbf{X}}}{\partial\mathbf{X}} = \begin{bmatrix} \frac{\partial v_i}{\partial r_i} & \frac{\partial v_i}{\partial r_j} & \frac{\partial v_i}{\partial r_k} & \frac{\partial v_i}{\partial v_i} & \frac{\partial v_i}{\partial v_j} & \frac{\partial v_i}{\partial v_k}\\ \frac{\partial v_j}{\partial r_i} & \frac{\partial v_j}{\partial r_j} & \frac{\partial v_j}{\partial r_k} & \frac{\partial v_j}{\partial v_i} & \frac{\partial v_j}{\partial v_j} & \frac{\partial v_j}{\partial v_k}\\ \frac{\partial v_k}{\partial r_i} & \frac{\partial v_k}{\partial r_j} & \frac{\partial v_k}{\partial r_k} & \frac{\partial v_k}{\partial v_i} & \frac{\partial v_k}{\partial v_j} & \frac{\partial v_k}{\partial v_k}\\ \frac{\partial a_i}{\partial r_i} & \frac{\partial a_i}{\partial r_j} & \frac{\partial a_i}{\partial r_k} & \frac{\partial a_i}{\partial v_i} & \frac{\partial a_i}{\partial v_j} & \frac{\partial a_i}{\partial v_k}\\ \frac{\partial a_j}{\partial r_i} & \frac{\partial a_j}{\partial r_j} & \frac{\partial a_j}{\partial r_k} & \frac{\partial a_j}{\partial v_i} & \frac{\partial a_j}{\partial v_j} & \frac{\partial a_j}{\partial v_k}\\ \frac{\partial a_k}{\partial r_i} & \frac{\partial a_k}{\partial r_j} & \frac{\partial a_k}{\partial r_k} & \frac{\partial a_k}{\partial v_i} & \frac{\partial a_k}{\partial v_j} & \frac{\partial a_k}{\partial v_k}\end{bmatrix}$$

$$= \begin{bmatrix} 0 & 0 & 0 & 1 & 0 & 0\\ 0 & 0 & 0 & 0 & 1 & 0\\ 0 & 0 & 0 & 0 & 0 & 1\\ -\frac{\mu}{r^3}+\frac{3\mu r_i^2}{r^5} & \frac{3\mu r_i r_j}{r^5} & \frac{3\mu r_i r_k}{r^5} & 0 & 0 & 0\\ \frac{3\mu r_i r_j}{r^5} & -\frac{\mu}{r^3}+\frac{3\mu r_j^2}{r^5} & \frac{3\mu r_j r_k}{r^5} & 0 & 0 & 0\\ \frac{3\mu r_i r_k}{r^5} & \frac{3\mu r_j r_k}{r^5} & -\frac{\mu}{r^3}+\frac{3\mu r_k^2}{r^5} & 0 & 0 & 0\end{bmatrix}$$

Once again, the four types of disturbing forces considered are non-spherical, drag, 3-body and solar radiation. These disturbing forces need to be added to the F matrix so that they become incorporated into the state transition matrix, Φ. Luckily the F matrices, for each disturbing forces, can be combined in the following way:

$$\mathbf{F} = \mathbf{F}_{2-\text{body}} + \mathbf{F}_{\text{nonspherical}} + \mathbf{F}_{\text{drag}} + \mathbf{F}_{3-\text{body}} + \mathbf{F}_{\text{SR}}$$

Therefore, the state matrices for each of the perturbing forces need to be developed. This is done by taking the partial derivatives of the perturbing acceleration with respect to the state vector. In the following sections, the state matrices for each of the perturbing accelerations are determined.

3.5.1 Earth's Oblateness

In Section 3.4.1, the acceleration on the satellite due to a non spherical Earth was determined to be

$$a_i = \left\{ [-\frac{3}{2}\frac{\mu {R_\oplus}^2 C_{2,0}}{r^4}\{3\sin^2\left(\phi_{gc_{sat}}\right) - 1\}] - \frac{r_k}{r^2\sqrt{r_i^2 + r_j^2}}[3\frac{\mu {R_\oplus}^2 C_{2,0}}{r^3}\sin\left(\phi_{gc_{sat}}\right)\cos\left(\phi_{gc_{sat}}\right)] \right\} r_i$$

$$a_j = \left\{ [-\frac{3}{2}\frac{\mu {R_\oplus}^2 C_{2,0}}{r^4}\{3\sin^2\left(\phi_{gc_{sat}}\right) - 1\}] - \frac{r_k}{r^2\sqrt{r_i^2 + r_j^2}}[3\frac{\mu {R_\oplus}^2 C_{2,0}}{r^3}\sin\left(\phi_{gc_{sat}}\right)\cos\left(\phi_{gc_{sat}}\right)] \right\} r_j$$

$$a_k = [-\frac{3}{2}\frac{\mu {R_\oplus}^2 C_{2,0}}{r^4}\{3\sin^2\left(\phi_{gc_{sat}}\right) - 1\}] r_k + \frac{\sqrt{r_i^2 + r_j^2}}{r^2} 3\frac{\mu {R_\oplus}^2 C_{2,0}}{r^3}\sin\left(\phi_{gc_{sat}}\right)\cos\left(\phi_{gc_{sat}}\right)$$

The state matrix for this perturbing force is then

$$\mathbf{F}_{\text{spherical}} = \frac{\partial \dot{\mathbf{X}}_{\text{spherical}}}{\partial \mathbf{X}} = = \begin{bmatrix} 0 & 0 & 0 & 1 & 0 & 0 \\ 0 & 0 & 0 & 0 & 1 & 0 \\ 0 & 0 & 0 & 0 & 0 & 1 \\ \frac{\partial \mathrm{a_i}}{\partial \mathrm{r_i}} & \frac{\partial \mathrm{a_i}}{\partial \mathrm{r_j}} & \frac{\partial \mathrm{a_i}}{\partial \mathrm{r_k}} & & & \\ \frac{\partial \mathrm{a_j}}{\partial \mathrm{r_i}} & \frac{\partial \mathrm{a_j}}{\partial \mathrm{r_j}} & \frac{\partial \mathrm{a_j}}{\partial \mathrm{r_k}} & 0 & 0 & 0 \\ \frac{\partial \mathrm{a_k}}{\partial \mathrm{r_i}} & \frac{\partial \mathrm{a_k}}{\partial \mathrm{r_j}} & \frac{\partial \mathrm{a_k}}{\partial \mathrm{r_k}} & 0 & 0 & 0 \end{bmatrix}$$

Appendix A shows how each of these partial derivatives are found. Below is just the first of the partial derivatives of the acceleration with respect to position

$$\frac{\partial \mathrm{a_i}}{\partial \mathrm{r_i}} = -\frac{3}{2}\frac{\mu {R_\oplus}^2 C_{2,0}}{r^4}\{3\sin^2\left(\phi_{gc_{sat}}\right) - 1\} - \frac{r_k}{r^2\sqrt{r_i^2 + r_j^2}}[3\frac{\mu {R_\oplus}^2 C_{2,0}}{r^3}\sin\left(\phi_{gc_{sat}}\right)\cos\left(\phi_{gc_{sat}}\right)$$
$$+ r_i\left(6r_i\frac{\mu {R_\oplus}^2 C_{2,0}}{r^3}\{3\sin^2\left(\phi_{gc_{sat}}\right) - 1\}\right.$$
$$+ \frac{15r_k r_i}{r^7\sqrt{r_i^2 + r_j^2}}[\mu {R_\oplus}^2 C_{2,0}\sin\left(\phi_{gc_{sat}}\right)\cos\left(\phi_{gc_{sat}}\right)$$
$$\left.+ \frac{3r_k r_i}{r^5\left(r_i^2 + r_j^2\right)^{3/2}}[\mu {R_\oplus}^2 C_{2,0}\sin\left(\phi_{gc_{sat}}\right)\cos\left(\phi_{gc_{sat}}\right)]\right)$$

Although the derivation is lengthy, once programmed, the state matrix for Earth's oblateness just depends on the current position of the satellite.

3.5.2 Earth's Atmospheric Drag

In Section 3.4.2, the acceleration due to atmospheric drag was defined as

$$\vec{\mathbf{a}}_{\mathrm{drag}} = -\frac{1}{2}\frac{\mathrm{c_D A}}{\mathrm{m}}\gamma_0 \mathrm{e}^{-\left(\sqrt{\mathrm{r_i}^2+\mathrm{r_j}^2+\mathrm{r_k}^2}-\mathrm{R}_\oplus\right)/\mathrm{h}_0}\sqrt{\mathrm{v_i}^2+\mathrm{v_j}^2+\mathrm{v_k}^2}\begin{bmatrix}\mathrm{v_i}+\omega_\oplus \mathrm{r_j}\\ \mathrm{v_j}+\omega_\oplus \mathrm{r_i}\\ \mathrm{v_k}\end{bmatrix}$$

The state matrix is then

$$\mathbf{F}_{\mathrm{drag}} = \frac{\partial \dot{\mathbf{X}}}{\partial \mathbf{X}} = \begin{bmatrix} 0 & 0 & 0 & 1 & 0 & 0 \\ 0 & 0 & 0 & 0 & 1 & 0 \\ 0 & 0 & 0 & 0 & 0 & 1 \\ \frac{\partial \mathrm{a_i}}{\partial \mathrm{r_i}} & \frac{\partial \mathrm{a_i}}{\partial \mathrm{r_j}} & \frac{\partial \mathrm{a_i}}{\partial \mathrm{r_k}} & \frac{\partial \mathrm{a_i}}{\partial \mathrm{v_i}} & \frac{\partial \mathrm{a_i}}{\partial \mathrm{v_j}} & \frac{\partial \mathrm{a_i}}{\partial \mathrm{v_k}} \\ \frac{\partial \mathrm{a_j}}{\partial \mathrm{r_i}} & \frac{\partial \mathrm{a_j}}{\partial \mathrm{r_j}} & \frac{\partial \mathrm{a_j}}{\partial \mathrm{r_k}} & \frac{\partial \mathrm{a_j}}{\partial \mathrm{v_i}} & \frac{\partial \mathrm{a_j}}{\partial \mathrm{v_j}} & \frac{\partial \mathrm{a_j}}{\partial \mathrm{v_k}} \\ \frac{\partial \mathrm{a_k}}{\partial \mathrm{r_i}} & \frac{\partial \mathrm{a_k}}{\partial \mathrm{r_j}} & \frac{\partial \mathrm{a_k}}{\partial \mathrm{r_k}} & \frac{\partial \mathrm{a_k}}{\partial \mathrm{v_i}} & \frac{\partial \mathrm{a_k}}{\partial \mathrm{v_j}} & \frac{\partial \mathrm{a_k}}{\partial \mathrm{v_k}} \end{bmatrix}$$

where

$$\frac{\partial \mathbf{a}}{\partial \mathbf{r}} = \begin{bmatrix} \frac{\partial a_i}{\partial r_i} & \frac{\partial a_i}{\partial r_j} & \frac{\partial a_i}{\partial r_k} \\ \frac{\partial a_j}{\partial r_i} & \frac{\partial a_j}{\partial r_j} & \frac{\partial a_j}{\partial r_k} \\ \frac{\partial a_k}{\partial r_i} & \frac{\partial a_k}{\partial r_j} & \frac{\partial a_k}{\partial r_k} \end{bmatrix}$$

$$= -\frac{1}{2}\frac{c_D A \gamma_0}{m h_0} e^{-(|r|-R_\oplus)/h_0} \begin{bmatrix} -r_i(v_i + \omega_\oplus r_j)\frac{|v_{rel}|}{|r|} & \omega_\oplus |v_{rel}| - r_j(v_i + \omega_\oplus r_j)\frac{|v_{rel}|}{|r|} & -r_k(v_i + \omega_\oplus r_j)\frac{|v_{rel}|}{|r|} \\ \omega_\oplus |v_{rel}| - r_i(v_j + \omega_\oplus r_i)\frac{|v_{rel}|}{|r|} & -r_j(v_j + \omega_\oplus r_i)\frac{|v_{rel}|}{|r|} & r_k(v_j + \omega_\oplus r_i)\frac{|v_{rel}|}{|r|} \\ -v_k r_i \frac{|v_{rel}|}{|r|} & -v_k r_j \frac{|v_{rel}|}{|r|} & -v_k r_k \frac{|v_{rel}|}{|r|} \end{bmatrix}$$

and

$$\frac{\partial \mathbf{a}}{\partial \mathbf{v}} = \begin{bmatrix} \frac{\partial a_i}{\partial v_i} & \frac{\partial a_i}{\partial v_j} & \frac{\partial a_i}{\partial v_k} \\ \frac{\partial a_j}{\partial v_i} & \frac{\partial a_j}{\partial v_j} & \frac{\partial a_j}{\partial v_k} \\ \frac{\partial a_k}{\partial v_i} & \frac{\partial a_k}{\partial v_j} & \frac{\partial a_k}{\partial v_k} \end{bmatrix}$$

$$= -\frac{1}{2}\frac{c_D A \gamma_0}{m} e^{-(|r|-R_\oplus)/h_0} \begin{bmatrix} |v_{rel}| + \frac{v_i(v_i + \omega_\oplus r_j)}{|v_{rel}|} & \frac{v_j(v_i + \omega_\oplus r_j)}{|v_{rel}|} & \frac{v_k(v_i + \omega_\oplus r_j)}{|v_{rel}|} \\ \frac{v_i(v_j + \omega_\oplus r_i)}{|v_{rel}|} & |v_{rel}| + \frac{v_j(v_j + \omega_\oplus r_i)}{|v_{rel}|} & \frac{v_k(v_j + \omega_\oplus r_i)}{|v_{rel}|} \\ \frac{v_i v_k}{|v_{rel}|} & \frac{v_j v_k}{|v_{rel}|} & |v_{rel}| + \frac{{v_k}^2}{|v_{rel}|} \end{bmatrix}$$

The state matrix for atmospheric drag perturbations changes with time and depends on the current position and velocity of the satellite.

3.5.3 Moon's Gravitational Force

The acceleration of the satellite due to the Moon's gravitational force is

$$\vec{\mathbf{a}}_{Moon} = GM_{Moon}\left[\frac{1}{\left[(r_{i_m} - r_{i_{sat}})^2 + (r_{j_m} - r_{j_{sat}})^2 + (r_{k_m} - r_{k_{sat}})^2\right]^{3/2}}\begin{bmatrix} r_{i_m} - r_{i_{sat}} \\ r_{j_m} - r_{j_{sat}} \\ r_{k_m} - r_{k_{sat}} \end{bmatrix} - \frac{1}{|\vec{\mathbf{r}}_{moon}|^3}\begin{bmatrix} r_{i_{moon}} \\ r_{j_{moon}} \\ r_{k_{moon}} \end{bmatrix}\right]$$

The state matrix is then

$$\mathbf{F}_{\text{Moon}} = \frac{\partial \dot{\mathbf{X}}}{\partial \mathbf{X}} = \begin{bmatrix} 0 & 0 & 0 & 1 & 0 & 0 \\ 0 & 0 & 0 & 0 & 1 & 0 \\ 0 & 0 & 0 & 0 & 0 & 1 \\ \frac{\partial \mathrm{a_i}}{\partial \mathrm{r_i}} & \frac{\partial \mathrm{a_i}}{\partial \mathrm{r_j}} & \frac{\partial \mathrm{a_i}}{\partial \mathrm{r_k}} & & & \\ \frac{\partial \mathrm{a_j}}{\partial \mathrm{r_i}} & \frac{\partial \mathrm{a_j}}{\partial \mathrm{r_j}} & \frac{\partial \mathrm{a_j}}{\partial \mathrm{r_k}} & 0 & 0 & 0 \\ \frac{\partial \mathrm{a_k}}{\partial \mathrm{r_i}} & \frac{\partial \mathrm{a_k}}{\partial \mathrm{r_j}} & \frac{\partial \mathrm{a_k}}{\partial \mathrm{r_k}} & 0 & 0 & 0 \end{bmatrix}$$

where

$$\frac{\partial \mathbf{a}}{\partial \mathbf{r}} = \begin{bmatrix} \frac{\partial \mathrm{a_i}}{\partial \mathrm{r_i}} & \frac{\partial \mathrm{a_i}}{\partial \mathrm{r_j}} & \frac{\partial \mathrm{a_i}}{\partial \mathrm{r_k}} \\ \frac{\partial \mathrm{a_j}}{\partial \mathrm{r_i}} & \frac{\partial \mathrm{a_j}}{\partial \mathrm{r_j}} & \frac{\partial \mathrm{a_j}}{\partial \mathrm{r_k}} \\ \frac{\partial \mathrm{a_k}}{\partial \mathrm{r_i}} & \frac{\partial \mathrm{a_k}}{\partial \mathrm{r_j}} & \frac{\partial \mathrm{a_k}}{\partial \mathrm{r_k}} \end{bmatrix}$$

$$= \mathrm{GM_{Moon}} \begin{bmatrix} \frac{3(r_{i_m} - r_{i_{sat}})^2}{|\vec{\mathrm{r}}_{\text{moon}} - \vec{\mathrm{r}}_{\text{sat}}|^5} - \frac{1}{|\vec{\mathrm{r}}_{\text{moon}} - \vec{\mathrm{r}}_{\text{sat}}|^3} & \frac{3(r_{i_m} - r_{i_{sat}})(r_{j_m} - r_{j_{sat}})}{|\vec{\mathrm{r}}_{\text{moon}} - \vec{\mathrm{r}}_{\text{sat}}|^5} & \frac{3(r_{i_m} - r_{i_{sat}})(r_{k_m} - r_{k_{sat}})}{|\vec{\mathrm{r}}_{\text{moon}} - \vec{\mathrm{r}}_{\text{sat}}|^5} \\ \frac{3(r_{i_m} - r_{i_{sat}})(r_{j_m} - r_{j_{sat}})}{|\vec{\mathrm{r}}_{\text{moon}} - \vec{\mathrm{r}}_{\text{sat}}|^5} & \frac{3(r_{j_m} - r_{j_{sat}})^2}{|\vec{\mathrm{r}}_{\text{moon}} - \vec{\mathrm{r}}_{\text{sat}}|^5} - \frac{1}{|\vec{\mathrm{r}}_{\text{moon}} - \vec{\mathrm{r}}_{\text{sat}}|^3} & \frac{3(r_{j_m} - r_{j_{sat}})(r_{k_m} - r_{k_{sat}})}{|\vec{\mathrm{r}}_{\text{moon}} - \vec{\mathrm{r}}_{\text{sat}}|^5} \\ \frac{3(r_{i_m} - r_{i_{sat}})(r_{k_m} - r_{k_{sat}})}{|\vec{\mathrm{r}}_{\text{moon}} - \vec{\mathrm{r}}_{\text{sat}}|^5} & \frac{3(r_{j_m} - r_{j_{sat}})(r_{k_m} - r_{k_{sat}})}{|\vec{\mathrm{r}}_{\text{moon}} - \vec{\mathrm{r}}_{\text{sat}}|^5} & \frac{3(r_{k_m} - r_{k_{sat}})^2}{|\vec{\mathrm{r}}_{\text{moon}} - \vec{\mathrm{r}}_{\text{sat}}|^5} - \frac{1}{|\vec{\mathrm{r}}_{\text{moon}} - \vec{\mathrm{r}}_{\text{sat}}|^3} \end{bmatrix}$$

Once again, the position of the Moon is assumed to be constant over the period of the satellite orbit, so the state matrix for the lunar perturbations only depends on the current position of the satellite.

3.5.4 Solar Radiation Pressure

Finally, the acceleration of the satellite due to solar radiation pressure is

$$\vec{a}_{SR} = -\frac{p_{SR} c_R A_\odot}{m} \frac{1}{\sqrt{(r_{i_\odot} - r_{i_{sat}})^2 + (r_{j_\odot} - r_{j_{sat}})^2 + (r_{k_\odot} - r_{k_{sat}})^2}} \begin{bmatrix} r_{i_\odot} - r_{i_{sat}} \\ r_{j_\odot} - r_{j_{sat}} \\ r_{k_\odot} - r_{k_{sat}} \end{bmatrix}$$

Therefore the state matrix becomes,

$$\mathbf{F}_{\mathrm{SR}} = \frac{\partial \dot{\mathbf{X}}}{\partial \mathbf{X}} = \begin{bmatrix} 0 & 0 & 0 & 1 & 0 & 0 \\ 0 & 0 & 0 & 0 & 1 & 0 \\ 0 & 0 & 0 & 0 & 0 & 1 \\ \frac{\partial \mathrm{a_i}}{\partial \mathrm{r_i}} & \frac{\partial \mathrm{a_i}}{\partial \mathrm{r_j}} & \frac{\partial \mathrm{a_i}}{\partial \mathrm{r_k}} & & & \\ \frac{\partial \mathrm{a_j}}{\partial \mathrm{r_i}} & \frac{\partial \mathrm{a_j}}{\partial \mathrm{r_j}} & \frac{\partial \mathrm{a_j}}{\partial \mathrm{r_k}} & 0 & 0 & 0 \\ \frac{\partial \mathrm{a_k}}{\partial \mathrm{r_i}} & \frac{\partial \mathrm{a_k}}{\partial \mathrm{r_j}} & \frac{\partial \mathrm{a_k}}{\partial \mathrm{r_k}} & 0 & 0 & 0 \end{bmatrix}$$

where

$$\frac{\partial \mathbf{a}}{\partial \mathbf{r}} = \begin{bmatrix} \frac{\partial \mathrm{a_i}}{\partial \mathrm{r_i}} & \frac{\partial \mathrm{a_i}}{\partial \mathrm{r_j}} & \frac{\partial \mathrm{a_i}}{\partial \mathrm{r_k}} \\ \frac{\partial \mathrm{a_j}}{\partial \mathrm{r_i}} & \frac{\partial \mathrm{a_j}}{\partial \mathrm{r_j}} & \frac{\partial \mathrm{a_j}}{\partial \mathrm{r_k}} \\ \frac{\partial \mathrm{a_k}}{\partial \mathrm{r_i}} & \frac{\partial \mathrm{a_k}}{\partial \mathrm{r_j}} & \frac{\partial \mathrm{a_k}}{\partial \mathrm{r_k}} \end{bmatrix}$$

$$= -\frac{p_{SR} c_R A_{\odot}}{m} \begin{bmatrix} \frac{(r_{i_{\odot}} - r_{i_{sat}})^2}{\vec{r}_{sat\odot}{}^3} - \frac{1}{|\vec{r}_{sat\odot}|} & \frac{(r_{i_{\odot}} - r_{i_{sat}})(r_{j_{\odot}} - r_{j_{sat}})}{\vec{r}_{sat\odot}{}^3} & \frac{(r_{i_{\odot}} - r_{i_{sat}})(r_{k_{\odot}} - r_{k_{sat}})}{\vec{r}_{sat\odot}{}^3} \\ \frac{(r_{i_{\odot}} - r_{i_{sat}})(r_{j_{\odot}} - r_{j_{sat}})}{\vec{r}_{sat\odot}{}^3} & \frac{(r_{j_{\odot}} - r_{j_{sat}})^2}{\vec{r}_{sat\odot}{}^3} - \frac{1}{|\vec{r}_{sat\odot}|} & \frac{(r_{k_{\odot}} - r_{k_{sat}})(r_{j_{\odot}} - r_{j_{sat}})}{\vec{r}_{sat\odot}{}^3} \\ \frac{(r_{i_{\odot}} - r_{i_{sat}})(r_{k_{\odot}} - r_{k_{sat}})}{\vec{r}_{sat\odot}{}^3} & \frac{(r_{k_{\odot}} - r_{k_{sat}})(r_{j_{\odot}} - r_{j_{sat}})}{\vec{r}_{sat\odot}{}^3} & \frac{(r_{k_{\odot}} - r_{k_{sat}})^2}{\vec{r}_{sat\odot}{}^3} - \frac{1}{|\vec{r}_{sat\odot}|} \end{bmatrix}$$

After the initial values pertaining to the satellites reflectivity, surface area, etc. are inputted along with the position of the Sun, the state matrix for solar pressure only depends on the current location of the satellite.

Now that each of the state matrices for the perturbing forces has been defined, they can be summed to get the final state matrix to be used in the Kalman filter.

$$\mathbf{F} = \mathbf{F}_{2-\mathrm{body}} + \mathbf{F}_{\mathrm{nonspherical}} + \mathbf{F}_{\mathrm{drag}} + \mathbf{F}_{3-\mathrm{body}} + \mathbf{F}_{\mathrm{SR}}$$

3.6 Kalman Filter Implementation for Site Track Orbit Determination

The first of the two cases studied in this thesis, determines the satellite orbit using input measurements from a ground stations site track. When the satellite passes in view of the ground station antenna, the antenna's orientation and signal collection determines the satellite range, elevation and azimuth and relays this information to the satellite every time step. For the orbit and ground station used in this thesis, the measurements are received once every two orbits, or once a day.

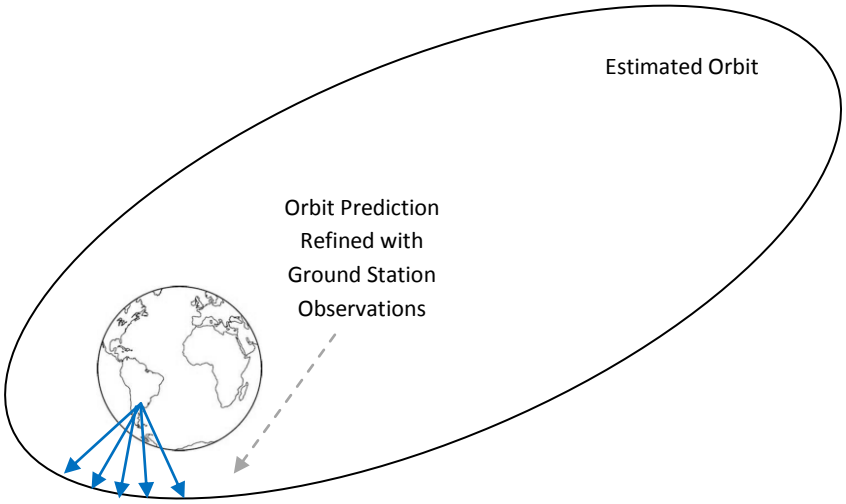

Figure 3.8: Visualization of Orbit and Occurrence of Measurements from Ground Station

The range of the satellite, ρ, is determined using the following equation

$$\rho = \frac{c\Delta t}{2}$$

where c is the speed of light and Δt is the total time required to transmit the signal to the satellite and then receive a signal from the satellite. Range accuracy using this type of calculation has errors of about 3 meters. The range rate, $\dot{\rho}$, is determined from the frequency shift of the signal, or Doppler shift.

$$f_d = -\frac{2\dot{\rho}}{\lambda}$$

where λ is the wavelength of the signal and f_d is the change in frequency of the signal from the initial frequency sent by the antenna and the frequency that the satellite receives. The

azimuth and elevation of the satellite are determined using the gimbal angles from the antenna when collecting the satellite signal.

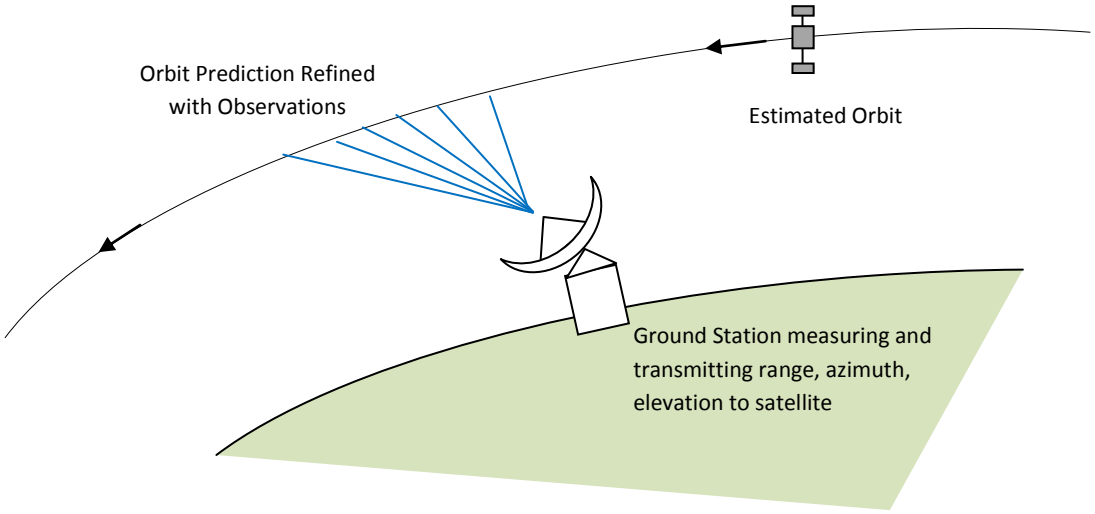

Figure 3.8: Visualization of ground station collecting and sending range data to satellite

The state matrix found in the previous section applies to all orbit determining cases in this thesis. The difference between the two cases, site track and GPS sensor, lies in the form and occurrence of the measurements inputted into the Kalman filter. For the site track case, the measurements are in the form of range, ρ, azimuth, β, and elevation, el, where

$$\rho_{SEZ} = \sqrt{{\rho_S}^2 + {\rho_E}^2 + {\rho_Z}^2}$$

$$\beta = ATAN(-\frac{\rho_S}{\rho_E})$$

$$el = ASIN(\frac{\rho_Z}{\sqrt{{\rho_S}^2 + {\rho_E}^2 + {\rho_Z}^2}})$$

In the case of orbit determination using site track observations, the H matrix is complex since the measurements are in the SEZ reference frame and need to be transformed in to the ECI frame. This is done using the chain rule

$$H = \frac{\partial observation}{\partial \hat{X}} = \left[\frac{\partial obs}{\partial \hat{X}_{ECEF}}\right] = \left[\frac{\partial obs}{\partial \hat{X}_{SEZ}} \times \frac{\partial \hat{X}_{SEZ}}{\partial \hat{X}_{ECI_{site}}} \times \frac{\partial \hat{X}_{ECI_{site}}}{\partial \hat{X}_{ECI}}\right]$$

$$= \left[\frac{\partial obs}{\partial \vec{\rho}_{SEZ}} \times \frac{\partial \vec{\rho}_{SEZ}}{\partial \vec{\rho}_{ECI}} \times \frac{\partial \vec{\rho}_{ECI}}{\partial \vec{r}_{ECI}} \quad \frac{\partial obs}{\partial \dot{\vec{\rho}}_{SEZ}} \times \frac{\partial \dot{\vec{\rho}}_{SEZ}}{\partial \dot{\vec{\rho}}_{ECI}} \times \frac{\partial \dot{\vec{\rho}}_{ECI}}{\partial \vec{v}_{ECI}}\right]$$

From the definitions of range, ρ, azimuth, β, and elevation, el the partial derivatives of each with respect to the position portion of the state vector in the SEZ frame are

$$\frac{\partial obs}{\partial \vec{\rho}_{SEZ}} = \begin{bmatrix} \frac{\partial \rho}{\partial \rho_S} & \frac{\partial \rho}{\partial \rho_E} & \frac{\partial \rho}{\partial \rho_Z} \\ \frac{\partial \beta}{\partial \rho_S} & \frac{\partial \beta}{\partial \rho_E} & \frac{\partial \beta}{\partial \rho_Z} \\ \frac{\partial el}{\partial \rho_S} & \frac{\partial el}{\partial \rho_E} & \frac{\partial el}{\partial \rho_Z} \end{bmatrix}$$

$$= \begin{bmatrix} \frac{\rho_S}{\rho} & \frac{\rho_E}{\rho} & \frac{\rho_Z}{\rho} \\ \frac{-1}{{\rho_S}^2(\frac{{\rho_E}^2}{{\rho_S}^2}+1)} & \frac{\rho_S}{{\rho_E}^2(\frac{{\rho_E}^2}{{\rho_S}^2}+1)} & 0 \\ \frac{\rho_S\rho_Z}{\rho^3\sqrt{-\frac{{\rho_Z}^2}{{\rho_S}^2+{\rho_E}^2+{\rho_Z}^2}+1}} & \frac{-\rho_E\rho_Z}{\rho^3\sqrt{-\frac{{\rho_Z}^2}{{\rho_S}^2+{\rho_E}^2+{\rho_Z}^2}+1}} & \frac{\rho_S\rho_Z}{\rho^3\sqrt{-\frac{{\rho_Z}^2}{\rho^2}+1}} \end{bmatrix}$$

In Section 3.1.2 the rotation matrix needed to transform the SEZ to an earth centered frame was defined as

$$\frac{\partial \vec{\rho}_{SEZ}}{\partial \vec{\rho}_{ECI}} = \begin{bmatrix} \sin(\emptyset_{gd})\cos(\lambda) & \sin(\emptyset_{gd})\sin(\lambda) & -\cos(\emptyset_{gd}) \\ -\sin(\lambda) & \cos(\lambda) & 0 \\ \cos(\emptyset_{gd})\cos(\lambda) & \cos(\emptyset_{gd})\sin(\lambda) & \sin(\emptyset_{gd}) \end{bmatrix}$$

where $\emptyset_{gd}$and λ are the latitude and longitude of the ground station.

Finally, since $\vec{r}_{ECI} = \vec{r}_{site\ ECI} + \vec{\rho}_{ECI}$, and $\vec{v}_{ECI} = \dot{\vec{\rho}}_{ECI}$

$$\frac{\partial \hat{X}_{ECI_{site}}}{\partial \hat{X}_{ECI}} = \begin{bmatrix} \frac{\partial \vec{\rho}_{ECI}}{\partial \vec{r}_{ECI}} \\ \frac{\partial \dot{\vec{\rho}}_{ECI}}{\partial \vec{v}_{ECI}} \end{bmatrix} = [I]$$

The observation matrix is then

$$H = \frac{\partial observation}{\partial \hat{X}} = \begin{bmatrix} \frac{\partial obs}{\partial \vec{\rho}_{SEZ}} \times \frac{\partial \vec{\rho}_{SEZ}}{\partial \vec{\rho}_{ECI}} & 0 \end{bmatrix}$$

Now that both the state matrix and observation matrix have been determined, the orbit can be estimated by running the Kalman filter algorithm over multiple orbits and imputing measurements when the satellite is over the ground station. Only one ground station was used throughout this thesis, therefore the measurements are sent to the satellite once a day when the satellite is over that station. A sample set of site track measurement data is seen in Table 3.1. The

measurement errors of the site track are assumed to be 0.1 degrees for azimuth and elevation and 3 meters for range.

Measurement	Range, ρ, (km)	Azimuth, β, (degrees)	Elevation, el, (degrees)
1	1338	240.8	17.9
2	1816	160.3	45.2
3	2824	128.4	50.7
4	3531	116.2	51.0
5	4329	107.1	52.4

Table 3.1: Sample set of site track data

Figure 3.10 shows the actual and predicted orbit obtained using the orbit determining Kalman filter with site track measurements.

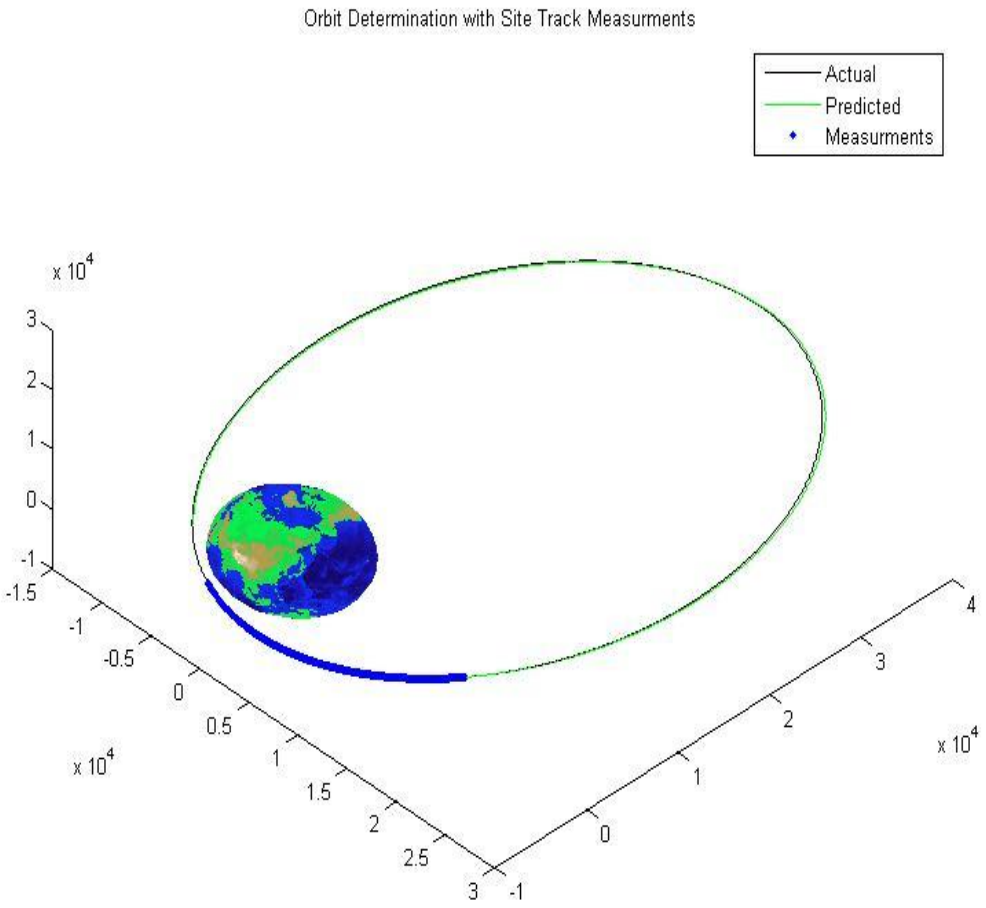

Figure 3.10: Predicted and actual orbit determined using site track

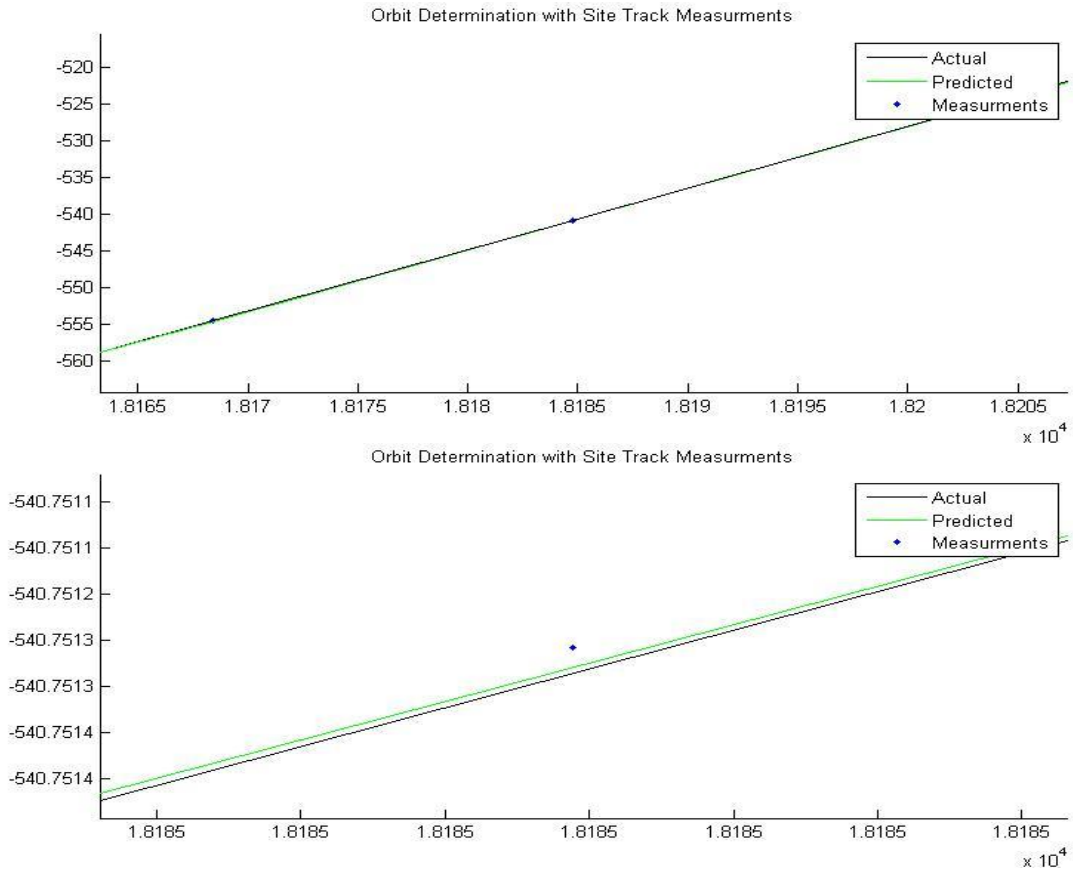

Figure 3.11: Close up of Predicted and Actual Orbit Determined using Site Track

Figure 3.11 shows sample sections of the orbit with the predicted, actual and measurement data plotted. It shows how the Kalman filter takes in to account the measurement as well as the past position in order to best predict the current location of the satellite.

Figure 3.12 plots the difference in actual and predicted orbits. The plot is over two periods. The error increases as time from last measurement update increases. The algorithm was iterated over multiple orbits and days; however the errors did not seem to decrease much as shown in Figure 3.13.

Although, the site track method has quite a bit of errors, if they are within the requirements for the satellite, this method is computationally less expensive and requires no on-board sensors unlike the next case, in which an on-board GPS receiver is used to input measurements of position and velocity in to the Kalman filter at each time step throughout the orbit. This case has much smaller errors but forces the algorithm to update itself with measurements multiple times a second, which is computationally expensive.

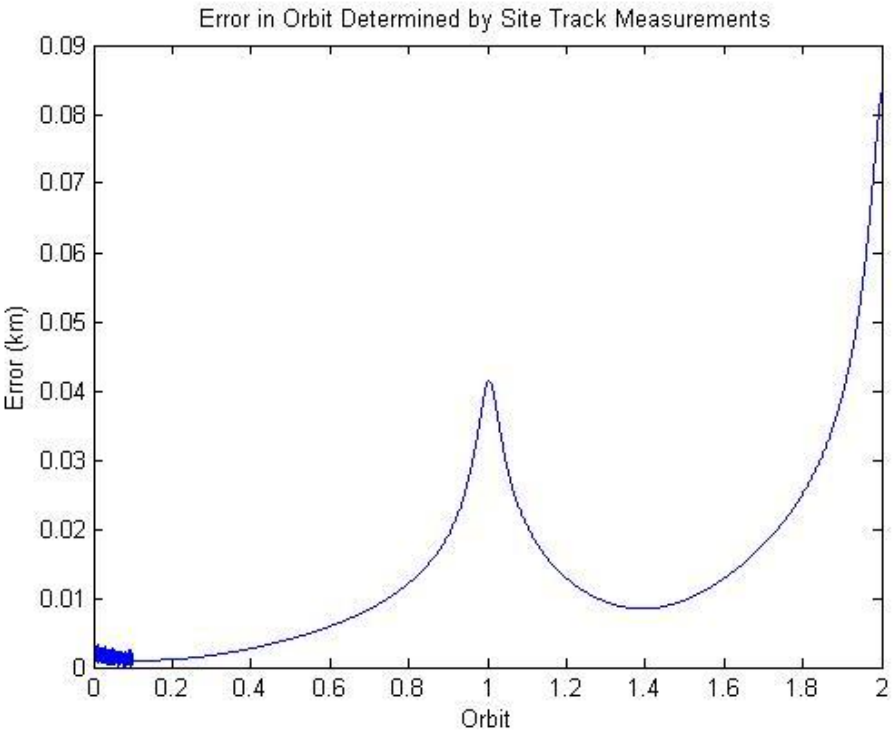

Figure 3.12: Error of Orbit Determined using Site Track over one Orbit

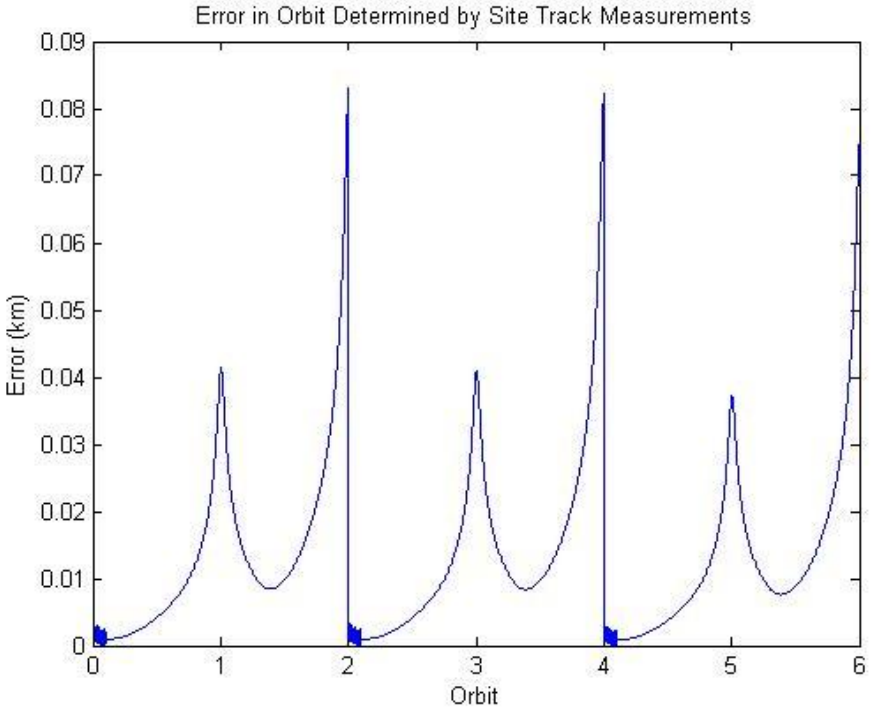

Figure 3.13: Error of Orbit Determined using Site Track over multiple orbits

3.7 Orbit Determining Kalman Filter Implementation with GPS

The same method used in Section 3.6 can easily be applied to the case using measurements from an onboard GPS sensor. The only differences are the observation matrix, H, and the frequency in which the algorithm corrects the predict phase with measurements.

For the case of GPS sensor date in the form of ECI position and velocity, the observation matrix is simply

$$H = \frac{\partial observation}{\partial \hat{X}} = \begin{bmatrix} \frac{\partial r_i}{\partial r_i} & \frac{\partial r_i}{\partial r_j} & \frac{\partial r_i}{\partial r_k} & \frac{\partial r_i}{\partial v_i} & \frac{\partial r_i}{\partial v_j} & \frac{\partial r_i}{\partial v_k} \\ \frac{\partial r_j}{\partial r_i} & \frac{\partial r_j}{\partial r_j} & \frac{\partial r_j}{\partial r_k} & \frac{\partial r_j}{\partial v_i} & \frac{\partial r_j}{\partial v_j} & \frac{\partial r_j}{\partial v_k} \\ \frac{\partial r_k}{\partial r_i} & \frac{\partial r_k}{\partial r_j} & \frac{\partial r_k}{\partial r_k} & \frac{\partial r_k}{\partial v_i} & \frac{\partial r_k}{\partial v_j} & \frac{\partial r_k}{\partial v_k} \\ \frac{\partial v_i}{\partial r_i} & \frac{\partial v_i}{\partial r_j} & \frac{\partial v_i}{\partial r_k} & \frac{\partial v_i}{\partial v_i} & \frac{\partial v_i}{\partial v_j} & \frac{\partial v_i}{\partial v_k} \\ \frac{\partial v_j}{\partial r_i} & \frac{\partial v_j}{\partial r_j} & \frac{\partial v_j}{\partial r_k} & \frac{\partial v_j}{\partial v_i} & \frac{\partial v_j}{\partial v_j} & \frac{\partial v_j}{\partial v_k} \\ \frac{\partial v_k}{\partial r_i} & \frac{\partial v_k}{\partial r_j} & \frac{\partial v_k}{\partial r_k} & \frac{\partial v_k}{\partial v_i} & \frac{\partial v_k}{\partial v_j} & \frac{\partial v_k}{\partial v_k} \end{bmatrix} = \begin{bmatrix} 1 & 0 & 0 & 0 & 0 & 0 \\ 0 & 1 & 0 & 0 & 0 & 0 \\ 0 & 0 & 1 & 0 & 0 & 0 \\ 0 & 0 & 0 & 1 & 0 & 0 \\ 0 & 0 & 0 & 0 & 1 & 0 \\ 0 & 0 & 0 & 0 & 0 & 1 \end{bmatrix} = \mathbf{I}$$

The state matrix, F, is the same as it was in the site track case, since it is independent of what type of measurement is used. Now the Kalman filter is run inputting measurements over the entire orbit rather than just a brief time during ground site overpass which results in a much more accurate prediction of the satellite orbit. The simulated GPS measurements were created using the *rand* function in MatLab which produces normally distributed pseudorandom numbers, using a chosen error and rate. The error for the sensor used in this thesis is 0.5 meters.

Figure 3.14 shows the actual orbit and the predicated orbit and Figure 3.15 shows the element break down of the position vector. Figure 3.16 and 3.17 then show a close up of the actual and predicted position.

Figure 3.18 shows the errors seen between the actual and predicted orbit over one orbit with measurements inputted every second. Figure 3.19 shows the errors over one orbit with measurements inputted every two minutes. The plot begins and ends at the orbits perigee, where the satellite is traveling much faster than at apogee. Therefore, the distance traveled between each time step and measurement update is greater than when it is at apogee. Interestingly, the errors increase when the satellite is a perigee due to this greater distance between measurement updates. This increased error at perigee is not seen when the time step is one second. Therefore, the accuracy of the orbit determining Kalman filter depends on both the accuracy of the measurements as well as the time between updates.

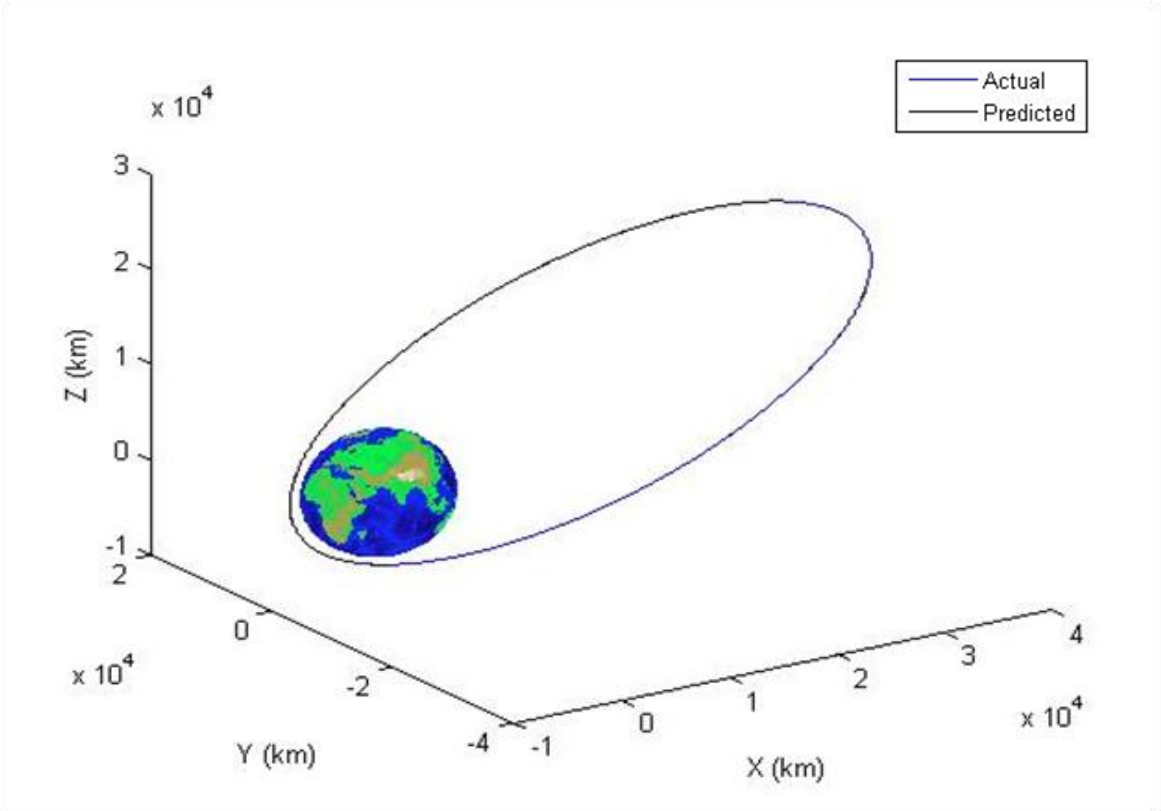

Figure 3.14: Error of Orbit Determined using GPS sensor

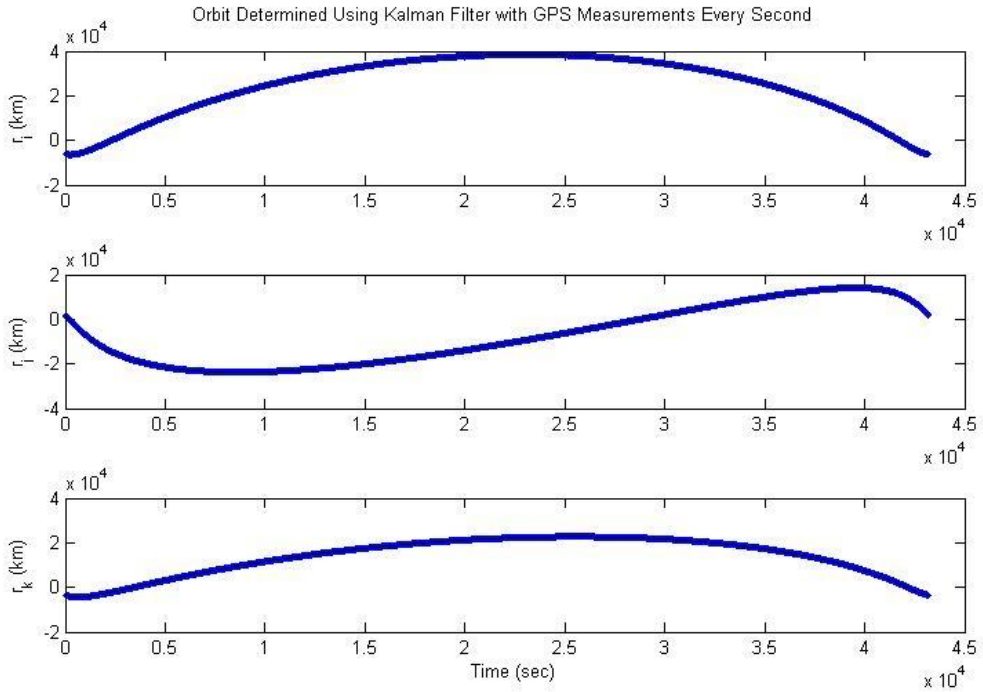

Figure 3.15: Orbit Determined using GPS sensor

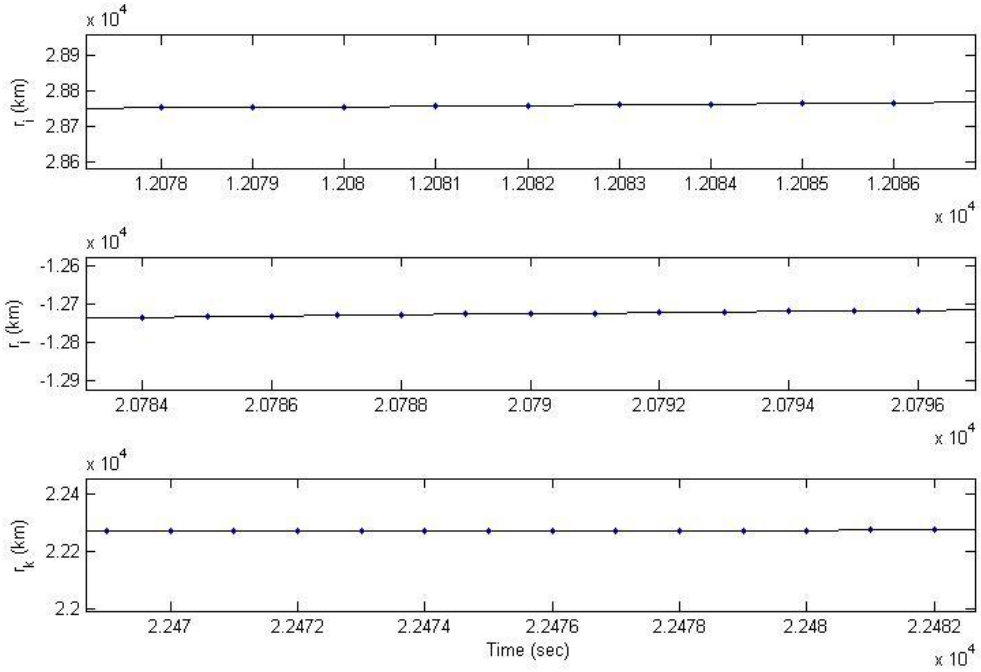

Figure 3.16: Zoomed In Orbit Determined using GPS sensor

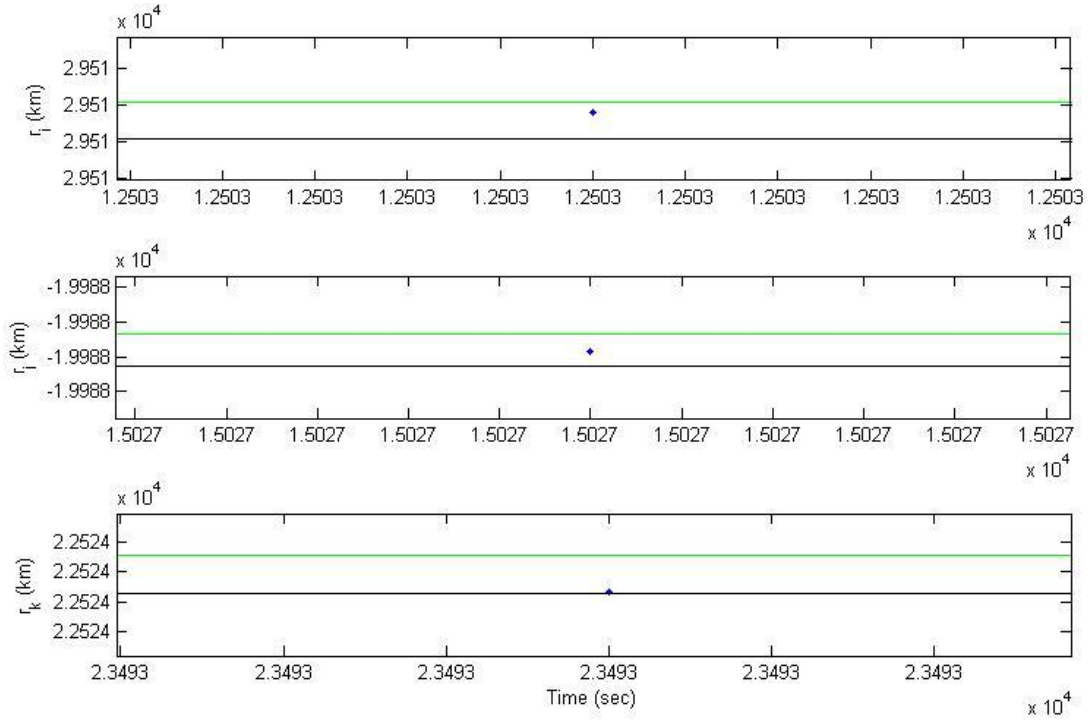

Figure 3.17: Zoomed in orbit determined using GPS sensor

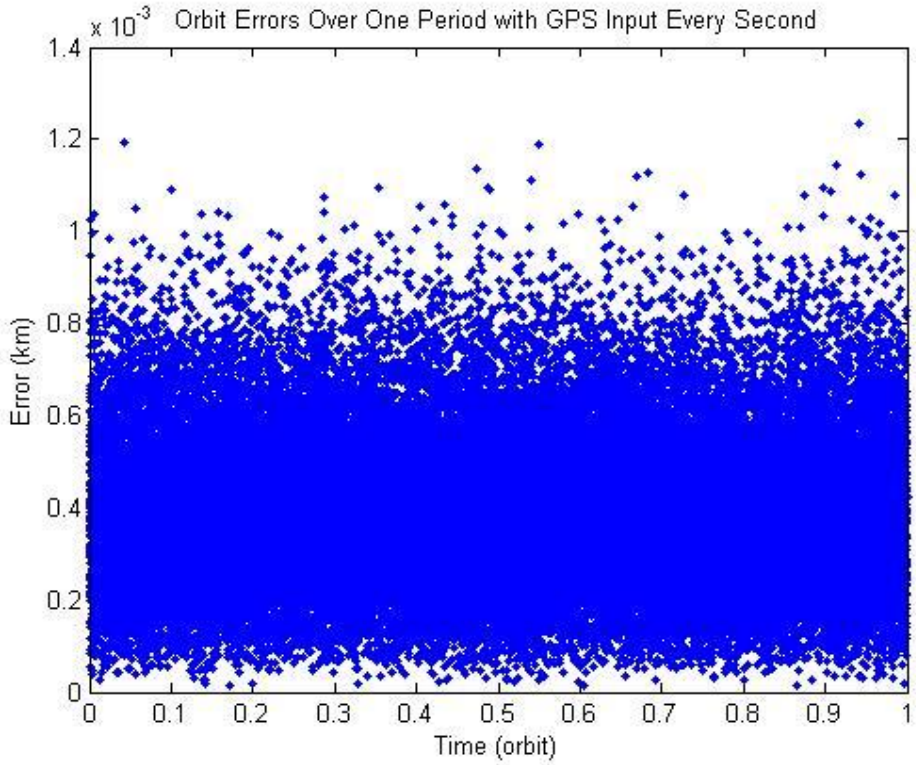

Figure 3.18: Errors in orbit determined using GPS sensor with measurement updates every second

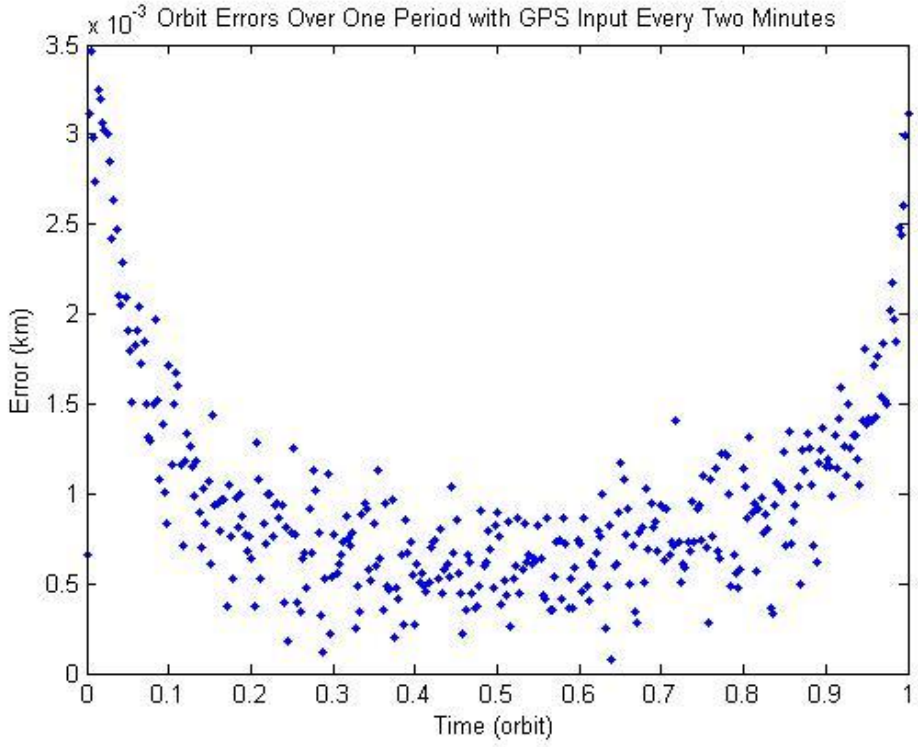

Figure 3.18: Errors in orbit determined using GPS sensor with measurement updates every two minutes

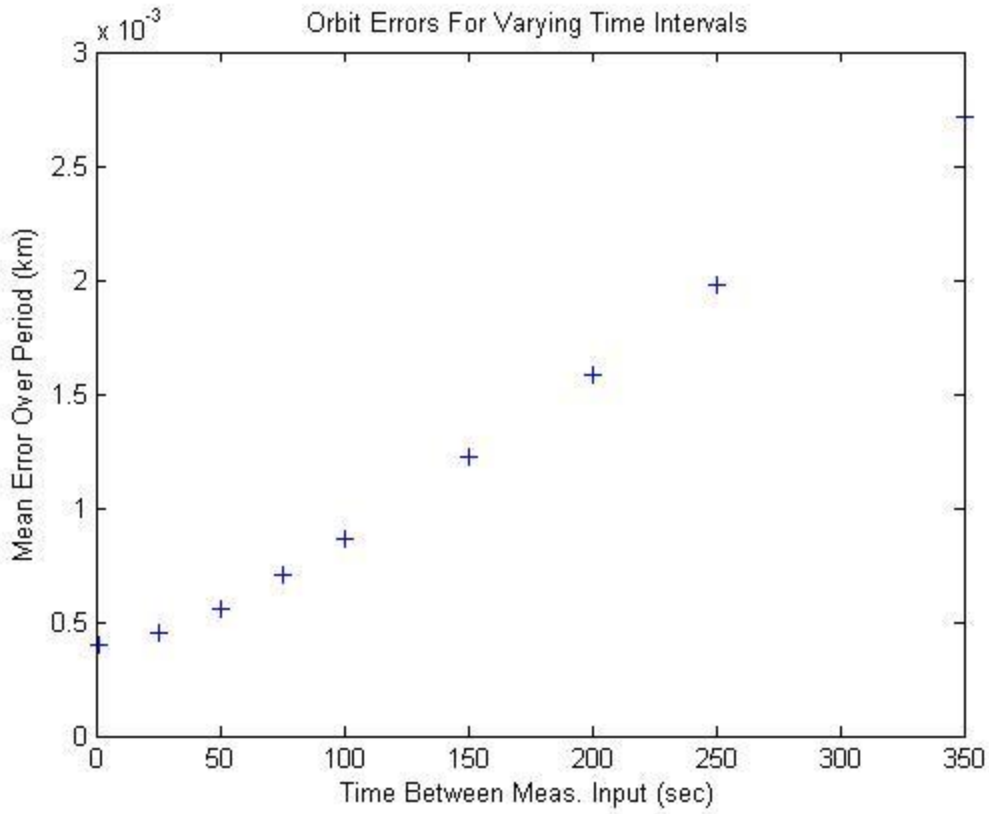

Figure 3.20: Mean errors in orbit verse time between measurement updates

Figure 3.20 shows how the decrease in time between measurement updates decreases the errors of the orbit determining Kalman filter. This shows the importance of both an accurate measurement as well as a small time between measurement update. The decrease in time between measurement updates increases the number of iterations per second the filter must compute, increase the computational effort. Therefore when designing an orbit determining algorithm, a trade study can be performed to find the largest time interval that meets the desired accuracy requirements.

In summary, the orbit determining Kalman filter designed in this thesis is clearly more accurate when run with GPS measurements updated throughout the orbit than using site-track measurements. However, if the GPS receiver somehow failed, the orbit can be determined using a ground station site track. This allows for orbit determination redundancy for the satellite. Now that the orbit has been determined, the satellite attitude will be determined using a similar method. The rotational equations of motion will be defined and the attitude will be estimated, taking in to consideration environmental forces on the satellite. Then the Kalman filter will be defined and implemented using a multiple of attitude determining sensors.

Chapter 4

Attitude Determination

Similarly to orbit determination, satellite attitude determination is an essential part of a satellite mission. Determining and controlling the attitude of a satellite allows for successful pointing of the satellite antennas, sensors and solar arrays. In order for a satellite to successfully perform the mission it was designed for, it must be able to accurately estimate and control its attitude. Also similar to the orbit of a satellite, the attitude of a satellite is affected by the environment in which it is in such as by atmospheric drag or solar radiation pressure. These environmental forces create disturbing torques on the satellite that need to be estimated in order to accurately determine the attitude of the satellite.

4.1 Representing Attitude

The attitude of a satellite is defined as the orientation of the satellite's body frame with respect to a constant reference frame. The next section defines the reference frames used in determining the attitude of the spacecraft in this thesis.

4.1.1 Reference Frames

In order to define a satellites orientation, an orbital reference frame, consisting of a triad of orthonormal vectors, must be defined. The orbital frame is constant under orbital variations with, $\widehat{\boldsymbol{o}}_3$, pointing in the direction of the satellite's position vector, described in Section 3.1.1. The attitude of a satellite is the orientation of the satellite's body frame with respect to this orbital frame, shown in Figure 4.1.

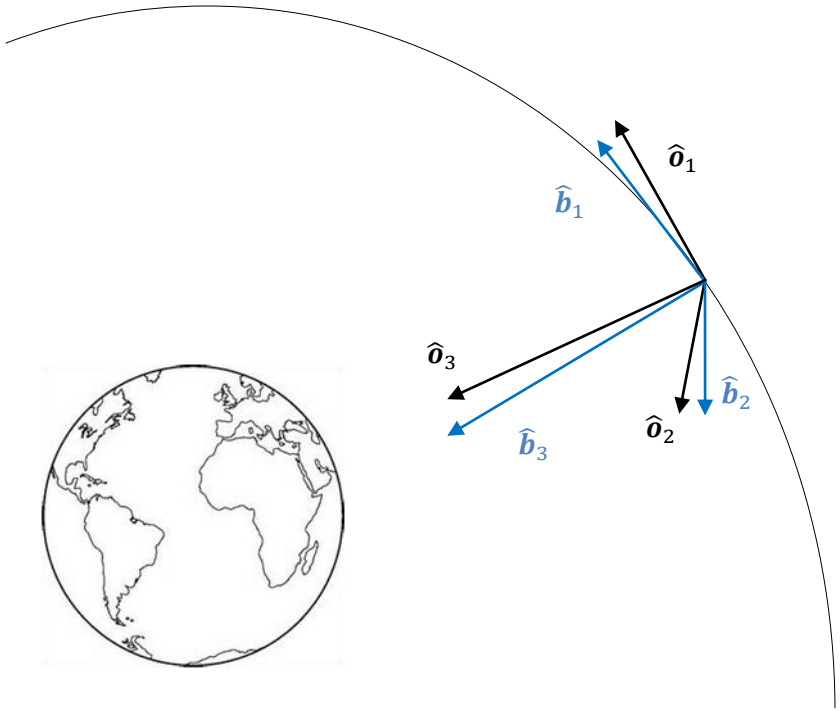

Figure 4.1: Orbital and Body Frame Representations

The angles between the body frame and the orbital frame are called Euler angles and define the orientation of the body frame with respect to the orbital frame.

4.1.2 Euler Angles

A satellite's orientation can be described by three angles, called Euler angles. Each Euler angle represents a rotation of the body frame about an axis of the orbital frame. These Euler angles are commonly referred to as roll, pitch and yaw. For a satellite, roll is the rotation of the satellite about $\hat{\boldsymbol{o}}_3$, the satellite's position vector. Yaw is defined as the rotation of the satellite about $\hat{\boldsymbol{o}}_2$. Last, pitch is defined as the rotation about $\hat{\boldsymbol{o}}_1$, the satellite's velocity vector. The roll Euler angle, θ_3, is the angle with which the body frame rotates about $\hat{\boldsymbol{o}}_3$. In other words, the roll angle is the angle between the body frame and orbital frame along the $\hat{\boldsymbol{o}}_1$ and $\hat{\boldsymbol{o}}_2$ axes. Similarly, the yaw Euler angle, θ_2, is the angle with which the body frame rotates about $\hat{\boldsymbol{o}}_2$. Last, the pitch Euler angle, θ_1, is defined as the rotation about $\hat{\boldsymbol{o}}_1$. These angles are summarized in Figure 4.2.

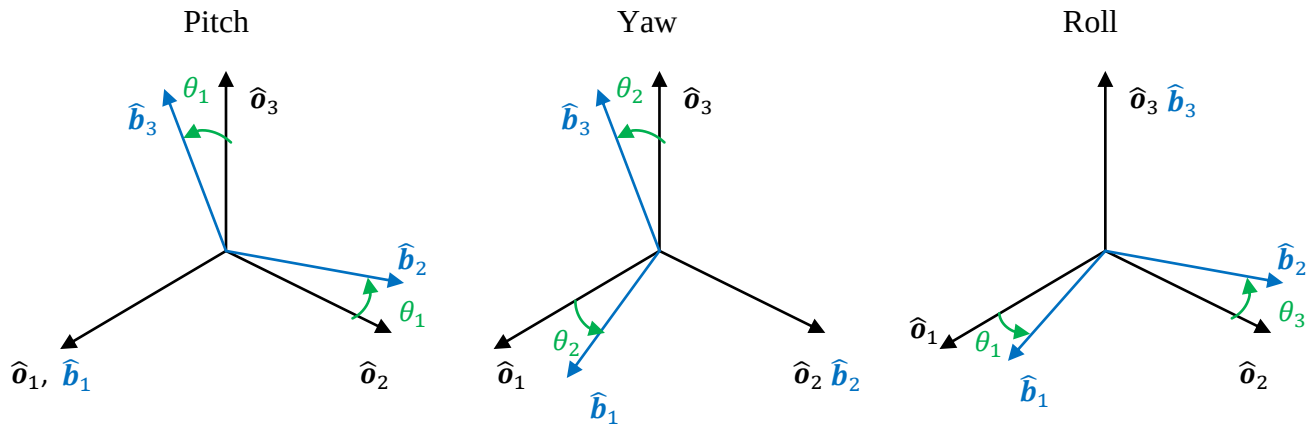

Figure 4.2: Euler Angles

Similar to the rotation matrix created to transform the SEZ frame to the ECI frame, rotation matrices are developed to represent a rotation about each of the three possible orbital axes. Below are the corresponding rotation matrices for roll pitch and yaw.

$$R_{Pitch}(\theta_1) = R_1(\theta_1) = \begin{bmatrix} 1 & 0 & 0 \\ 0 & \cos\theta_1 & -\sin\theta_1 \\ 0 & \sin\theta_1 & \cos\theta_1 \end{bmatrix}$$

$$R_{Yaw}(\theta_2) = R_2(\theta_2) = \begin{bmatrix} \cos\theta_2 & 0 & \sin\theta_2 \\ 0 & 1 & 0 \\ -\sin\theta_2 & 0 & \cos\theta_2 \end{bmatrix}$$

$$R_{Roll}(\theta_3) = R_3(\theta_3) = \begin{bmatrix} \cos\theta_3 & -\sin\theta_3 & 0 \\ \sin\theta_3 & \cos\theta_3 & 0 \\ 0 & 0 & 1 \end{bmatrix}$$

Combining these three rotations gives the rotation matrix.

$$R^{bo} = R_3(\theta_3)R_2(\theta_2)R_1(\theta_1)$$

$$R^{bo} = \begin{bmatrix} \cos\theta_2\cos\theta_3 & \cos\theta_3\sin\theta_1\sin\theta_2 + \cos\theta_1\sin\theta_3 & \sin\theta_1\sin\theta_3 - \cos\theta_1\cos\theta_3\sin\theta_2 \\ -\cos\theta_2\sin\theta_3 & \cos\theta_1\cos\theta_3 - \sin\theta_1\sin\theta_2\sin\theta_3 & \cos\theta_1\sin\theta_2\sin\theta_3 + \cos\theta_3\sin\theta_1 \\ \sin\theta_2 & -\cos\theta_2\sin\theta_1 & \cos\theta_3\cos\theta_3 \end{bmatrix}$$

This will be the rotation matrix used to transform any vectors in the orbital frame to the body frame. The same process can be used to determine the rotation matrix needed to transform any vector in the body frame to the orbital frame. Next, the rotational equations of motion must be formed in order to propagate the satellites attitude over the orbit.

4.2 Rotational Equations of Motion

The equations of motion for the satellite rotating about the orbital frame is derived using the satellites angular momentum and moment of inertia, defined as

$$\boldsymbol{h} = \mathrm{I}\boldsymbol{\omega}$$

where $\boldsymbol{\omega} = \begin{bmatrix}\omega_1\\ \omega_2\\ \omega_3\end{bmatrix} = \begin{bmatrix}\dot{\theta}_1\\ \dot{\theta}_2\\ \dot{\theta}_3\end{bmatrix}$ and is the time derivative of the Euler angles.

From Euler's Laws the time derivative of the satellite angular momentum is then

$$\frac{\mathrm{d}\boldsymbol{h}}{\mathrm{dt}} = \dot{\boldsymbol{h}} = -\boldsymbol{\omega}^{\times}\boldsymbol{h} + \boldsymbol{\tau} = \frac{\mathrm{d}(\mathrm{I}\boldsymbol{\omega})}{\mathrm{dt}} = \mathrm{I}\dot{\boldsymbol{\omega}}$$

where

$$\boldsymbol{\omega}^{\times} = \begin{bmatrix}0 & -\omega_3 & \omega_2\\ \omega_3 & 0 & -\omega_1\\ -\omega_2 & \omega_1 & 0\end{bmatrix}$$

and $\boldsymbol{\tau}$ is the torque acting on the satellite.

By rearranging the equation

$$\dot{\boldsymbol{\omega}} = -\mathbf{I}^{-1}\boldsymbol{\omega}^{\times}\mathbf{I}\boldsymbol{\omega} + \mathbf{I}^{-1}\boldsymbol{\tau}$$

where I^{-1} for the principal moments of inertia found in Section 1.2 is

$$\mathrm{I}^{-1} = \begin{bmatrix}1/\mathrm{I}_1 & 0 & 0\\ 0 & 1/\mathrm{I}_2 & 0\\ 0 & 0 & 1/\mathrm{I}_3\end{bmatrix}$$

Therefore the final rotational equations of motion are

$$\begin{bmatrix}\dot{\omega}_1\\ \dot{\omega}_2\\ \dot{\omega}_3\end{bmatrix} = \begin{bmatrix}\frac{\mathrm{I}_2 - \mathrm{I}_3}{\mathrm{I}_1}\omega_2\omega_3 + \frac{\tau_1}{\mathrm{I}_1}\\ \frac{\mathrm{I}_3 - \mathrm{I}_1}{\mathrm{I}_2}\omega_1\omega_3 + \frac{\tau_2}{\mathrm{I}_2}\\ \frac{\mathrm{I}_1 - \mathrm{I}_2}{\mathrm{I}_3}\omega_1\omega_2 + \frac{\tau_3}{\mathrm{I}_3}\end{bmatrix}$$

As done in Chapter 3, the Cowell's Formulation will be applied to the rotational equations of motion to propagate the satellite attitude over time using numerical integration. The state vector is defined as

$$X = \begin{bmatrix} x_1 \\ x_2 \\ x_3 \\ x_4 \\ x_5 \\ x_6 \end{bmatrix} = \begin{bmatrix} \theta_1 \\ \theta_2 \\ \theta_3 \\ \dot{\theta}_1 \\ \dot{\theta}_2 \\ \dot{\theta}_3 \end{bmatrix} = \begin{bmatrix} \theta_1 \\ \theta_2 \\ \theta_3 \\ \omega_1 \\ \omega_2 \\ \omega_3 \end{bmatrix}$$

The time derivative of the state vector is then

$$\dot{X} = \begin{bmatrix} \dot{\theta}_1 \\ \dot{\theta}_2 \\ \dot{\theta}_3 \\ \ddot{\theta}_1 \\ \ddot{\theta}_2 \\ \ddot{\theta}_3 \end{bmatrix} = \begin{bmatrix} \omega_1 \\ \omega_2 \\ \omega_3 \\ \dot{\omega}_1 \\ \dot{\omega}_2 \\ \dot{\omega}_3 \end{bmatrix} = \begin{bmatrix} \omega_1 \\ \omega_2 \\ \omega_3 \\ \frac{\mathrm{I}_2 - \mathrm{I}_3}{\mathrm{I}_1}\omega_2\omega_3 + \frac{\tau_1}{\mathrm{I}_1} \\ \frac{\mathrm{I}_3 - \mathrm{I}_1}{\mathrm{I}_2}\omega_1\omega_3 + \frac{\tau_2}{\mathrm{I}_2} \\ \frac{\mathrm{I}_1 - \mathrm{I}_2}{\mathrm{I}_3}\omega_1\omega_2 + \frac{\tau_3}{\mathrm{I}_3} \end{bmatrix} = \begin{bmatrix} x_4 \\ x_5 \\ x_6 \\ \frac{\mathrm{I}_2 - \mathrm{I}_3}{\mathrm{I}_1}x_5x_6 + \frac{\tau_{total_1}}{\mathrm{I}_1} \\ \frac{\mathrm{I}_3 - \mathrm{I}_1}{\mathrm{I}_2}x_4x_6 + \frac{\tau_{total_2}}{\mathrm{I}_2} \\ \frac{\mathrm{I}_1 - \mathrm{I}_2}{\mathrm{I}_3}x_4x_5 + \frac{\tau_{total_3}}{\mathrm{I}_3} \end{bmatrix}$$

Also seen in the previous chapter, perturbing forces, or in this case disturbing torques, are added to the angular acceleration in order to best estimate the attitude of the satellite. The disturbing acceleration is defined as

$$\begin{bmatrix} \dot{\omega}_1 \\ \dot{\omega}_2 \\ \dot{\omega}_3 \end{bmatrix}_{dist} = \begin{bmatrix} \frac{\tau_1}{I_1} \\ \frac{\tau_2}{I_2} \\ \frac{\tau_3}{I_3} \end{bmatrix}_{dist}$$

Similarly to Chapter 2, the disturbing torques can be summed to find the total disturbance on the satellite attitude. In this thesis, four disturbing environmental torques are considered as well as a control torque, which will counteract the disturbing torques and orient the satellite to the desired position. The torques are summed together below.

$$\tau_{total} = \tau_{disturb} + \tau_{control} = \tau_{gg} + \tau_{SR} + \tau_{mag} + \tau_{aero} + \tau_{control}$$

4.3 Disturbing Torques

The four disturbing torques studied in this thesis are: gravity gradient torque, solar radiation pressure torque, magnetic torque and aerodynamic drag torque. These are the four most prominent environmental torques experienced by a satellite in a Molniya orbit. Figure 4.3 shows generally how the magnitudes of the four disturbing torques vary with altitude. Since the Molniya orbit's altitude is similar to a LEO orbit while at perigee and a GEO orbit while at apogee, all four torques must be considered. The magnitudes shown in Figure 4.3 also vary depending on the satellite shape and weight.

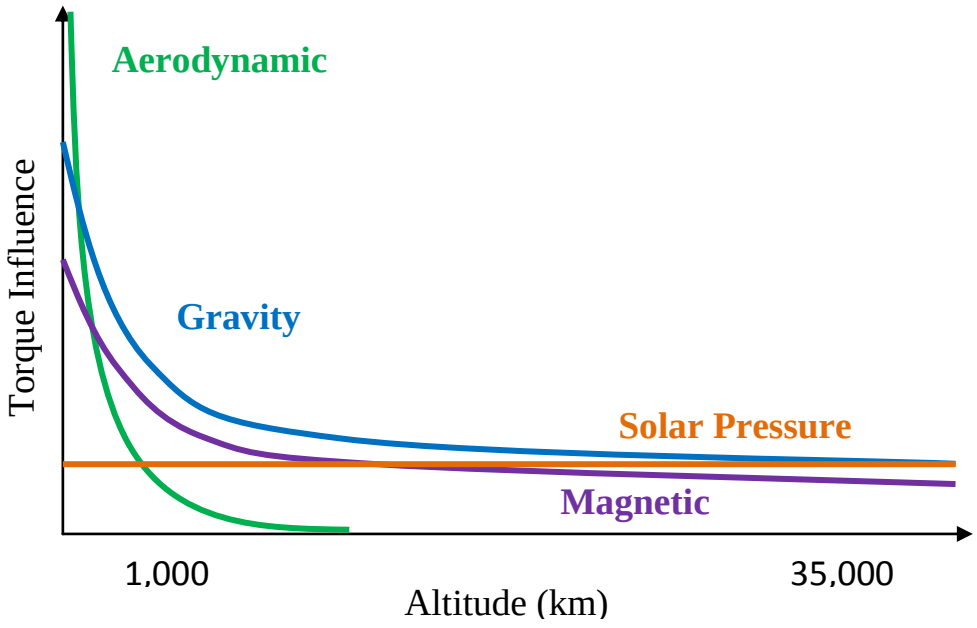

Figure 4.3: Disturbance Torque Effects vs. Altitude

In the following sections, the angular acceleration due to each of the disturbing torques will be derived. Then, in order to implement the Kalman filter, the state matrix, F, made up of the accelerations partial derivatives, must be determined.

4.3.1 Solar Radiation Pressure Torque

Particles and energy from the sun bombard the satellite throughout the orbit creating pressure and torque on the satellite. The torque is created when the location of the satellite's center of mass is not the location of the satellite's center of solar pressure, as it is in this thesis. The variations in the satellite attitude due to solar radiation pressure torque are periodic and depend on the reflectivity of the satellite as well as the direction of the sun.

The solar radiation torque can be calculated using the following equation

$$\tau_{SR} = \frac{F_s}{c} A(1+q)\cos(\emptyset_{inc})\,(C_{ps} - cm)$$

where F_s is the solar constant (1358 W/m^2), c is the speed of light, and A is the surface area of the satellite that is towards the Sun. The reflectance factor, q, the center of solar pressure, C_{ps}, and the center of mass, *cm*, are all characteristics of the satellite and must be taken in to account during its design. See Table 1.1 for these quantities. Last the incidence angle of the sun is $\emptyset_{inc}$, which determines the direction of the disturbing torque

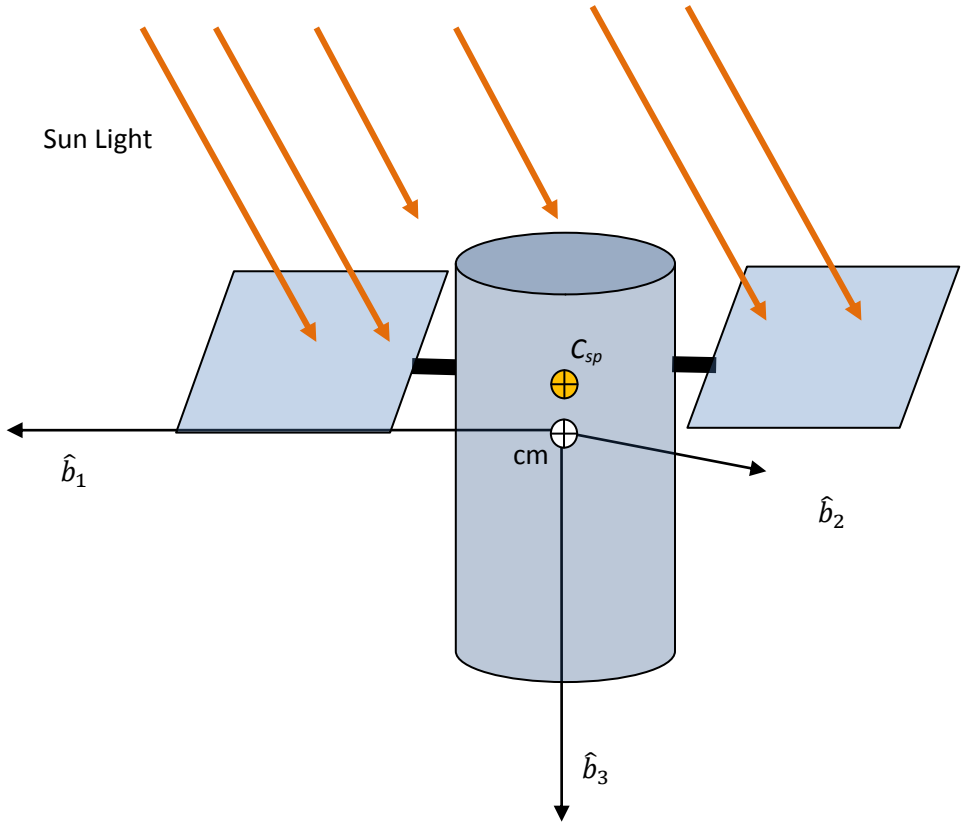

Figure 4.4: Sunlight on Satellite

Similarly to the solar radiation pressure perturbing force calculated in Chapter 3, the vector from the sun to the satellite must be inputted in to the Kalman filter in order to determine the disturbing torque created by the pressure. The vector from the sun to the satellite is

$$\vec{r}_{sat\odot} = \vec{r}_{\odot} - \vec{r}_{sat} = \begin{bmatrix} r_{i_\odot} - r_{i_{sat}} \\ r_{j_\odot} - r_{j_{sat}} \\ r_{k_\odot} - r_{k_{sat}} \end{bmatrix}$$

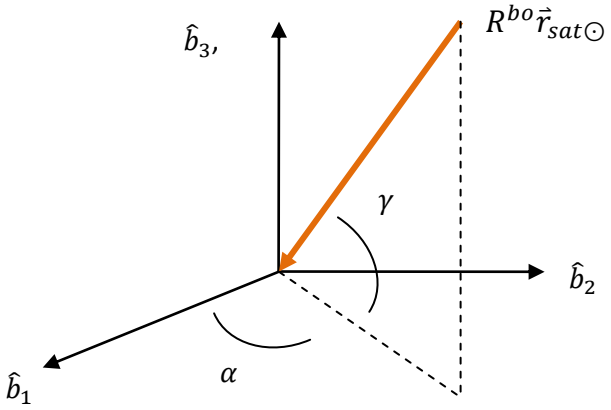

Figure 4.5: Incident angles of Sunlight with respect to Body Frame

Then the incident angle of the sun with respect to the body frame can be defined by the angles α and γ shown in Figure 4.5 as

$$\alpha = tan^{-1}\left(\frac{\vec{r}_{sat\odot 2}}{\vec{r}_{sat\odot 1}}\right) \qquad \gamma = sin^{-1}(\vec{r}_{sat\odot 3})$$

Then the disturbance torque due to solar radiation, represented in the body frame is

$$\tau_{SR}{}^{b} = \begin{bmatrix}\tau_1\\ \tau_2\\ \tau_3\end{bmatrix} = \frac{F_s}{c}(1+q)\begin{bmatrix}A_1\cos(\alpha)(C_{ps}-cm)_1\\ A_2\sin(\alpha)(C_{ps}-cm)_2\\ A_3\sin(\gamma)(C_{ps}-cm)_3\end{bmatrix} = \frac{F_s}{c}(1+q)\begin{bmatrix}A_1\cos(\alpha)\Delta_1\\ A_2\sin(\alpha)\Delta_2\\ A_3\sin(\gamma)\Delta_3\end{bmatrix}$$

The center of pressure and center of mass components are equal except for along the $\hat{b}_3$ axis. Assuming the satellite is always oriented such that the normal vector of the solar arrays is always pointing toward the Sun; the solar radiation pressure torque creates a motion only about the $\hat{b}_1$ axis, or pitch angle.

4.2.2 Gravity Gradient Torque

One of the assumptions of the two body problem was that the Earth and satellite were spherically symmetric. Chapter 3 discussed the effects due to Earth not being spherically symmetric, now the fact that the satellite is not spherically symmetric will be addressed. As previously explained, Newton's law of gravitational force states that the force due to gravity on a satellite is proportional to the distance the satellite is to the central body. Since the satellite in this thesis is not spherically symmetric, the portion of the satellite closest to Earth will experience a larger gravitational force than the portion furthest from Earth. The difference between the gravity experienced by the closest and furthest part of the satellite is called the gravity gradient.

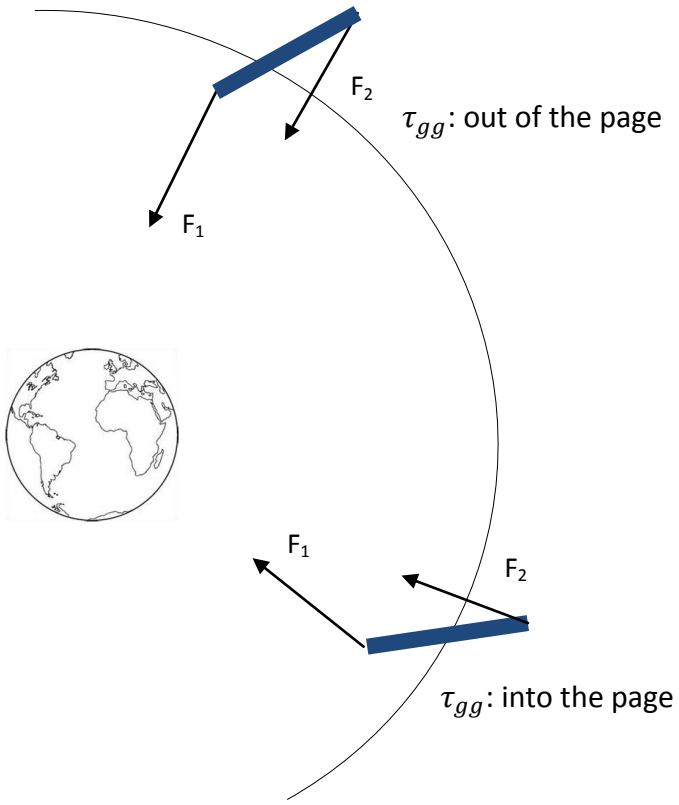

Figure 4.7: Gravity Gradient Torque

The gravity gradient creates a torque given as

$$\tau_{gg}{}^{o} = 3\omega_o^2 \hat{o}_3^{\times} I \hat{o}_3$$

where

$$\hat{o}_3 = R^{ob}\hat{b}_3 = R^{ob}\begin{bmatrix}0\\0\\1\end{bmatrix} = \begin{bmatrix}R_{13}\\R_{23}\\R_{33}\end{bmatrix}$$

Therefore

$$\tau_{gg}{}^{o} = 3\omega_o^2 \hat{o}_3^{\times} I \hat{o}_3 = 3\omega_o^2 \begin{bmatrix}0 & -R_{33} & R_{23}\\ R_{33} & 0 & -R_{13}\\ -R_{23} & R_{13} & 0\end{bmatrix}\begin{bmatrix}I_1 & 0 & 0\\ 0 & I_2 & 0\\ 0 & 0 & I_3\end{bmatrix}\begin{bmatrix}R_{13}\\R_{23}\\R_{33}\end{bmatrix} = 3\omega_o^2 \begin{bmatrix}(I_3-I_2)R_{23}R_{33}\\ (I_1-I_3)R_{13}R_{33}\\ (I_2-I_1)R_{13}R_{23}\end{bmatrix}$$

$$= 3\omega_o^2 \begin{bmatrix}(I_3 - I_2)\cos\theta_3\cos\theta_3\,(\cos\theta_1\sin\theta_2\sin\theta_3 + \cos\theta_3\sin\theta_1)\\ (I_1 - I_3)\cos\theta_3\cos\theta_3\,(\sin\theta_1\sin\theta_3 - \cos\theta_1\cos\theta_3\sin\theta_2)\\ (I_2 - I_1)(\sin\theta_1\sin\theta_3 - \cos\theta_1\cos\theta_3\sin\theta_2)(\cos\theta_1\sin\theta_2\sin\theta_3 + \cos\theta_3\sin\theta_1)\end{bmatrix}$$

4.2.3 Magnetic Field Torque

Magnetic field torque is caused by the interactions between the Earth's magnetic field and the residual magnetic dipole of the satellite. The torque depends on the Earth's magnetic field and therefore it varies depending on the satellite's position in its orbit. The distubing torque due to Earth's magnetic field is

$$\vec{\tau}_{mag} = \vec{D} \times \vec{B}$$

where D is the satellite's residual dipole and B is the strength and direction of the Earth's magnetic field at the radius of the satellite. Therefore, to calculate the torque acting on the satellite a model of the Earth's magnetic field, or a magnetometer, is required on board the satellite. Using an on-board model of the Earth's magnetic field is computational expensive but does not require a magnetometer sensor on board. A magnetometer will be explained in the following section.

4.2.4 Aerodynamic Torque

Aerodynamic torque is caused by particles in the Earth's atmosphere bombarding the satellite. If the satellite's center of mass and center of drag are not co-located, the particles hitting the satellite create a torque. Since the torque is caused by the Earth's atmosphere, as the satellite's altitude increases, the aerodynamic torque decreases. The torque on the satellite is

$$\tau_{mag} = \frac{1}{2}\rho C_d A v^2 (C_{pa} - cm)$$

where C_d is the coefficient of drag for the satellite, A is the cross-sectional area and *v* is the velocity. C_{pa} is the center of aerodynamic pressure, ρ is the atmospheric density and cm is the satellites center of mass. The atmospheric density model explained in Chapter 3 can be used again here to determine the atmospheric density at the current location of the satellite. Similarly to the other disturbing torques, knowledge of the location of the satellite is necessary to determine the torque acting on the satellite.

To summarize, the four disturbing torques considered, in this thesis, are gravity gradient, solar radiation pressure, magnetic and drag. These torques add together to form the disturbance torque seen in the equation for total torque

$$\tau_{total} = \tau_{disturb} + \tau_{control} = \tau_{gg} + \tau_{SR} + \tau_{mag} + \tau_{aero} + \tau_{control}$$

The next step is to define the control torque needed to maneuver the satellite in the desired motion. Once the control torque is determined the final equations of motions will be numerically integrated and used as the "prediction" phase of the Kalman filter implementation.

4.4 Attitude Control

In order to perform a desired mission, a satellite must not only accurately determine its attitude but control its attitude. The satellite in this thesis uses both control moment gyros and thrusters to control the attitude. Control momentum gyros (CMG) are a commonly used in satellite attitude control systems since they have low power requirements. CMGs are made up of a spinning rotor and motorized gimbals that use the conservation of angular momentum to change the satellite attitude. The spinning rotor is tilted by the gimbals to create a gyroscopic torque that changes the satellite attitude. Another form of attitude control is thrusters. Thrusters are attached along all three axis of the satellite and positioned at the satellite's center of mass. Fuel consumption and hardware degradation are the limiting factors of thrusters. In this thesis, it is assumed that the satellite's CMGs and thrusters are able to change the attitude of the satellite in the desired control motion seen in Figure 4.11.

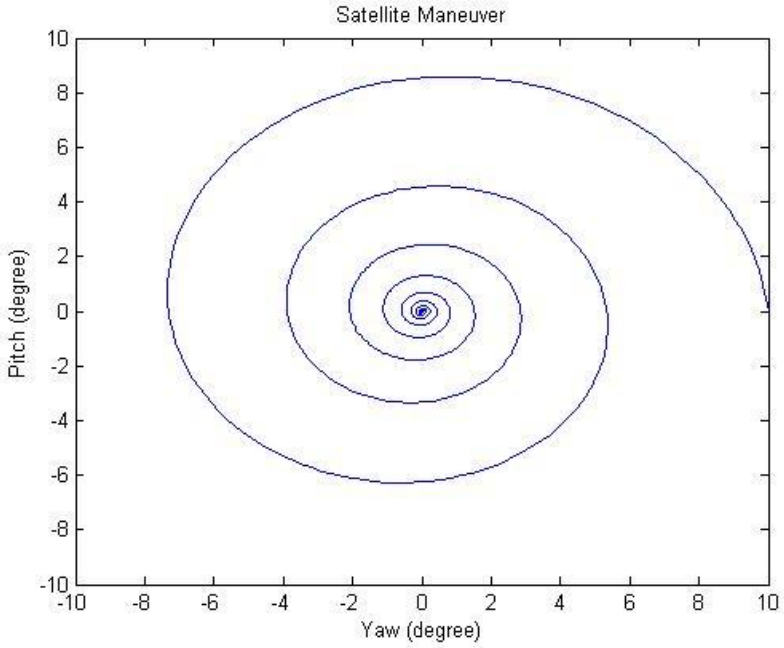

Figure 4.11: Desired motion of satellite

As derived in the previous section, the rotational equations of motion applied in this thesis are

$$\dot{X} = \begin{bmatrix} \dot{\theta}_1 \\ \dot{\theta}_2 \\ \dot{\theta}_3 \\ \ddot{\theta}_1 \\ \ddot{\theta}_2 \\ \ddot{\theta}_3 \end{bmatrix} = \begin{bmatrix} \omega_1 \\ \omega_2 \\ \omega_3 \\ \dot{\omega}_1 \\ \dot{\omega}_2 \\ \dot{\omega}_3 \end{bmatrix} = \begin{bmatrix} \omega_1 \\ \omega_2 \\ \omega_3 \\ \frac{\mathrm{I}_2 - \mathrm{I}_3}{\mathrm{I}_1}\omega_2\omega_3 + \frac{\tau_1}{\mathrm{I}_1} \\ \frac{\mathrm{I}_3 - \mathrm{I}_1}{\mathrm{I}_2}\omega_1\omega_3 + \frac{\tau_2}{\mathrm{I}_2} \\ \frac{\mathrm{I}_1 - \mathrm{I}_2}{\mathrm{I}_3}\omega_1\omega_2 + \frac{\tau_3}{\mathrm{I}_3} \end{bmatrix} = \begin{bmatrix} x_4 \\ x_5 \\ x_6 \\ \frac{\mathrm{I}_2 - \mathrm{I}_3}{\mathrm{I}_1}x_5x_6 + \frac{\tau_{total_1}}{\mathrm{I}_1} \\ \frac{\mathrm{I}_3 - \mathrm{I}_1}{\mathrm{I}_2}x_4x_6 + \frac{\tau_{total_2}}{\mathrm{I}_2} \\ \frac{\mathrm{I}_1 - \mathrm{I}_2}{\mathrm{I}_3}x_4x_5 + \frac{\tau_{total_3}}{\mathrm{I}_3} \end{bmatrix}$$

where the torque applied to the system is a sum of the disturbing torques as well as the control torque seen below

$$\tau_{total} = \tau_{disturb} + \tau_{control} = \tau_{gg} + \tau_{SR} + \tau_{mag} + \tau_{aero} + \tau_{control}$$

This section will focus on developing the control torque needed to maneuver the satellite in a spiral type motion seen in Figure 4.11. This motion will test the accuracy of the Kalman Filter algorithm since the Euler angles change rather quickly.

The desired motion is

$$\begin{bmatrix} \theta_1 \\ \theta_2 \\ \theta_3 \end{bmatrix} = \begin{bmatrix} 10e^{-0.02t}\sin(11.4592t) \\ 10e^{-0.02t}\cos(11.4592t) \\ \sin(2.8648t) \end{bmatrix}$$

where the angles are in degrees. The needed acceleration to perform this maneuver is

$$\begin{bmatrix} \dot{\omega}_1 \\ \dot{\omega}_2 \\ \dot{\omega}_3 \end{bmatrix} = \begin{bmatrix} -0.002e^{0.009t}\theta_1 \\ -0.002e^{0.009t}\theta_2 \\ -0.0002\theta_3 \end{bmatrix}$$

The time derivative of the state vector becomes

$$\dot{X} = \begin{bmatrix} \omega_1 \\ \omega_2 \\ \omega_3 \\ -0.002e^{0.009t}\theta_1 \\ -0.002e^{0.009t}\theta_2 \\ -0.0002\theta_3 \end{bmatrix} = \begin{bmatrix} x_4 \\ x_5 \\ x_6 \\ -0.002e^{0.009t}x_1 \\ -0.002e^{0.009t}x_2 \\ -0.0002x_3 \end{bmatrix}$$

The satellites attitude is seen in Figure 4.12. This is the motion that will be used in the Kalman filter.

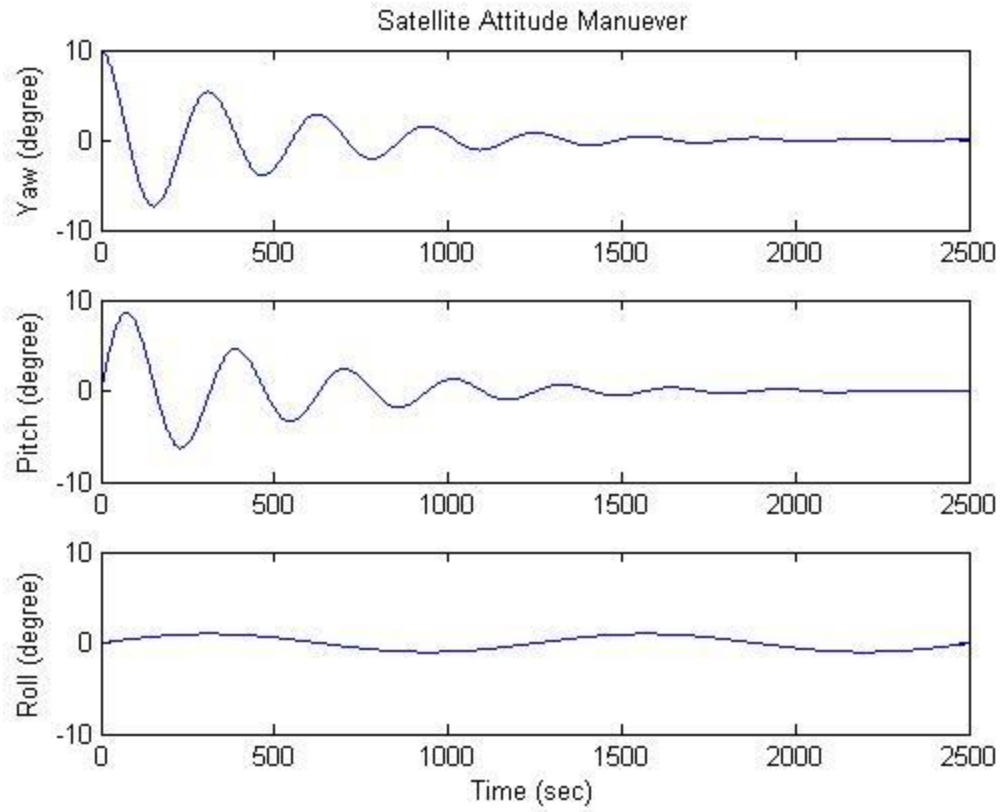

Figure 4.12: Satellite Maneuver

Now that the rotational equations of motion have been defined they can be used to find the state transition matrix for the prediction phase of the Kalman filter. Next the sensors used to input measurements in to the correction phase of the filter will be explained.

4.5 On-Board Attitude Sensors

In order to conduct the desired mission, the satellite must accurately determine and control the attitude. A satellite's attitude can be determined by a variety of on-board sensors. Each type of sensor has its advantages and disadvantages. The four cases of attitude determination in the thesis correspond to four sensors on board the satellite and are: magnetometer, Earth sensor, Sun sensor and star trackers. How each sensor works and their typical errors are explained in the following sections.

4.5.1 Magnetometer

A magnetometer determines the attitude of the satellite by measuring the magnetic field in the satellite's body frame and comparing the measured field to that of the predicated field in the satellite's orbital frame. The predicted magnetic field of the Earth in the satellite's orbital frame

is derived from a chosen model. Therefore, the Euler angles can be determined from the rotation matrix needed to transform the magnetic field in the satellites orbital frame to the measured field in the satellite's body frame.

$$M_{body} = R^{bo} M_{orbital}$$

Therefore

$$R^{bo} = M_{body} {M_{orbital}}^{-1}$$

Then

$$yaw = \theta_2 = \sin^{-1}(R_{31}^{bo})$$

$$pitch = \theta_1 = \sin^{-1}(-\frac{R_{32}^{bo}}{\cos\theta_2})$$

$$roll = \theta_3 = \cos^{-1}(\frac{R_{11}^{bo}}{\cos\theta_2})$$

An advantage to magnetometer attitude sensors is that they are lightweight and have low power consumptions. A disadvantage to magnetometer sensors is the rather large inaccuracies, about 1 degree, when compared to the other attitude sensors available. These errors arise from the errors of the Earth's magnetic field model. The magnetometer has the highest errors of the attitude sensors used in this thesis.

4.5.2 Earth Sensor

An Earth sensor uses the location of the Earth to determine the attitude of the satellite. Typically, infrared cameras are continuously determining the location of the Earth relative to the satellite's body frame. Then the location of the Earth relative to the satellite's body frame is compared to that of the orbital frame to determine the Euler angles. The math is similar to the magnetometer derivation above, except for rather than a magnetic field vector, it the vector from the Earth to the satellite's body and orbital frame. Earth sensors are more accurate than magnetometers as well as being low cost and reliable. The Earth sensor used in this thesis has typical errors of 0.2 degrees.

4.5.3 Sun Sensor

Similar to the Earth sensor, a Sun sensor determines the orientation of the satellite by comparing the Sun's position vector measured in the satellite's body reference frame to the Sun's position vector known in the orbital reference frame. The sun sensor uses on-board photocells to determine the incident angle of the Sun. The Sun sensor used in this thesis has errors of 0.15 degrees.

4.5.4 Star Sensor

Star sensors determine the attitude of the satellite by capturing images of stars seen in the satellite's body frame and comparing them to a catalog of star constellations. A star sensor is highly accurate but requires more power and is the heaviest of the four sensors used in this thesis. Therefore, the engineers designing the attitude control system for the satellite must weigh the cost and benefits of each of these four sensors in order to design the satellite to best meet the mission requirements.

To summarize, four attitude determining cases will be studied corresponding to the four attitude sensors explained above. A summary of the errors and update rates of the four sensors are shown in Table 4.1. The update rate is important since not only are small errors required to best determine attitude, but also short durations between measurement inputs in to the Kalman Filter. Therefore, a very accurate sensor that only inputs measurements ever minute may be less effective at determining attitude than a less accurate sensor that updates once a second.

	Error	Update rate
Magnetometers	1°	0.1 sec
Earth Sensor	0.2°	0.1 sec
Sun Sensor	0.15°	0.25 sec
Star Sensor	5.6×10^{-4} °	0.25 sec

Table 4.1: Errors and update times for Attitude Sensors

4.6 Kalman Filter Implementation for Attitude Determination

Now that the acceleration of the Euler angles and the measurement devices used to determine the attitude of the satellite have been explained, the Kalman filter can be implemented. First, the observation matrix must be formed. Since the attitude sensors measure the position and velocity of the Euler angles, the observation matrix is just the identity matrix.

$$\mathbf{H} = \frac{\partial \mathbf{z}}{\partial \mathbf{X}} = \begin{bmatrix} \frac{\partial \theta_1}{\partial \theta_1} & \frac{\partial \theta_1}{\partial \theta_2} & \frac{\partial \theta_1}{\partial \theta_3} & \frac{\partial \theta_1}{\partial \omega_1} & \frac{\partial \theta_1}{\partial \omega_2} & \frac{\partial \theta_1}{\partial \omega_3} \\ \frac{\partial \theta_2}{\partial \theta_1} & \frac{\partial \theta_2}{\partial \theta_2} & \frac{\partial \theta_2}{\partial \theta_3} & \frac{\partial \theta_2}{\partial \omega_1} & \frac{\partial \theta_2}{\partial \omega_2} & \frac{\partial \theta_2}{\partial \omega_3} \\ \frac{\partial \theta_3}{\partial \theta_1} & \frac{\partial \theta_3}{\partial \theta_2} & \frac{\partial \theta_3}{\partial \theta_3} & \frac{\partial \theta_3}{\partial \omega_1} & \frac{\partial \theta_3}{\partial \omega_2} & \frac{\partial \theta_3}{\partial \omega_3} \\ \frac{\partial \omega_1}{\partial \theta_1} & \frac{\partial \omega_1}{\partial \theta_2} & \frac{\partial \omega_1}{\partial \theta_3} & \frac{\partial \omega_1}{\partial \omega_1} & \frac{\partial \omega_1}{\partial \omega_2} & \frac{\partial \omega_1}{\partial \omega_3} \\ \frac{\partial \omega_2}{\partial \theta_1} & \frac{\partial \omega_2}{\partial \theta_2} & \frac{\partial \omega_2}{\partial \theta_3} & \frac{\partial \omega_2}{\partial \omega_1} & \frac{\partial \omega_2}{\partial \omega_2} & \frac{\partial \omega_2}{\partial \omega_3} \\ \frac{\partial \omega_3}{\partial \theta_1} & \frac{\partial \omega_3}{\partial \theta_2} & \frac{\partial \omega_3}{\partial \theta_3} & \frac{\partial \omega_3}{\partial \omega_1} & \frac{\partial \omega_3}{\partial \omega_2} & \frac{\partial \omega_3}{\partial \omega_3} \end{bmatrix} = \begin{bmatrix} 1 & 0 & 0 & 0 & 0 & 0 \\ 0 & 1 & 0 & 0 & 0 & 0 \\ 0 & 0 & 1 & 0 & 0 & 0 \\ 0 & 0 & 0 & 1 & 0 & 0 \\ 0 & 0 & 0 & 0 & 1 & 0 \\ 0 & 0 & 0 & 0 & 0 & 1 \end{bmatrix}$$

The state matrix, F, is developed by linearizing the state vector by taking the partial derivatives of each element with respect to the position and velocity components. For the undisturbed rotational equations of motion

$$\dot{X} = \begin{bmatrix} \dot{\theta}_1 \\ \dot{\theta}_2 \\ \dot{\theta}_3 \\ \ddot{\theta}_1 \\ \ddot{\theta}_2 \\ \ddot{\theta}_3 \end{bmatrix} = \begin{bmatrix} \omega_1 \\ \omega_2 \\ \omega_3 \\ \dot{\omega}_1 \\ \dot{\omega}_2 \\ \dot{\omega}_3 \end{bmatrix} = \begin{bmatrix} \omega_1 \\ \omega_2 \\ \omega_3 \\ \frac{I_2 - I_3}{I_1}\omega_2\omega_3 \\ \frac{I_3 - I_1}{I_2}\omega_1\omega_3 \\ \frac{I_1 - I_2}{I_3}\omega_1\omega_2 \end{bmatrix}$$

the state matrix is

$$\mathbf{F} = \begin{bmatrix} \frac{\partial \omega_1}{\partial \theta_1} & \frac{\partial \omega_1}{\partial \theta_2} & \frac{\partial \omega_1}{\partial \theta_3} & \frac{\partial \omega_1}{\partial \omega_1} & \frac{\partial \omega_1}{\partial \omega_2} & \frac{\partial \omega_1}{\partial \omega_3} \\ \frac{\partial \omega_2}{\partial \theta_1} & \frac{\partial \omega_2}{\partial \theta_2} & \frac{\partial \omega_2}{\partial \theta_3} & \frac{\partial \omega_2}{\partial \omega_1} & \frac{\partial \omega_2}{\partial \omega_2} & \frac{\partial \omega_2}{\partial \omega_3} \\ \frac{\partial \omega_3}{\partial \theta_1} & \frac{\partial \omega_3}{\partial \theta_2} & \frac{\partial \omega_3}{\partial \theta_3} & \frac{\partial \omega_3}{\partial \omega_1} & \frac{\partial \omega_3}{\partial \omega_2} & \frac{\partial \omega_3}{\partial \omega_3} \\ \frac{\partial \dot{\omega}_1}{\partial \theta_1} & \frac{\partial \dot{\omega}_1}{\partial \theta_2} & \frac{\partial \dot{\omega}_1}{\partial \theta_3} & \frac{\partial \dot{\omega}_1}{\partial \omega_1} & \frac{\partial \dot{\omega}_1}{\partial \omega_2} & \frac{\partial \dot{\omega}_1}{\partial \omega_3} \\ \frac{\partial \dot{\omega}_2}{\partial \theta_1} & \frac{\partial \dot{\omega}_2}{\partial \theta_2} & \frac{\partial \dot{\omega}_2}{\partial \theta_3} & \frac{\partial \dot{\omega}_2}{\partial \omega_1} & \frac{\partial \dot{\omega}_2}{\partial \omega_2} & \frac{\partial \dot{\omega}_2}{\partial \omega_3} \\ \frac{\partial \dot{\omega}_3}{\partial \theta_1} & \frac{\partial \dot{\omega}_3}{\partial \theta_2} & \frac{\partial \dot{\omega}_3}{\partial \theta_3} & \frac{\partial \dot{\omega}_3}{\partial \omega_1} & \frac{\partial \dot{\omega}_3}{\partial \omega_2} & \frac{\partial \dot{\omega}_3}{\partial \omega_3} \end{bmatrix} = \begin{bmatrix} 0 & 0 & 0 & 1 & 0 & 0 \\ 0 & 0 & 0 & 0 & 1 & 0 \\ 0 & 0 & 0 & 0 & 0 & 1 \\ 0 & 0 & 0 & 0 & \frac{I_2 - I_3}{I_1}\omega_3 & \frac{I_2 - I_3}{I_1}\omega_2 \\ 0 & 0 & 0 & \frac{I_3 - I_1}{I_2}\omega_3 & 0 & \frac{I_3 - I_1}{I_2}\omega_1 \\ 0 & 0 & 0 & \frac{I_1 - I_2}{I_3}\omega_1 & \frac{I_1 - I_2}{I_3}\omega_1 & 0 \end{bmatrix}$$

For the perturbed rotational equations of motion

$$\dot{X} = \begin{bmatrix} \dot{\theta}_1 \\ \dot{\theta}_2 \\ \dot{\theta}_3 \\ \ddot{\theta}_1 \\ \ddot{\theta}_2 \\ \ddot{\theta}_3 \end{bmatrix} = \begin{bmatrix} \omega_1 \\ \omega_2 \\ \omega_3 \\ \dot{\omega}_1 \\ \dot{\omega}_2 \\ \dot{\omega}_3 \end{bmatrix} = \begin{bmatrix} \omega_1 \\ \omega_2 \\ \omega_3 \\ \frac{I_2 - I_3}{I_1}\omega_2\omega_3 + \frac{\tau_1}{I_1} \\ \frac{I_3 - I_1}{I_2}\omega_1\omega_3 + \frac{\tau_2}{I_2} \\ \frac{I_1 - I_2}{I_3}\omega_1\omega_2 + \frac{\tau_3}{I_3} \end{bmatrix}$$

the state matrix, F, is then

$$\begin{bmatrix} 0 & 0 & 0 & & & & 1 & 0 & 0 & \\ 0 & 0 & 0 & & & & 0 & 1 & 0 & \\ 0 & 0 & 0 & & & & 0 & 0 & 1 & \\ \frac{1}{I_1}\frac{\partial\tau_1}{\partial\theta_1} & \frac{1}{I_1}\frac{\partial\tau_1}{\partial\theta_2} & \frac{1}{I_1}\frac{\partial\tau_1}{\partial\theta_3} & \frac{1}{I_1}\frac{\partial\tau_1}{\partial\omega_1} & \frac{I_2 - I_3}{I_1}\omega_3 + \frac{1}{I_1}\frac{\partial\tau_1}{\partial\omega_2} & \frac{I_2 - I_3}{I_1}\omega_2 + \frac{1}{I_1}\frac{\partial\tau_1}{\partial\omega_3} \\ \frac{1}{I_2}\frac{\partial\tau_2}{\partial\theta_1} & \frac{1}{I_2}\frac{\partial\tau_2}{\partial\theta_2} & \frac{1}{I_2}\frac{\partial\tau_2}{\partial\theta_3} & \frac{I_3 - I_1}{I_2}\omega_3 + \frac{1}{I_2}\frac{\partial\tau_2}{\partial\omega_1} & \frac{1}{I_2}\frac{\partial\tau_2}{\partial\omega_2} & \frac{I_3 - I_1}{I_2}\omega_1 + \frac{1}{I_2}\frac{\partial\tau_2}{\partial\omega_3} \\ \frac{1}{I_3}\frac{\partial\tau_3}{\partial\theta_1} & \frac{1}{I_3}\frac{\partial\tau_3}{\partial\theta_2} & \frac{1}{I_3}\frac{\partial\tau_3}{\partial\theta_3} & \frac{I_1 - I_2}{I_3}\omega_1 + \frac{1}{I_3}\frac{\partial\tau_3}{\partial\omega_1} & \frac{I_1 - I_2}{I_3}\omega_1 + \frac{1}{I_3}\frac{\partial\tau_3}{\partial\omega_2} & \frac{1}{I_3}\frac{\partial\tau_3}{\partial\omega_3} \end{bmatrix}$$

Just as in the orbit determining Kalman filter each of the perturbation forces have individual state matrices that can be added to one another.

$$\mathbf{F} = \mathbf{F}_{\text{torque free}} + \mathbf{F}_{\text{control}} + \mathbf{F}_{\text{gg}} + \mathbf{F}_{\text{SR}} + \mathbf{F}_{\text{mag}} + \mathbf{F}_{\text{drag}}$$

Where the state matrix corresponding to each torque is

$$\mathbf{F} = \begin{bmatrix} 0 & 0 & 0 & & & & 1 & 0 & 0 & \\ 0 & 0 & 0 & & & & 0 & 1 & 0 & \\ 0 & 0 & 0 & & & & 0 & 0 & 1 & \\ \frac{1}{I_1}\frac{\partial\tau_1}{\partial\theta_1} & \frac{1}{I_1}\frac{\partial\tau_1}{\partial\theta_2} & \frac{1}{I_1}\frac{\partial\tau_1}{\partial\theta_3} & \frac{1}{I_1}\frac{\partial\tau_1}{\partial\omega_1} & \frac{1}{I_1}\frac{\partial\tau_1}{\partial\omega_2} & \frac{1}{I_1}\frac{\partial\tau_1}{\partial\omega_3} \\ \frac{1}{I_2}\frac{\partial\tau_2}{\partial\theta_1} & \frac{1}{I_2}\frac{\partial\tau_2}{\partial\theta_2} & \frac{1}{I_2}\frac{\partial\tau_2}{\partial\theta_3} & \frac{1}{I_2}\frac{\partial\tau_2}{\partial\omega_1} & \frac{1}{I_2}\frac{\partial\tau_2}{\partial\omega_2} & \frac{1}{I_2}\frac{\partial\tau_2}{\partial\omega_3} \\ \frac{1}{I_3}\frac{\partial\tau_3}{\partial\theta_1} & \frac{1}{I_3}\frac{\partial\tau_3}{\partial\theta_2} & \frac{1}{I_3}\frac{\partial\tau_3}{\partial\theta_3} & \frac{1}{I_3}\frac{\partial\tau_3}{\partial\omega_1} & \frac{1}{I_3}\frac{\partial\tau_3}{\partial\omega_2} & \frac{1}{I_3}\frac{\partial\tau_3}{\partial\omega_3} \end{bmatrix}$$

In Section 4.4, the time derivative of the state vector was formed in order to perform the desired maneuver. The time derivative of the state vector is

$$\dot{X} = \begin{bmatrix} \omega_1 \\ \omega_2 \\ \omega_3 \\ -0.002e^{0.009t}\theta_1 \\ -0.002e^{0.009t}\theta_2 \\ -0.0002\theta_3 \end{bmatrix} = \begin{bmatrix} x_4 \\ x_5 \\ x_6 \\ -0.002e^{0.009t}x_1 \\ -0.002e^{0.009t}x_2 \\ -0.0002x_3 \end{bmatrix}$$

Therefore the state matrix is

$$\mathbf{F} = \begin{bmatrix} \frac{\partial\omega_1}{\partial\theta_1} & \frac{\partial\omega_1}{\partial\theta_2} & \frac{\partial\omega_1}{\partial\theta_3} & \frac{\partial\omega_1}{\partial\omega_1} & \frac{\partial\omega_1}{\partial\omega_2} & \frac{\partial\omega_1}{\partial\omega_3} \\ \frac{\partial\omega_2}{\partial\theta_1} & \frac{\partial\omega_2}{\partial\theta_2} & \frac{\partial\omega_2}{\partial\theta_3} & \frac{\partial\omega_2}{\partial\omega_1} & \frac{\partial\omega_2}{\partial\omega_2} & \frac{\partial\omega_2}{\partial\omega_3} \\ \frac{\partial\omega_3}{\partial\theta_1} & \frac{\partial\omega_3}{\partial\theta_2} & \frac{\partial\omega_3}{\partial\theta_3} & \frac{\partial\omega_3}{\partial\omega_1} & \frac{\partial\omega_3}{\partial\omega_2} & \frac{\partial\omega_3}{\partial\omega_3} \\ \frac{\partial\dot{\omega}_1}{\partial\theta_1} & \frac{\partial\dot{\omega}_1}{\partial\theta_2} & \frac{\partial\dot{\omega}_1}{\partial\theta_3} & \frac{\partial\dot{\omega}_1}{\partial\omega_1} & \frac{\partial\dot{\omega}_1}{\partial\omega_2} & \frac{\partial\dot{\omega}_1}{\partial\omega_3} \\ \frac{\partial\dot{\omega}_2}{\partial\theta_1} & \frac{\partial\dot{\omega}_2}{\partial\theta_2} & \frac{\partial\dot{\omega}_2}{\partial\theta_3} & \frac{\partial\dot{\omega}_2}{\partial\omega_1} & \frac{\partial\dot{\omega}_2}{\partial\omega_2} & \frac{\partial\dot{\omega}_2}{\partial\omega_3} \\ \frac{\partial\dot{\omega}_3}{\partial\theta_1} & \frac{\partial\dot{\omega}_3}{\partial\theta_2} & \frac{\partial\dot{\omega}_3}{\partial\theta_3} & \frac{\partial\dot{\omega}_3}{\partial\omega_1} & \frac{\partial\dot{\omega}_3}{\partial\omega_2} & \frac{\partial\dot{\omega}_3}{\partial\omega_3} \end{bmatrix}$$

$$= \begin{bmatrix} 0 & 0 & 0 & 1 & 0 & 0 \\ 0 & 0 & 0 & 0 & 1 & 0 \\ 0 & 0 & 0 & 0 & 0 & 1 \\ -0.002e^{0.009t} & 0 & 0 & 0 & 0 & 0 \\ 0 & -0.002e^{0.009t} & 0 & 0 & 0 & 0 \\ 0 & 0 & -0.0002 & 0 & 0 & 0 \end{bmatrix}$$

Now that the observation matrix and state matrix have been defined, the Kalman filter can be implemented and run using the different types of attitude determining sensors to best estimate the attitude of the satellite.

4.7 Results of Attitude Determination Algorithm

Now that the Klaman filter algorthim has been developed, it can be run using different types of attitude determing sensors. Figure 4.12 shows the controlled attitude manuerver used to test the algorithm. This manueaver changes the pitch and yaw angles quite rapidly, which could lead to inaccurate attitude estimations if the algorithm is not robust enough. The next four sections correspond to the cases run for the four attitude sensors. First, the magnetometer sensor, which is the most inaccurate.

4.7.1 Magnetometer

The magnetometer sensor used in this thesis has the errors and sample rate listed in Table 4.1. The actual and estimated Euler angles and measurements are plotted in Figure 4.13. Zooming in, Figure 4.14, shows how the estimated attitude uses the measurements to update the predicted attitude but with fairly large errors. The errors are seen in Figure 4.14. The standard deviation of the errors for the attitude determined using a magnetometer sensor is 0.2 degrees. The normal distribution of the errors seen using a magnetometer is plotted in Figure 4.15.

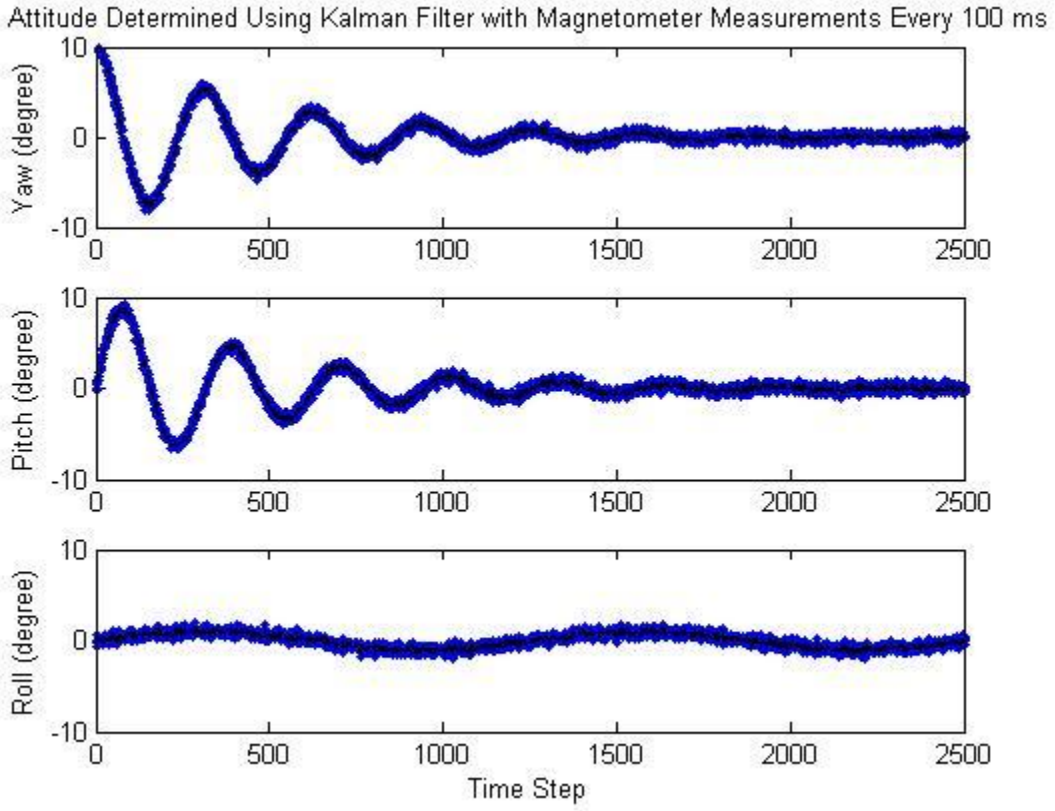

Figure 4.13: Satellite Attitude Determine Using Magnetometer

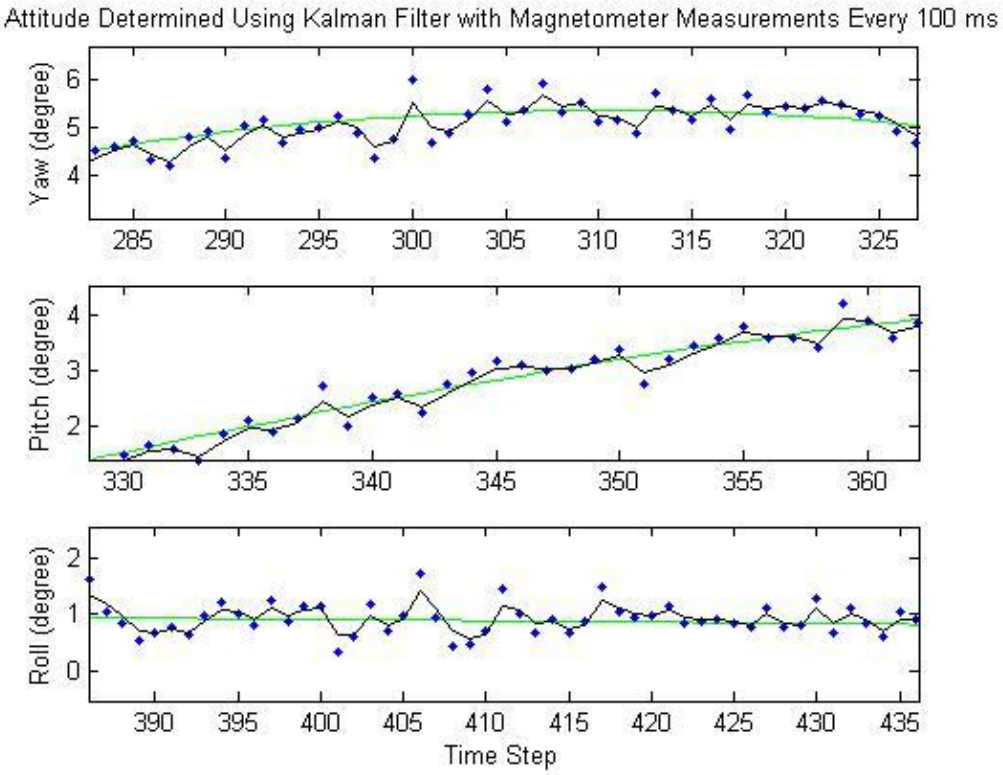

Figure 4.14: Satellite Attitude Determine Using Magnetometer

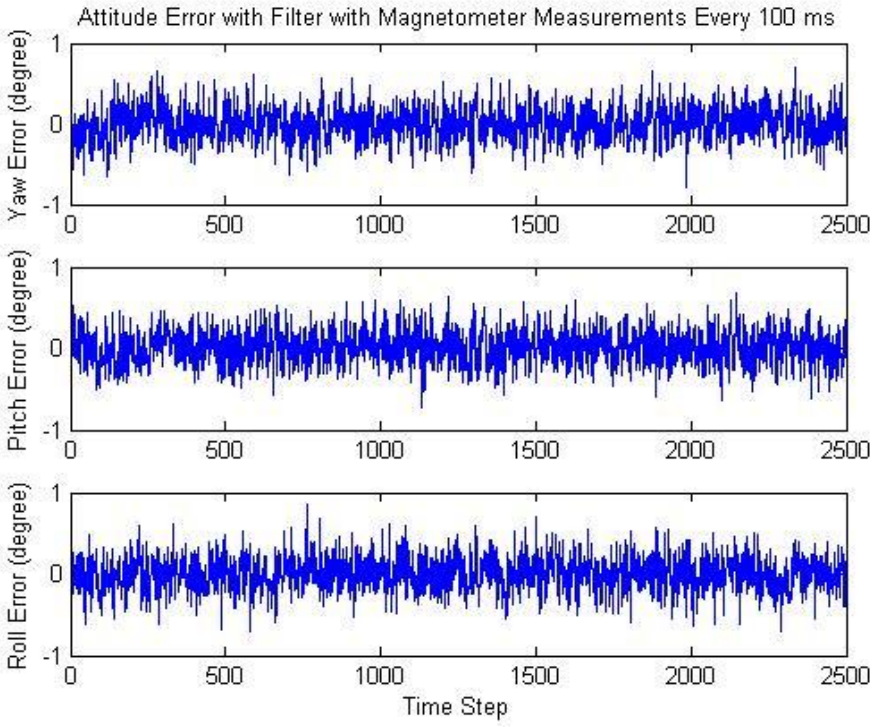

Figure 4.15: Errors in Satellite Attitude Determine Using Magnetometer

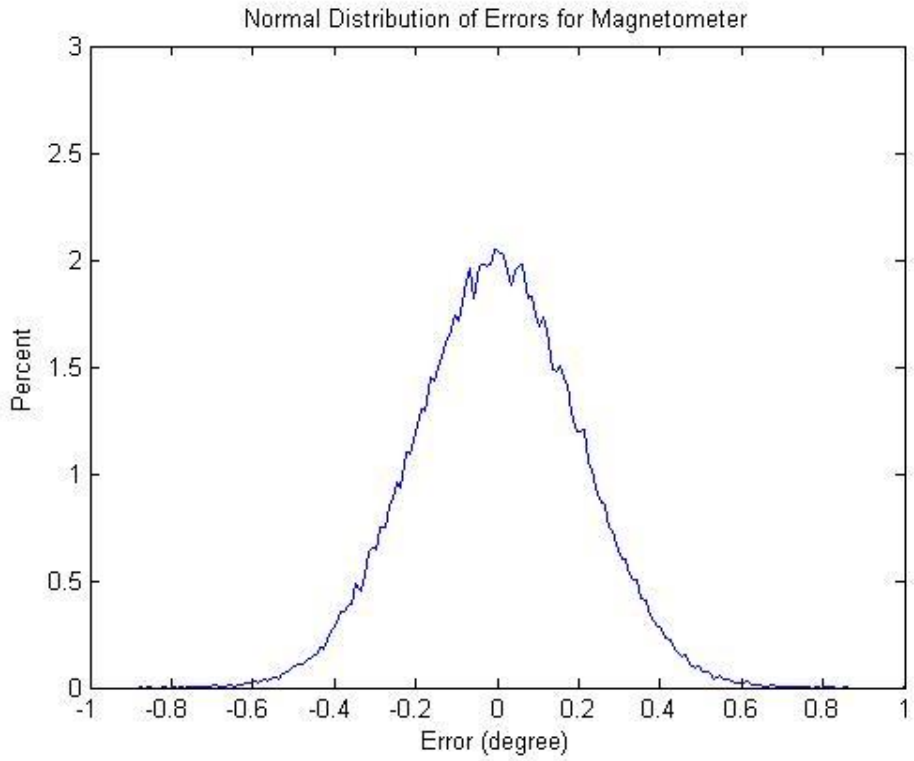

Figure 4.16: Probability Distribution of Errors in Satellite Attitude Determine Using Magnetometer

4.7.2 Earth Sensor

The Earth sensor used in this thesis has the errors and sample rate listed in Table 4.1. The actual and estimated Euler angles and measurements are plotted in Figure 4.17. Zooming in, Figure 4.18, shows how the estimated attitude is corrected with the inputted measurements to predict the attitude. The attitude is estimated more accurately than with the magnetometer measurement inputs. The errors in attitude for the three axes are seen in Figure 4.19. Notice that the errors are larger when the angular rate of change is higher. This confirms the findings found in Chapter 3, an increase in distance covered between measurement updates increases the errors determined by the filter. The error distribution is plotted in Figure 4.20.The first standard deviation of the errors for the attitude determined using an Earth sensor is 0.05 degrees.

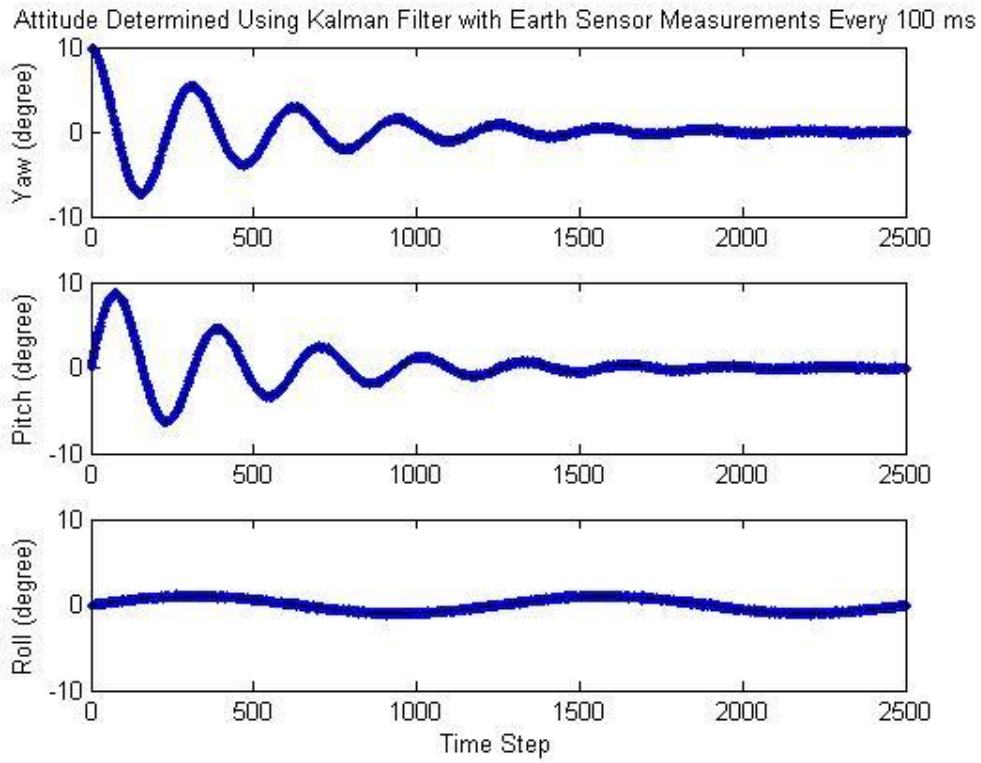

Figure 4.17: Satellite Attitude Determine Using Earth Sensor

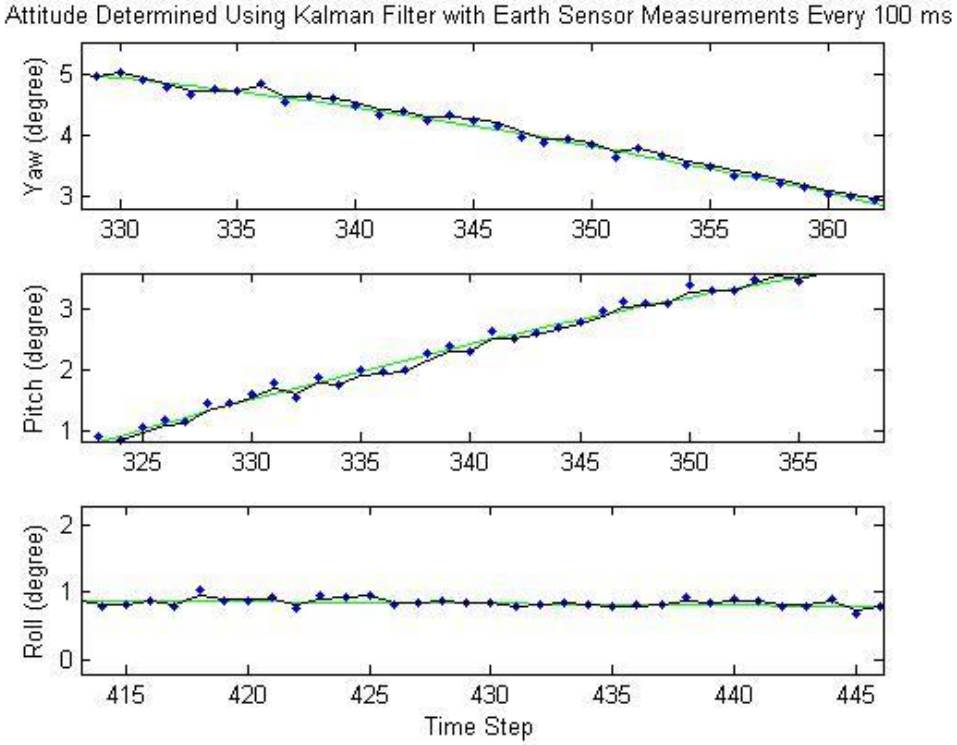

Figure 4.18: Satellite Attitude Determine Using Earth Sensor

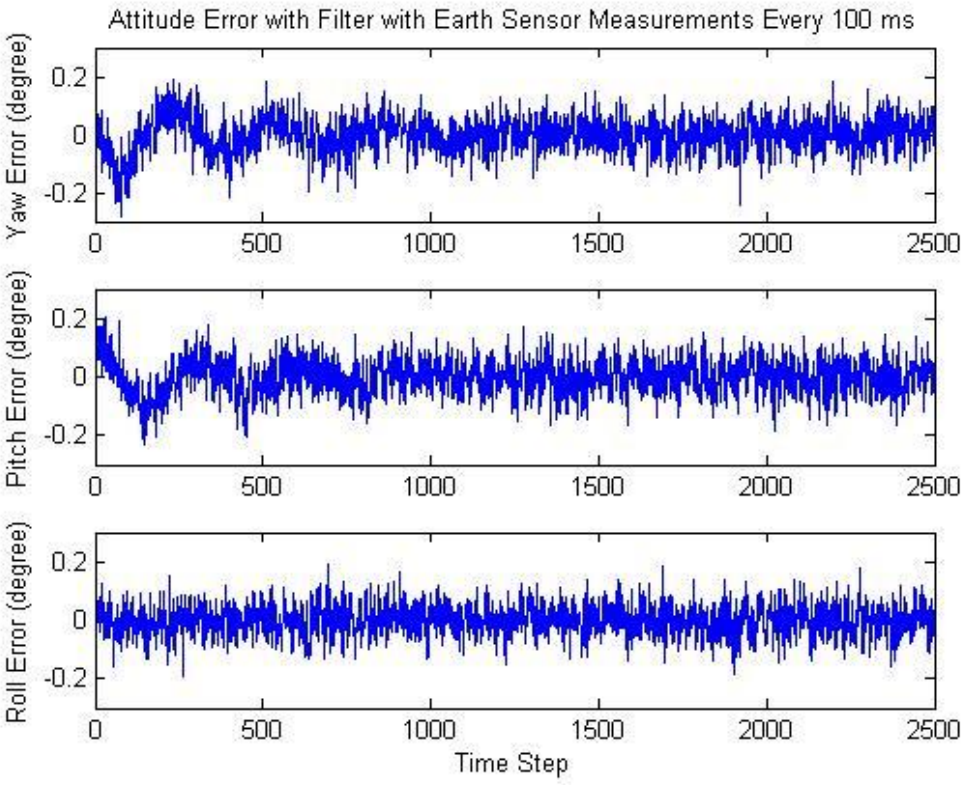

Figure 4.19: Errors in Satellite Attitude Determine Using Earth Sensor

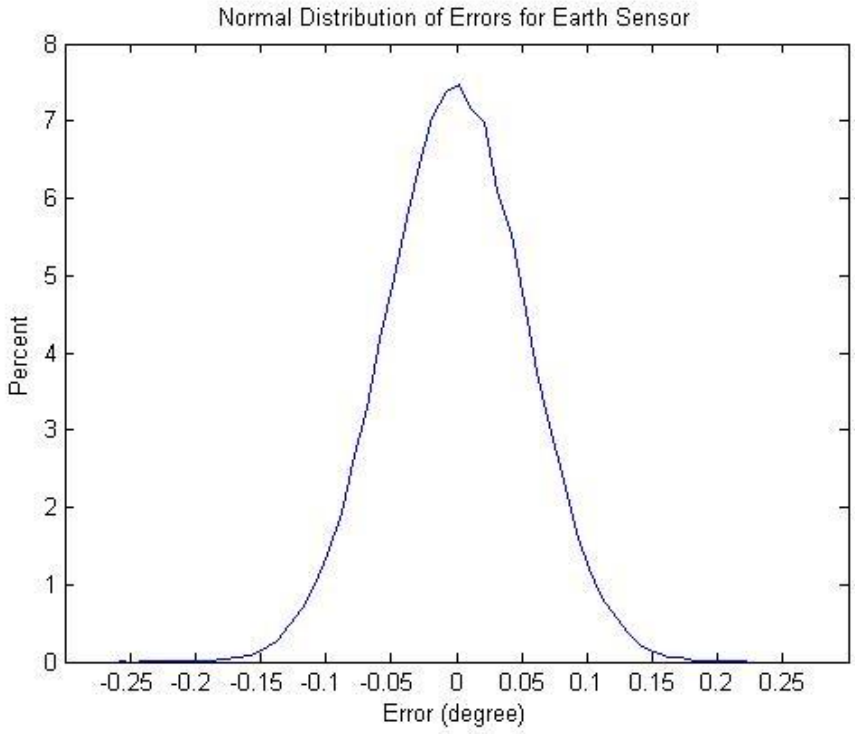

Figure 4.20: Probability Distribution of Errors in Satellite Attitude Determine Using Earth Sensor

4.7.3 Sun Sensor

Below are the results of the attitude determining Kalman Filter algorithm using the sun sensor attiude measurments every quarter of a second. From Figure 4.22, it is seen that the filter is esitmating the attitude quite accuratly. The attitude errors from the algorithm are seen in Figure 4.23. The fisrt satandard deviation of the errors computed using the sun sensor is 0.06 degrees.The errors are similar to the Earth sensor, even though the sun sensor has higher accuracy, since the sun sensor inputs measurements half as often as the earth sensor. Therefore it is shown that both accuracy and time interval between measuemenrts are important in computing the attiude of the satellite using the Kalman filter developed in this thesis. The error distribution for the attitude determined by the sun sensor is seen in Figure 4.24.

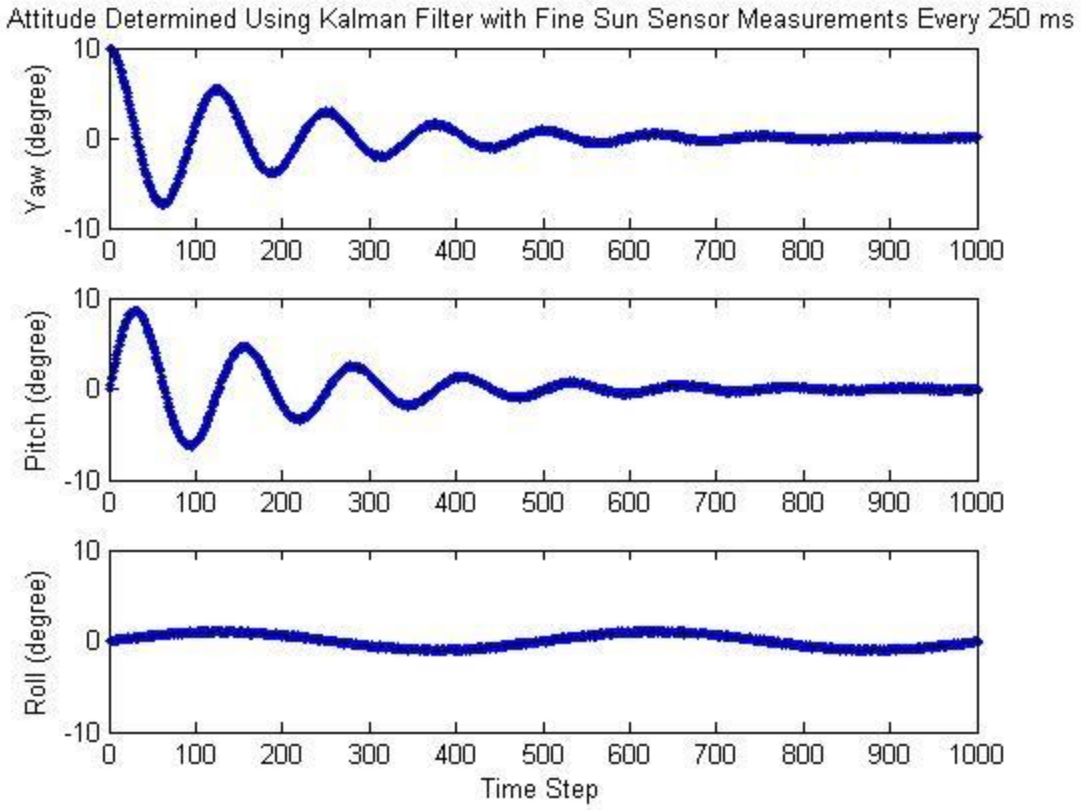

Figure 4.20: Satellite Attitude Determine Using Sun Sensor

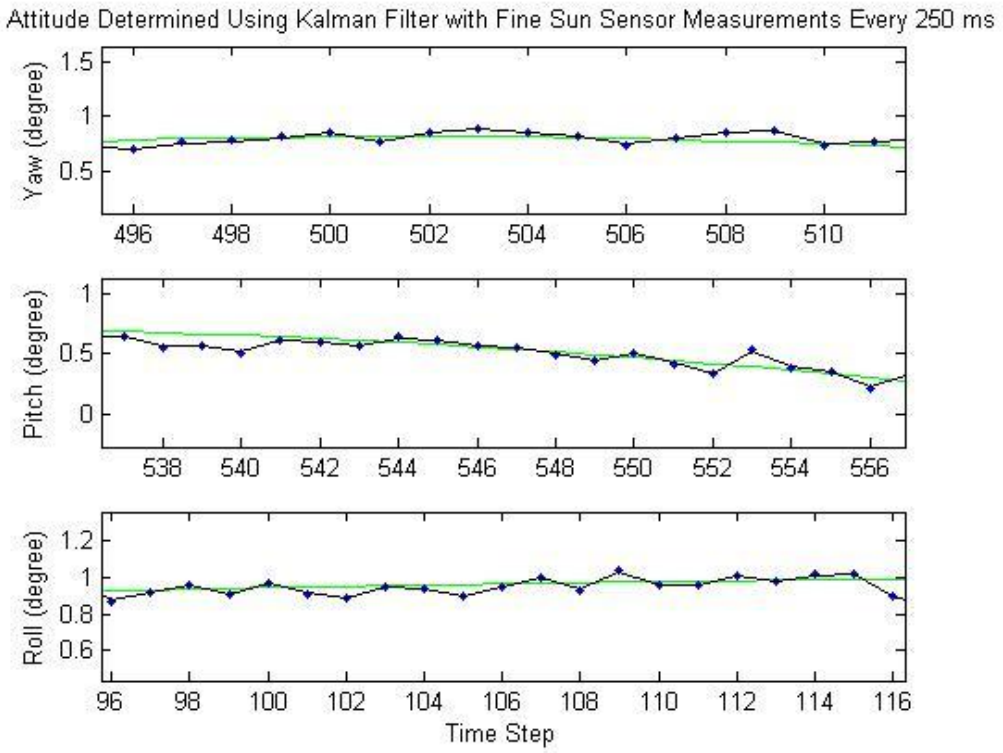

Figure 4.21: Satellite Attitude Determine Using Sun Sensor

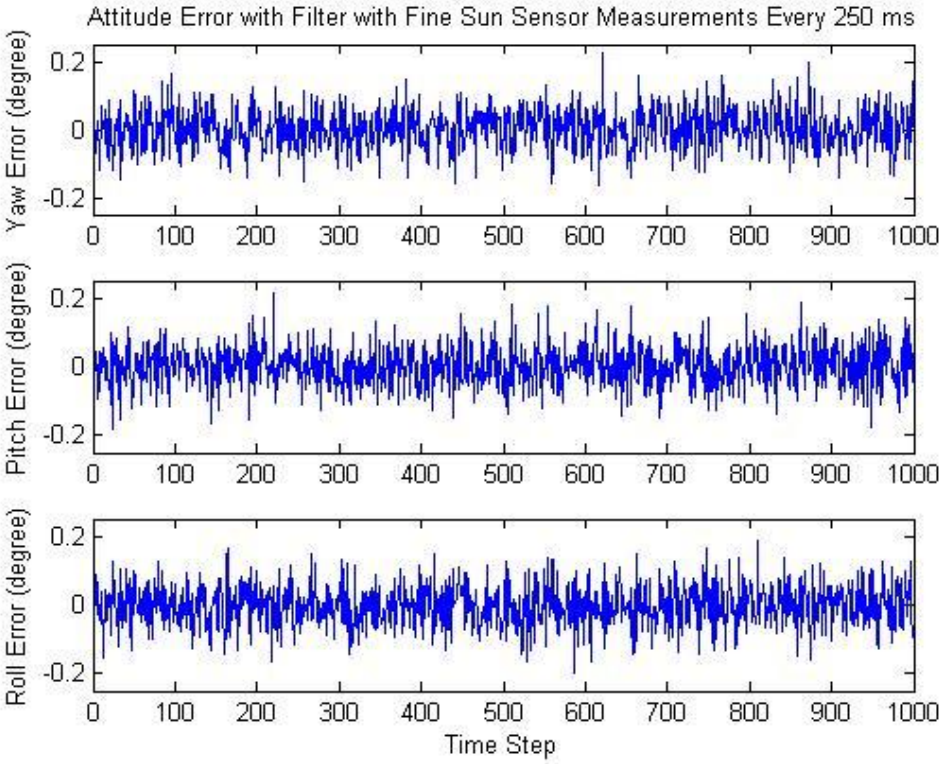

Figure 4.23: Errors in Satellite Attitude Determine Using Sun Sensor

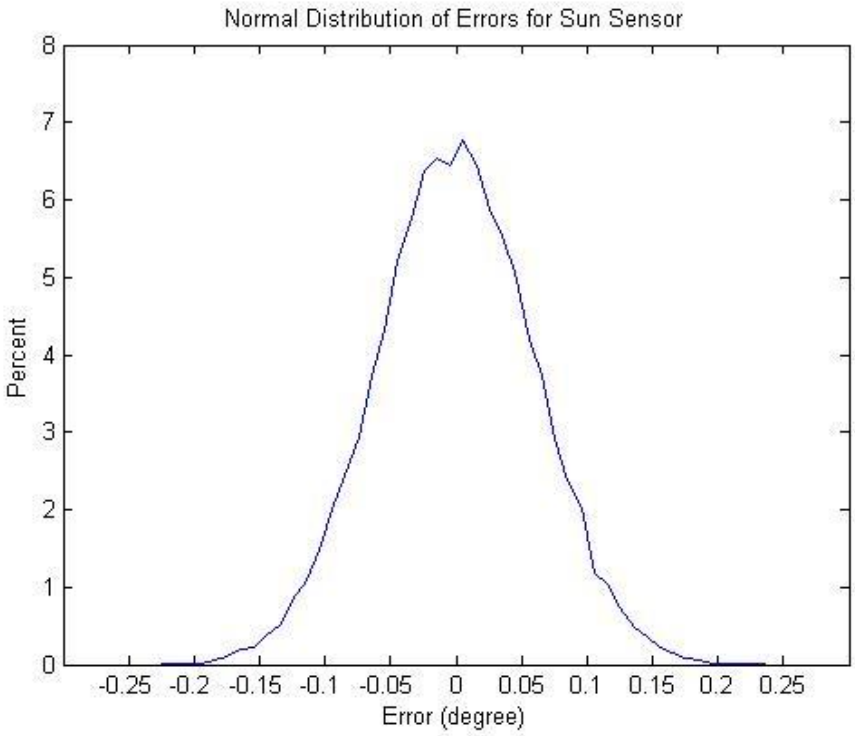

Figure 4.24: Distribution of errors in satellite attitude determined using sun sensor

4.7.4 Star Sensor

Last but not least, the attitude of the satellite is determined using star tracker measurements every quarter second. Star tracker measurements are far more accurate than the other three sensors used in this thesis. Therefore, even with the time step being a quarter second rather than a tenth of a second, the errors in attitude are far smaller with star tracker measurements than with the other three sensors. The standard deviation of the errors in attitude determined by the Kalman filter using star tracker measurements is 0.0006 degrees. The error distribution is plotted in Figure 4.28. A plot all four error distribution is seen in Figure 2.29.

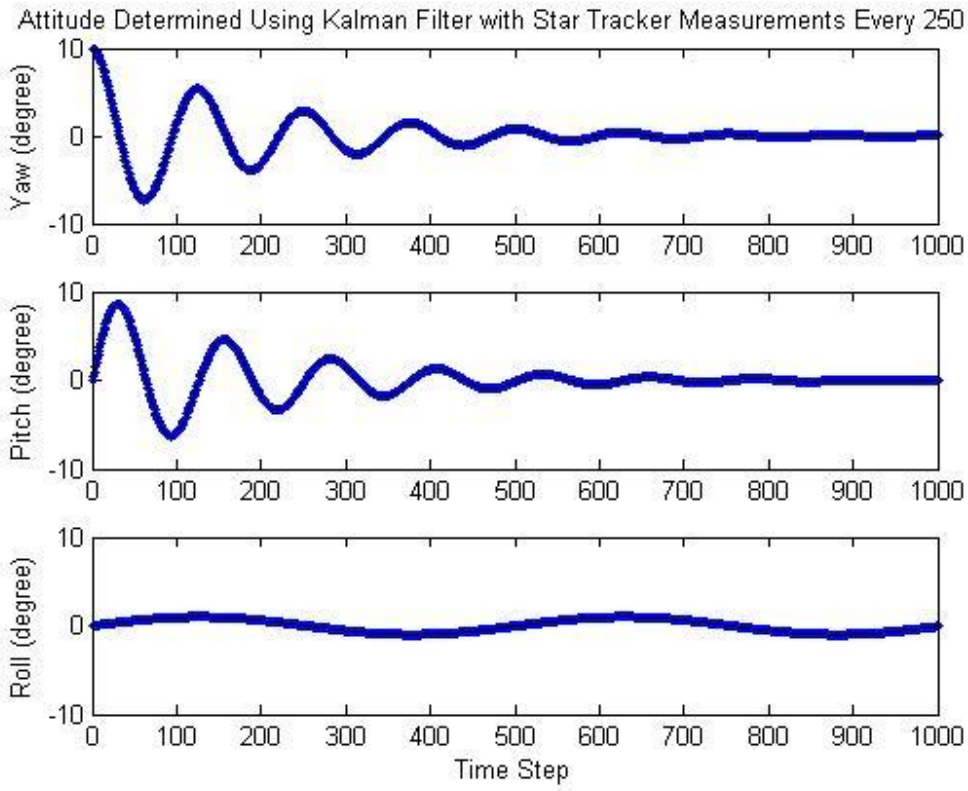

Figure 4.25: Satellite Attitude Determine Using Star Tracker

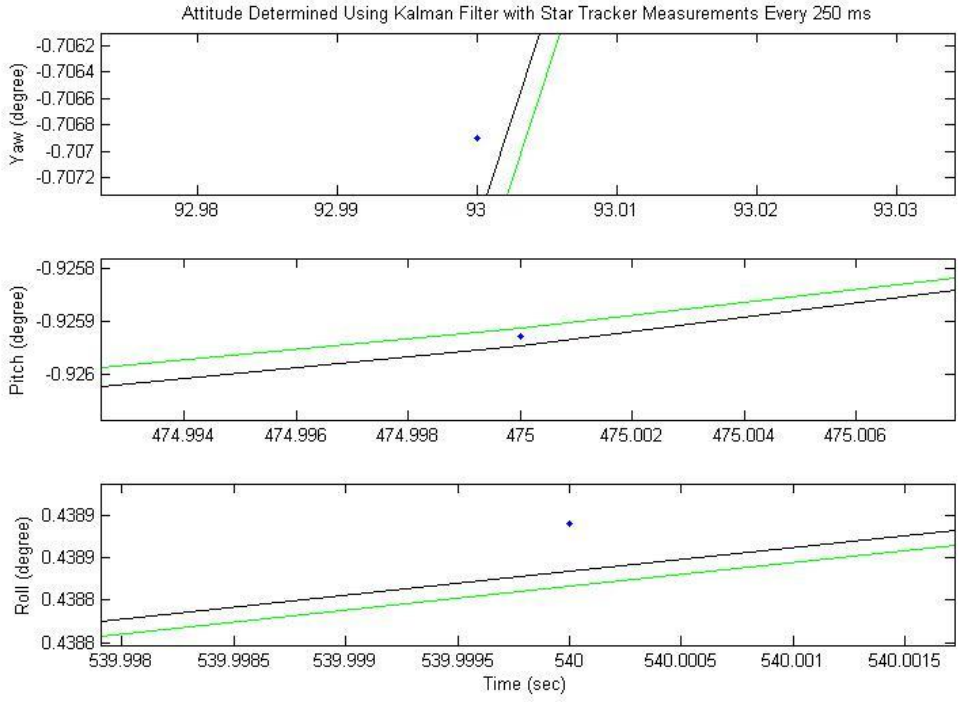

Figure 4.26: Satellite Attitude Determine Using Star Tracker

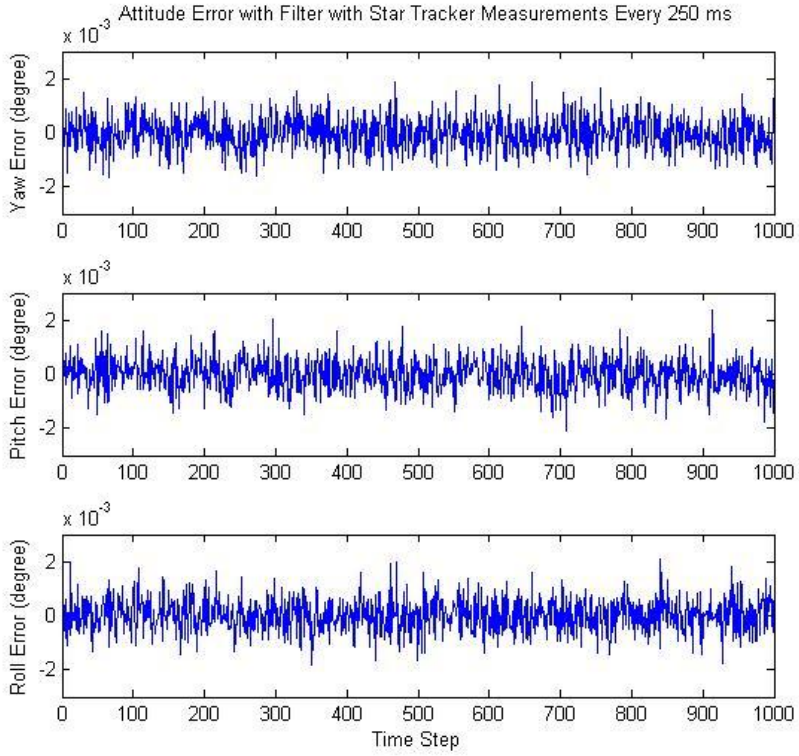

Figure 4.27: Errors in Satellite Attitude Determine Using Star Tracker

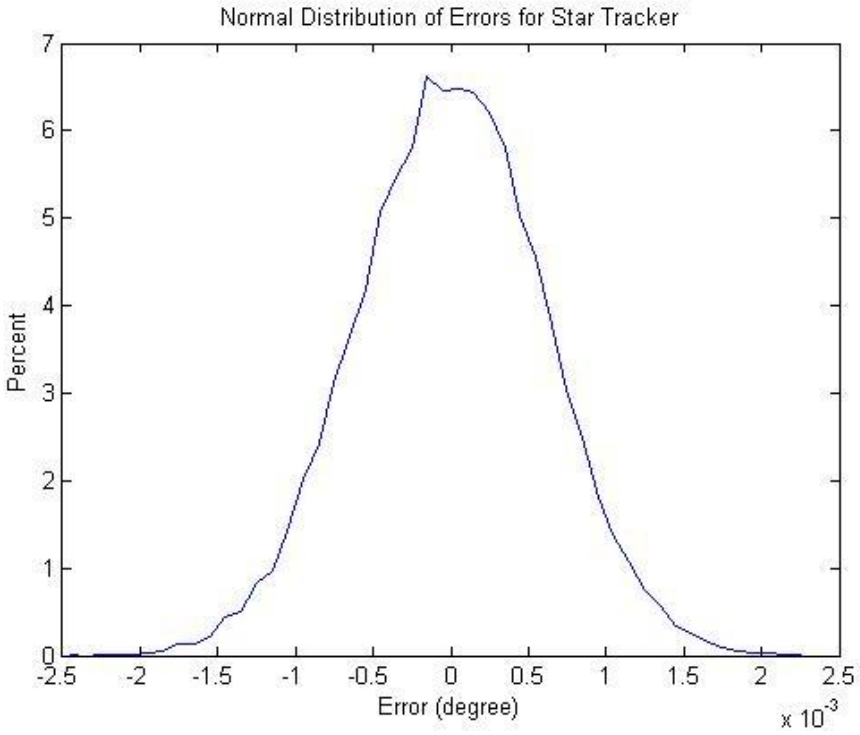

Figure 4.28: Distribution of errors in satellite attitude determined using star tracker

4.7.4 Summary

To summarize, both the accuracy of sensors as well as time between measurement updates influences the total accuracy of the attitude determining Kalman filter developed in this thesis. It is shown that star tracker sensor determines the satellite attitude with 300 times the accuracy then the magnetometer. However with accuracy comes greater weight and power consumptions. When designing the attitude control system of a satellite, the engineers will need to perform a trade study on attitude accuracy requirements with weight and power availability to determine the best sensors for the satellite.

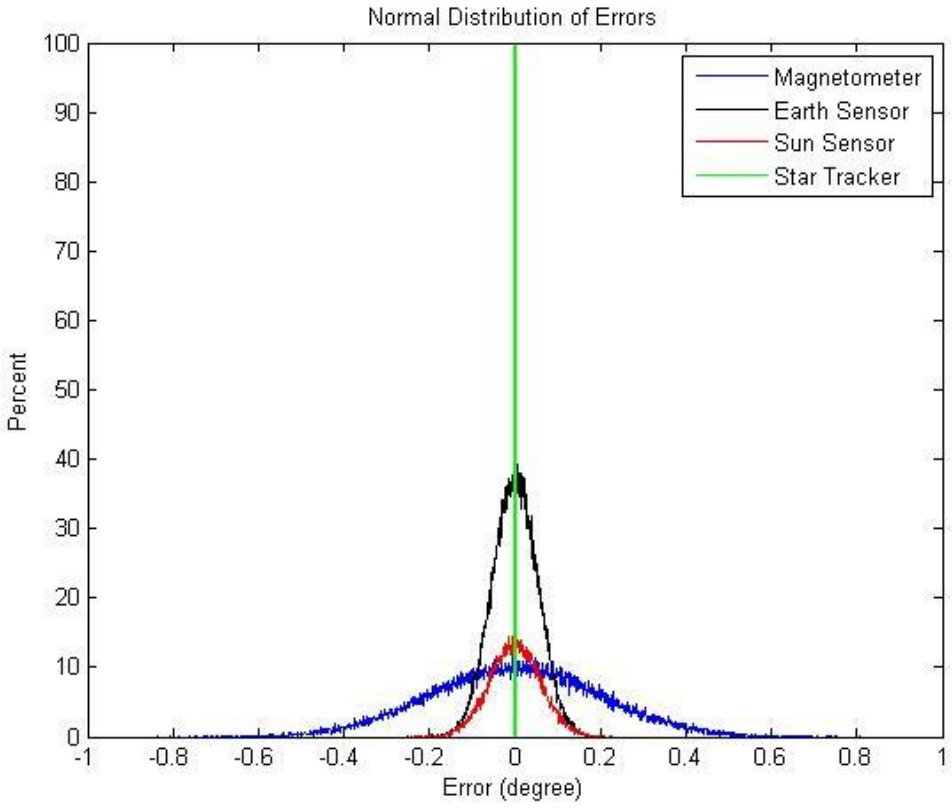

Figure 4.28: Summary of distribution of errors in satellite attitude determined

Chapter 5

Conclusion

This thesis details the development and implementation of an attitude and orbit determining Kalman filter algorithm for a satellite in a Molniya orbit. For the Kalman filter to determine the orbit of the satellite, the equations of motion were propagated using the Cowell's formulation. Four types of perturbing forces were added to the two body problem in order to increase the accuracy of the orbit prediction. These four perturbing forces are: the Earth's oblateness, atmospheric drag, lunar gravitational forces and solar radiation pressure. All four perturbing forces were added to the model since the satellite is in a Molniya orbit and therefore both the perturbing forces that occur at low altitudes and high altitudes must be considered. Next, measurements of the satellite's position are added to the Kalman filter in order to correct the predicted orbit. Two cases were studied, the first being the implementation of site track measurements, inputted when the satellite was over the ground station. It is shown that with each ground site pass, the errors in the predicted orbit decrease. However, large errors, upwards of ninety meters grow as time from last measurement input increases. The next case studied was continuous measurement inputs from a GPS receiver on board the satellite throughout the orbit. This algorithm greatly decreased the errors seen in the orbit determining algorithm. This is due to the accuracy of the position measured by the GPS sensor and the constant measurement update throughout the orbit. In summary, the orbit determining algorithm using GPS measurements throughout the orbit is much more accurate than a site track orbit determining implementation.

Next the Kalman filter is applied to determine the satellite attitude. The rotational equations of motion are propagated using the Cowell's Formulation and numerical integration. To increase the fidelity of the model four disturbing torques are included in the rotational

equations of motion. These four disturbing torques are gravity gradient torque, solar pressure torque, magnetic torque, and aerodynamic torque. The measurement input stage of the Kalman filter used on-board attitude determining sensors. Four cases were studied, one for each of the on-board sensors: Magnetometer, Earth sensor, Sun sensor, and star tracker. A controlled attitude path was chosen to test the accuracy of each of these cases and it was shown that the algorithm using star tracker measurements was 300 times more accurate than that of the magnetometer algorithm.

Therefore, if attempting to design a light weight payload with a computationally inexpensive orbit and attitude determining system, trade studies can be evaluated to determine what type of sensors to use on-board the payload. If only a GPS sensor is used, for both the attitude and orbit determining system, models of the location of the Sun and Moon, and Earth's magnetic field will be needed on board if calculating the perturbing forces and disturbing torques. However, it is possible that the attitude and orbit can be determined without a GPS sensor by using the site track method along with an on-board Sun sensor and magnetometer. Trade studies between cases such as the ones described above can be performed in order to determine the best orbit and attitude determining system to use. If a payload can accurately determine the satellite orbit and attitude without interfacing with the host satellite, the number of interfaces between the host and payload is greatly reduced. By reducing the number of interfaces, the integration of the payload on to the host satellite is greatly simplified, reducing development time and cost.

5.1 Future Work

Like in any model, assumptions were made to simplify the model and reduce computation time. For future work, these assumptions could be changed or removed, adding to the complexity and accuracy of the model. For example, the atmospheric model chosen in this thesis was time-invariant, therefore did not take in to account the Sun's diurnal and sun spot cycle. The atmospheric model only took in to account the altitude of the satellite. Since both the atmospheric drag perturbation force and aerodynamic disturbing torque calculations used this model, the accuracy of both could be improved by introducing a more accurate model. Also, the solar radiation pressure that created a disturbing torque on the satellite, as well as perturbing force on the orbit, was found assuming the Sun was stationary over the orbit and duration of the algorithm. Therefore, to make this algorithm self sufficient for the life of the satellite, the sun's incident angle measured by the Sun sensor could be inputted alongside the measurements into the orbit determining algorithm. Similarly, the lunar gravitational effects on the orbit of the satellite were determined assuming the Moon's position relative to Earth remained constant over the time of the satellite orbit.

Another idea for future work would be to study how the Kalman filter accuracy would change when using dynamic weights in the error covariance matrices, R and Q, rather than the static ones used in this thesis. By adding dynamic weights or more accurate perturbation accelerations, the complexity and accuracy of the model increases. Therefore, an engineer developing a satellite attitude and orbit determining system will need to determine what level of accuracy and therefore complexity is required for the specific satellite.

Bibliography

[1] Auret, Jacoba. "Design of an Aerodynamic Attitude Control System for a CubeSat." Thesis. Stellenbosch University, 2012. Print.

[2] *Autonomous Star Sensor ASTRO 15*. Jenaoptronik, Feb. 2011. Data Sheet.

[3] Bamford, William, Luke Winternitz, and Michael Mareau. *Real-Time Geostationary Orbit Determination Using the Navigator GPS Receiver.* Web. 12 Feb. 2014.

[4] Bate, Roger R., Donald D. Mueller, and Jerry E. White. *Fundamentals of Astrodynamics*. New York: Dover Publications, 1971. Print.

[5] Bjelbole, Cecilie. "An Attitude Determination and Control System for CubeSTAR." Thesis. University of Oslo, 2013. Print.

[6] *Fine Sun Sensor*. Jenaoptronik, Apr. 2011. Data Sheet.

[7] Garcia, R. V., H. K. Kuga, and M. C. Zanardi. *Unscented Kalman Filter for Spacecraft Attitude Esimation Using Quaternions and Euler Angles*. Space Mechanics and Control Division, National Institute for Space Research, n.d. Web. 7 Feb. 2014.

[8] Hall, Chris. "Introduction to Attitude Dynamics and Control." Spacecraft Dynamics and Control. Virginia Polytechnic and State University, Blacksburg. 21 Jan. 2013. Lecture.

[9] Hobbs, David, and Preben Bohn. *Precise Orbit Determination for Low Earth Orbit Satellites*. Terma A/S, n.d. Web. 12 Feb. 2014.

[10] Ketsdever, Andrew. "Attitude Determination and Control." Massachusetts Institute of Technology, Boston. 21 Mar. 2014. Lecture.

[11] Kutlu, Aykut. "Design of Kalman Filter Based Attitude Determination Algorithm for a LEO Sattellite and for a Satellite Attitude Control Test Setup." Thesis. Middle East Technical University, 2008. Print.

[12] Marques, Sonia, Roberts Clements, and Pedro Lima. *Comparison of Small Atellite Attitude Determination Methods*. Instituto De Sistemas E Robotica, Instituto Superior Tecnico, n.d. Web. 30 Jan. 2014.

[13] Rohde, Jan. "Kalman Filter for Attitude Determination of Student Satellite." Thesis. Norwegian University of Science and Technology, 2007. Print.

[14] *TAM-1 Satellite Magnetometer*. Dulles: Macintyre Electronic Design Associates, Sept. 2005. Data Sheet.

[15] Tuthill, Jason. "Design and Simulation of a Nano-Satellite of a Nano-Satellite Attitude Determination System." Thesis. Naval Postgraduate School, 2009. Print.

[16] Vallado, David A., and Wayne D. McClain. *Fundamentals of Astrodynamics and Applications*. Dordrecht: Kluwer Academic, 2001. Print.

[17] Vergez, Paul, Luke Sauter, and Scott Dahlke. "An Improved Kalman Filter for Satellite Orbit Predictions." *The Journal of the Astronautical Sciences* 52.3 (2004): n. pag. Web.

[18] Weck, Olivier. "Attitude Determination and Control." 16.684 Space Systems Product Development. Massachusetts Institute of Technology, Boston. Spring 2001. Lecture.

[19] Yadlin, Roni. *Attitude Determination and Bias Estimation Using Kalman Filtering*. United States Air Force Academy, n.d. Web. 30 Jan. 2014.

APPENDIX

Development of State Matrix for Earth's Oblateness

Below are the individual partial derivatives that make up the State Matrix pertaining to Earth's oblateness.

$$\mathbf{F}_{\text{spherical}} = \frac{\partial \dot{\mathbf{X}}_{\text{spherical}}}{\partial \mathbf{X}} = = \begin{bmatrix} 0 & 0 & 0 & 1 & 0 & 0 \\ 0 & 0 & 0 & 0 & 1 & 0 \\ 0 & 0 & 0 & 0 & 0 & 1 \\ \frac{\partial \mathrm{a_i}}{\partial \mathrm{r_i}} & \frac{\partial \mathrm{a_i}}{\partial \mathrm{r_j}} & \frac{\partial \mathrm{a_i}}{\partial \mathrm{r_k}} & & & \\ \frac{\partial \mathrm{a_j}}{\partial \mathrm{r_i}} & \frac{\partial \mathrm{a_j}}{\partial \mathrm{r_j}} & \frac{\partial \mathrm{a_j}}{\partial \mathrm{r_k}} & 0 & 0 & 0 \\ \frac{\partial \mathrm{a_k}}{\partial \mathrm{r_i}} & \frac{\partial \mathrm{a_k}}{\partial \mathrm{r_j}} & \frac{\partial \mathrm{a_k}}{\partial \mathrm{r_k}} & 0 & 0 & 0 \end{bmatrix}$$

$$\frac{\partial \mathrm{a_i}}{\partial \mathrm{r_i}} = -\frac{3}{2}\frac{\mu {R_\oplus}^2 C_{2,0}}{r^4}\{3\sin^2\left(\phi_{gc_{sat}}\right) - 1\} - \frac{r_k}{r^2\sqrt{r_i^2 + r_j^2}}[3\frac{\mu {R_\oplus}^2 C_{2,0}}{r^3}\sin\left(\phi_{gc_{sat}}\right)\cos\left(\phi_{gc_{sat}}\right)$$

$$+ r_i\left(6r_i\frac{\mu {R_\oplus}^2 C_{2,0}}{r^3}\{3\sin^2\left(\phi_{gc_{sat}}\right) - 1\}\right.$$

$$+ \frac{15 r_k r_i}{r^7\sqrt{r_i^2 + r_j^2}}[\mu {R_\oplus}^2 C_{2,0}\sin\left(\phi_{gc_{sat}}\right)\cos\left(\phi_{gc_{sat}}\right)$$

$$\left. + \frac{3 r_k r_i}{r^5\left(r_i^2 + r_j^2\right)^{3/2}}[\mu {R_\oplus}^2 C_{2,0}\sin\left(\phi_{gc_{sat}}\right)\cos\left(\phi_{gc_{sat}}\right)]\right)$$

$$\frac{\partial \mathrm{a_i}}{\partial \mathrm{r_j}} = r_i \left(6r_j \frac{\mu {R_\oplus}^2 C_{2,0}}{r^3} \{3\sin^2\left(\phi_{gc_{sat}}\right) - 1\} + \frac{15 r_k r_j}{r^7 \sqrt{r_i^2 + r_j^2}} [\mu {R_\oplus}^2 C_{2,0} \sin\left(\phi_{gc_{sat}}\right) \cos\left(\phi_{gc_{sat}}\right) + \frac{3 r_k r_j}{r^5 (r_i^2 + r_j^2)^{3/2}} [\mu {R_\oplus}^2 C_{2,0} \sin\left(\phi_{gc_{sat}}\right) \cos\left(\phi_{gc_{sat}}\right)] \right)$$

$$\frac{\partial \mathrm{a_i}}{\partial \mathrm{r_k}} = r_i \left(6r_j \frac{\mu {R_\oplus}^2 C_{2,0}}{r^3} \{3\sin^2\left(\phi_{gc_{sat}}\right) - 1\} + \frac{15 {r_k}^2}{r^7 \sqrt{r_i^2 + r_j^2}} [\mu {R_\oplus}^2 C_{2,0} \sin\left(\phi_{gc_{sat}}\right) \cos\left(\phi_{gc_{sat}}\right) + \frac{3}{r^5 (r_i^2 + r_j^2)^{3/2}} [\mu {R_\oplus}^2 C_{2,0} \sin\left(\phi_{gc_{sat}}\right) \cos\left(\phi_{gc_{sat}}\right)] \right)$$

$$\frac{\partial \mathrm{a_j}}{\partial \mathrm{r_i}} = r_j \left(6r_i \frac{\mu {R_\oplus}^2 C_{2,0}}{r^3} \{3\sin^2\left(\phi_{gc_{sat}}\right) - 1\} + \frac{15 r_k r_i}{r^7 \sqrt{r_i^2 + r_j^2}} [\mu {R_\oplus}^2 C_{2,0} \sin\left(\phi_{gc_{sat}}\right) \cos\left(\phi_{gc_{sat}}\right) + \frac{3 r_k r_i}{r^5 (r_i^2 + r_j^2)^{3/2}} [\mu {R_\oplus}^2 C_{2,0} \sin\left(\phi_{gc_{sat}}\right) \cos\left(\phi_{gc_{sat}}\right)] \right)$$

$$\frac{\partial \mathrm{a_j}}{\partial \mathrm{r_j}} = -\frac{3}{2} \frac{\mu {R_\oplus}^2 C_{2,0}}{r^4} \{3\sin^2\left(\phi_{gc_{sat}}\right) - 1\} - \frac{r_k}{r^2 \sqrt{r_i^2 + r_j^2}} [3 \frac{\mu {R_\oplus}^2 C_{2,0}}{r^3} \sin\left(\phi_{gc_{sat}}\right) \cos\left(\phi_{gc_{sat}}\right) + r_j \left(6r_j \frac{\mu {R_\oplus}^2 C_{2,0}}{r^3} \{3\sin^2\left(\phi_{gc_{sat}}\right) - 1\} + \frac{15 r_k r_j}{r^7 \sqrt{r_i^2 + r_j^2}} [\mu {R_\oplus}^2 C_{2,0} \sin\left(\phi_{gc_{sat}}\right) \cos\left(\phi_{gc_{sat}}\right) + \frac{3 r_k r_j}{r^5 \left(r_i^2 + r_j^2\right)^{3/2}} [\mu {R_\oplus}^2 C_{2,0} \sin\left(\phi_{gc_{sat}}\right) \cos\left(\phi_{gc_{sat}}\right)] \right)$$

$$\frac{\partial \mathrm{a_j}}{\partial \mathrm{r_k}} = r_j \left(6r_k \frac{\mu {R_\oplus}^2 C_{2,0}}{r^3} \{3\sin^2\left(\phi_{gc_{sat}}\right) - 1\} + \frac{15{r_k}^2}{r^7\sqrt{r_i^2 + r_j^2}} [\mu {R_\oplus}^2 C_{2,0} \sin\left(\phi_{gc_{sat}}\right) \cos\left(\phi_{gc_{sat}}\right) + \frac{3}{r^5\left(r_i^2 + r_j^2\right)^{3/2}} [\mu {R_\oplus}^2 C_{2,0} \sin\left(\phi_{gc_{sat}}\right) \cos\left(\phi_{gc_{sat}}\right)] \right)$$

$$\frac{\partial \mathrm{a_k}}{\partial \mathrm{r_i}} = 6r_i r_k \frac{\mu {R_\oplus}^2 C_{2,0}}{r^6} \{3\sin^2\left(\phi_{gc_{sat}}\right) - 1\} - \frac{15r_i\sqrt{r_i^2 + r_j^2}}{r^7} [\mu {R_\oplus}^2 C_{2,0} \sin\left(\phi_{gc_{sat}}\right) \cos\left(\phi_{gc_{sat}}\right) + \frac{3r_i}{r^5\sqrt{r_i^2 + r_j^2}} [\mu {R_\oplus}^2 C_{2,0} \sin\left(\phi_{gc_{sat}}\right) \cos\left(\phi_{gc_{sat}}\right)]$$

$$\frac{\partial \mathrm{a_k}}{\partial \mathrm{r_j}} = 6r_i r_k \frac{\mu {R_\oplus}^2 C_{2,0}}{r^6} \{3\sin^2\left(\phi_{gc_{sat}}\right) - 1\} - \frac{15r_i\sqrt{r_i^2 + r_j^2}}{r^7} [\mu {R_\oplus}^2 C_{2,0} \sin\left(\phi_{gc_{sat}}\right) \cos\left(\phi_{gc_{sat}}\right) + \frac{3r_i}{r^5\sqrt{r_i^2 + r_j^2}} [\mu {R_\oplus}^2 C_{2,0} \sin\left(\phi_{gc_{sat}}\right) \cos\left(\phi_{gc_{sat}}\right)]$$

$$\frac{\partial \mathrm{a_k}}{\partial \mathrm{r_k}} = 6{r_k}^2 \frac{\mu {R_\oplus}^2 C_{2,0}}{r^6} \{3\sin^2\left(\phi_{gc_{sat}}\right) - 1\} + \frac{15r_k\sqrt{r_i^2 + r_j^2}}{r^7} [\mu {R_\oplus}^2 C_{2,0} \sin\left(\phi_{gc_{sat}}\right) \cos\left(\phi_{gc_{sat}}\right) - \frac{3}{2}\frac{\mu {R_\oplus}^2 C_{2,0}}{r^4} \{3\sin^2\left(\phi_{gc_{sat}}\right) - 1\}$$